SSL

SPACE SYSTEMS LABORATORY
DEPT. OF AERONAUTICS AND ASTRONAUTICS
MASSACHUSETTS INSTITUTE OF TECHNOLOGY
CAMBRIDGE, MA 02139

JOINT NONLINEARITY EFFECTS IN THE DESIGN OF

A FLEXIBLE TRUSS STRUCTURE CONTROL SYSTEM

Mathieu Mercadal

December 1986   SSL #22-86

JOINT NONLINEARITY EFFECTS IN THE DESIGN OF
A FLEXIBLE TRUSS STRUCTURE CONTROL SYSTEM

by

MATHIEU MERCADAL

Submitted to the Department of Aeronautics and
Astronautics on December 15, 1986 in partial fulfillment
of the requirements for the degree of
Master of Science in Aeronautics and Astronautics

ABSTRACT

Nonlinear effects are introduced in the dynamics of large space truss structures by the connecting joints which are designed with rather important tolerances to facilitate the assembly of the structures in space. The purpose of this work was to develop means to investigate the nonlinear dynamics of the structures, and particularly the limit cycles that might occur when active control is applied to the structures. An analytical method was sought and derived to predict the occurrence of limit cycles and to determine their stability. This method is mainly based on the quasi-linearization of every joint using describing functions. This approach was proven successful when simple dynamical systems were tested. Its applicability to larger systems depends however on the amount of computations it requires, and estimates of the computational task tend to indicate that the number of individual sources of nonlinearity should be limited. Alternate analytical approaches, which do not account for every single nonlinearity, or the simulation of a simplified model of the dynamical system should therefore be investigated to determine a more effective way to predict limit cycles in large dynamical systems with an important number of distributed nonlinearities.

Thesis Supervisor: Wallace E. Vander Velde
         Title: Professor of Aeronautics and Astronautics

Acknowledgements

A sincere note of gratitude goes to my advisor. Professor Wallace E. Vander Velde, whose experience in the variety of fields addressed by this study allowed me to always direct my efforts in the right direction. This research would have never been completed without him.

Many thanks also go to all the people of the Contol Division who have made my adaptation to a new life so easy.

Finally, I would like to express all my thanks to my parents and all my family for their comprehensive patience and their wholehearted support, without which I would not have been able to accomplish all I have undertaken.

Table of Contents

List of Figures

Figure:

List of Tables

CHAPTER ONE

INTRODUCTION

1.1 Presentation of some New Classes of Problems Associated with the Design of Large Space Structures.

A new stage in space development is approaching that sees an important increase in space-based activities. This increase should result in spacecraft of much bigger dimension, where size will be mainly determined by the need to collect and transmit more radiative energy like solar power or radio signals, the only form of energy that can be exchanged in outer space. The Hoop/Column antenna, as well as the current Large Space Station configuration should have, for example, dimensions exceeding 100 meters, and comparable, or even bigger spacecraft, stations or satellites are expected in a more distant future.

Truss structures offer a satisfactory answer to the problem of spanning large distances or large areas, and they are extensively used in the design of new spacecraft: they constitute, for example, the backbone of the space station, or so-called "power tower" configuration. The reason for this is that they have a very high stiffness to mass

ratio, which is even more important in the construction of edifices in space than it is on Earth.

However, the use of truss structures in space presents specific problems of vibration and instability. These problems arise from the inherent flexibility of structures which have very large geometrical characteristics, and which are built with a minimal amount of material, as weight is a limiting factor in the launch process. The situation is aggravated by the way the structures are assembled. Since it is not feasible to weld or bolt the different parts together in space, or to launch a structure in one piece, joints with rather large tolerances must be used so that structures can be erected by astronauts, or automatically deployed. The resulting stiffness is therefore reduced, and low frequency vibrations occur that may be very detrimental both for the hardware and for the completion of the mission. The behavior of the joints can even become predominant in the dynamics, and a lot of the benefits expected from a truss can be lost in joint dominated structures. A sometimes strongly nonlinear behavior of the joints induces other unwanted effects and complicates further the study of these problems.

Unfortunately, with the absence of gravity, a negligible internal energy dissipation in the material, and no possible energy loss with the non atmospheric environment, there is no natural phenomenon that can provide damping for the vibrations and assure stability.

All these characteristics make active dynamic control of a flexible structure compulsory, so that vibrations and geometric distortions be kept within an acceptable level. The National Aeronautics and Space Administration (NASA) is scheduling a series of experiments, referred to as Control Of Flexible Structure, or COFS program, in order to investigate, and to validate a technology data base for the suppression of inherent dynamic responses in large flexible spacecraft and the avoidance of undesirable interaction between flexible structures and controls. The COFS I experiment will be a 60 meter high truss mast bearing a 100 kg tip mass, and will be deployed from the cargo bay of the Space Shuttle. Figures 1-1 and 1-2 illustrate its characteristics in greater detail. The mast structure is made of more than 600 struts put together with about 1200 pinned-joints whose characteristics are described in figures 1-3 and 1-4. This study is a contribution to the COFS project, and is aimed at obtaining a better understanding of the effects of the joints on the structure dynamics.

1.2 Review of Previous Related Works.

Studies have already been conducted concerning the characteristics of the joints and their effects on the structure dynamics from a linear point of view, assuming that each joint has a constant stiffness and a constant viscous damping, or from a nonlinear point of view, assessing a more realistic behavior of the joints.

Among recent works, R.Y.-K. Lee, [1], examined the linear effects

of the joints on a three piece boom. He also derived nonlinear models for the joints, based on a physical understanding of what causes the nonlinear behavior, such as Coulomb friction or surface mating. These models were then used to simulate dynamic responses. Problems in simulation raised by the nonlinear character of the systems were also investigated for various integration schemes.

K.W. Belvin [2] also presented a thorough investigation on how to model the nonlinearities in the joints, how to obtain a simpler model more useful for larger problems, and how to use these models, along with an elaborate finite element analysis of a truss structure allowing large deflections, to simulate its dynamics. Next, he analyzed some of the effects of the joints on the dynamics of a plane truss structure with the new refined simulation technique, and obtained some interesting qualitative indications of its behavior. He also addressed the problem of parameter identification, and derived a method to fit optimally, in a least-square error sense, his model to experimental test results.

Parameter identification was the only goal of the thesis by K.J.O'Donnell, [3], where dynamic characteristics of the joints are found through force-state mapping techniques which yield very realistic and accurate models.

1.3 Thesis Objectives and Organization.

All of the aforementioned studies look only qualitatively by means of simulation at the effects of the joints on free structure dynamics.

They do not address the problem of the structure behavior under the effect of a control system, nor do they take into account the applicability of the simulation techniques to very large structures.

This present study is therefore aimed at filling this gap and at investigating some possible approaches to analyzing the behavior of nonlinear truss structures under active control.

Chapter 2 shows how to model the problem, and specifically how to transform the continuous mechanical problem into a finite state variable representation which is very well suited for the design and the study of control systems.

It would have been possible to investigate numbers of th system properties using the newly developed finite state description, but among the different issues, the major problem of stability was not addressed and the study was focused instead on the possible occurrence of limit cycles in the structure under active control. In fact, stability appears to be easy to guarantee for the particular type of problem found with the control of the COFS I Mast, and it is felt that the design of a controller that stabilizes the structure should be a rather simple task in this case. On the other hand, significant nonlinearities can interact with the control system and produce sustained oscillations, also called limit cycles, and because of the expected properties of the joints, those limit cycles seem likely to occur. The reasons for particularly studying limit cycles are developed more detail in Chapter 3, with the rest of the chapter being devoted to deriving analytical tools to

predict their occurrence.

Limit cycles are studied under a restrictive single harmonic hypothesis. The hypothesis allows the nonlinearities in the joints to be taken into account through the use of describing functions, giving means to derive methods applicable to large systems for the search of limit cycles and for the eventual determination of their stability. The special form of the COFS I Mast problem seems to indicate that the accuracy of the solutions found through these methods may not suffer too much from this simplifying hypothesis, and their use seems, therefore, to be rationalized.

In Chapter 4, the practical aspects are taken into account, and the section shows how the theoretical methodology of the previous chapter can be computationally implemented to determine limit cycle existence in real problems. Minimization methods are used in the limit cycle search algorithms derived. Some of the presumedly most effective minimization methods are reviewed in the section, and their pros and cons are discussed. The computational task associated with the different numerical implementations is evaluated in order to facilitate the selection of a most efficient algorithm, and also to permit the overall evaluation of the effectiveness of analytical methods, and ultimately to allow to compare it to the effectiveness of alternate methods.

Finally, some simple examples are derived as an illustration in Chapter 5. They allow comparisons between the different numerical techniques for very small order problems, and they confirm results previously obtained on their efficiency.

The conclusions that can be drawn from this first very general study about the applicability of analytical methods to predict limit cycles in very large structures under active control are presented in Chapter 6.

Possible improvements of the analytical methods, as well as alternate methods which should constitute the object of further studies, are indicated in this last section. Among the alternate methods, the determination of limit cycles through simulation is more specifically detailed, and a rough estimate of the computational task associated with it is given. The comparison of the estimates of the calculation requirements obtained for the two different approaches, the analytical approach and simulation, gives a strong indication that simulation should be in fact one of the most effective approaches to the determination of limit cycles in large structures comparable to the COFS I Mast. It is therefore believed that simulation techniques for large structural systems should be further studied in order to improve them and to reduce the computation they require, which still appears to be considerable when dealing with large dynamical systems like space structures.

CONTROL OF
FLEXIBLE STRUCTURES

MAST FLIGHT SYSTEM

Figure 1-1: General View of the COFS I Mast Experiment

ORIGINAL PAGE IS
OF POOR QUALITY
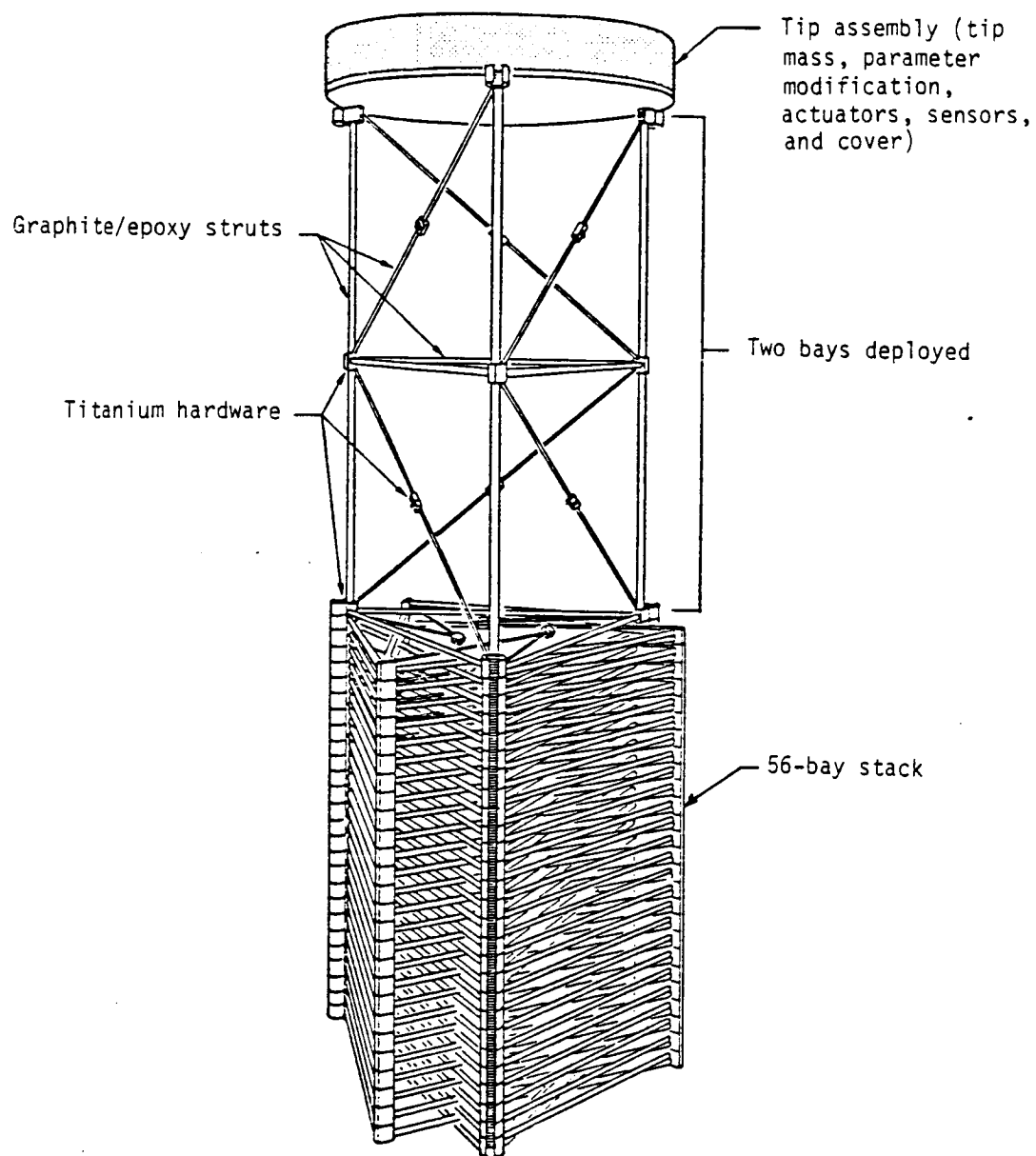
Figure 1-2:   Beam Subsystem During Extension
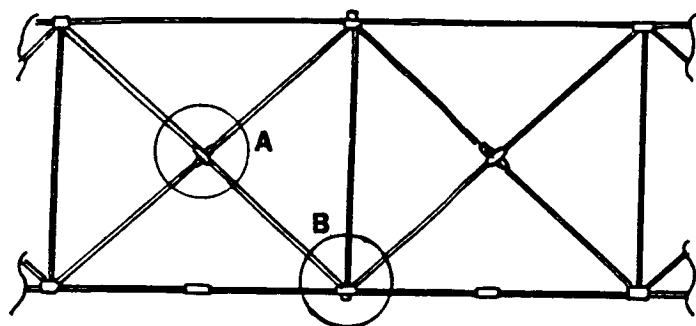
TYPICAL BEAM TWO BAY SECTION
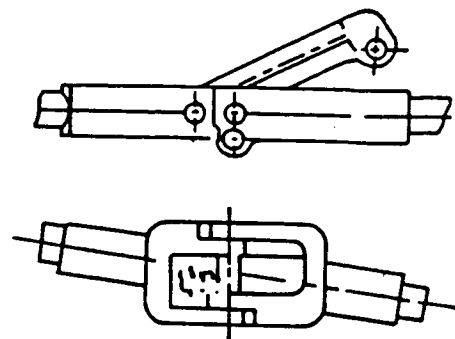
VIEW A
DIAGONAL JOINT ASSEMBLY

BATTEN END FITTING

DIAGONAL END FITTING

LONGERON END FITTING
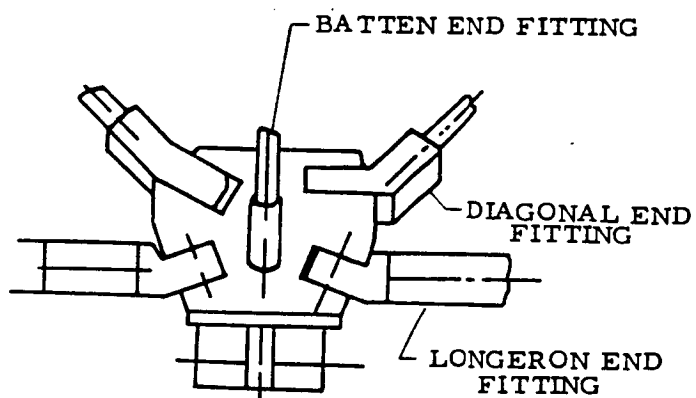
LONGERON JOINT ASSEMBLY
(TOP VIEW)
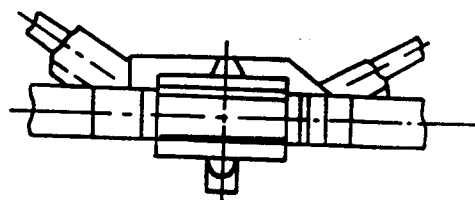
VIEW B
LONGERON JOINT ASSEMBLY
(SIDE VIEW)

Figure 1-3:   Mast Experiment Articulation Joints
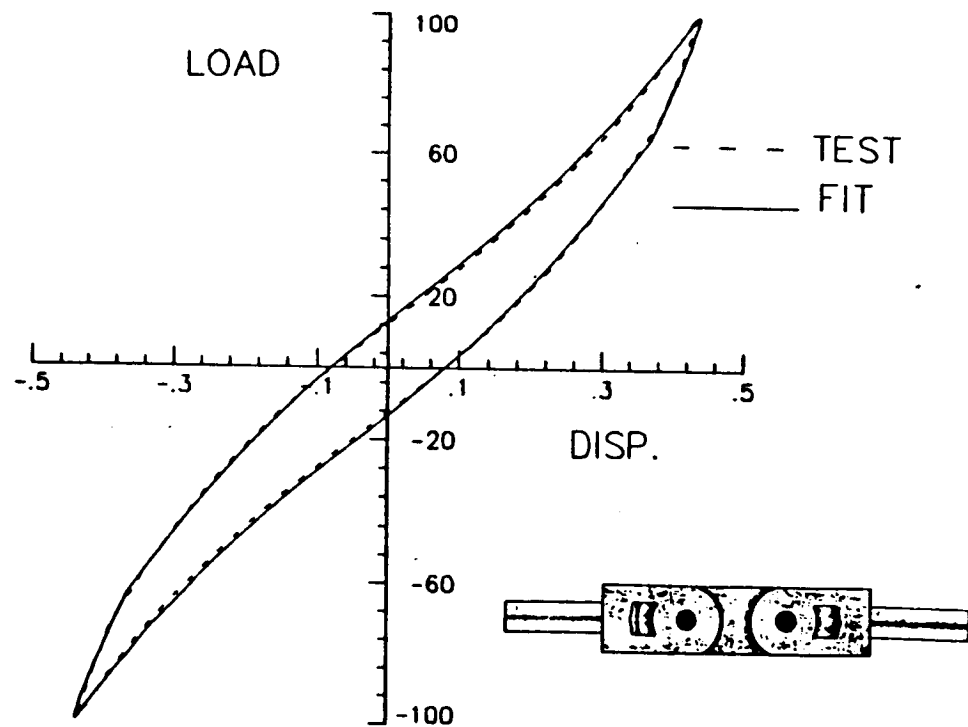
Figure 1-4: Load-Displacement Curve for a Pinned-Joint

CHAPTER 2

PROBLEM MODELING

2.1 Basic Hypothesis on the Nature of Problems in Structural Mechanics.

In most of the developments of Structural Mechanics, the hypothesis is made of the linear behavior of continuous materials. The strain, or local distortion of a body, is linked to the stress, or effort, through linear relations which use characteristic parameters of the material like the Poisson coefficient and Young's modulus for an isotropic material. This hypothesis is verified as long as the body is not subject to large deformations, and allows a great simplification of the study of the dynamics of the non-rigid body.

2.2 Review of a Common Approach for the Analysis of the Dynamics of Non-Rigid Bodies.

2.2.1 Problem Statement: the Modal Analysis.

The dynamics of a non-rigid body are governed by a set of partial

differential equations, along with a set of boundary conditions. Under the linear hypothesis, the general form of the problem can be written as follows (Meirovitch [4]):

$$L \, \underset{\sim}{u} + M \, \overset{..}{\underset{\sim}{u}} = \underset{\sim}{f} \quad , P \in D \tag{2-1}$$

$$B_i \, \underset{\sim}{u} = \underset{\sim}{0} \, , \, P \in S; \, i=1,2,\ldots p \tag{2-2}$$

where L is a differential operator matrix of order 2p, M is a mass matrix, $\underset{\sim}{u}(P,t)$ is the displacement vector at time t of the point P of the domain D occupied by the structure, $\overset{..}{\underset{\sim}{u}}$ being its second partial derivative relative to time, B_i's differential operator matrices of strictly smaller order than L, and S the boundary of D.

$\underset{\sim}{f}(P,t)$ represents the external loads which can be either distributed or discrete, where in the latter case it can be expressed as:

$$\underset{\sim}{f}(P,t) = \underset{\sim}{F}(t)\delta(P - P_o), \tag{2-3}$$

where $\delta(P - P_o)$ is a spatial Dirac delta function.

Because of its linear character, the problem can be solved in a particular way, through modal analysis: periodic solutions of (2-1) are sought when no external load is applied. Exponentially decaying solutions will be sought if damping is introduced, but the structure's internal damping is usually assumed to be zero. A mode r is then represented by a complex parameter λ_r that describes the frequency of the solution and a mode shape $\underset{\sim}{\phi}_r$ which is a function vector that associates the maximum amplitude of the displacement to each point of

the body. Looking for solutions of the form

$$\underset{\sim}{u}_r(P,t) = \underset{\sim}{\phi}_r(P) \, \exp(\lambda_r \cdot t) \tag{2-4}$$

in equations (2-1) and (2-2) yields the following equations for $(\underset{\sim}{\phi}_r, \lambda_r)$:

$$(L + M \, \lambda_r^2) \, \underset{\sim}{\phi}_r = \underset{\sim}{0} \; , \; P \in D \tag{2-5}$$

$$B_i \, \underset{\sim}{\phi}_r = \underset{\sim}{0} \; , P \in S \; , i=1,\ldots p \tag{2-6}$$

which is an eigenproblem ([4]).

The eigenfunctions $\underset{\sim}{\phi}_r$'s constitute an orthonormal basis of the space of the solutions, provided they have been normalized, and for a chosen dot product, they satisfy:

$$\int_D \underset{\sim}{\phi}_s^T M \, \underset{\sim}{\phi}_r \; dD = \delta_{rs} \; , \tag{2-7}$$

for any two modes r and s, where δ_{rs} is the Kroenecker symbol.

Solutions for any kind of loading can therefore be projected on the space spanned by the modal solutions. Writing the solution $\underset{\sim}{u}$ as

$$\underset{\sim}{u}(P,t) = \sum_{r=1}^{\infty} u_r(t) \, \underset{\sim}{\phi}_r(P) \; , \; u_r(t) \in \mathbb{R} \; , \tag{2-8}$$

transforms the partial differential problem into an infinite dimensional system of ordinary time differential equations satisfied by the modal

coordinates $u_r(t)$:

$$\ddot{u}_r - \lambda_r^2 \, u_r = f_r(t) \quad , \quad r=1\ldots\infty, \quad u_r \in \mathbb{R} \qquad (2\text{-}9)$$

where :

$$f_r(t) = \int_D \underset{\sim}{\phi}_r^T(P) \cdot \underset{\sim}{f}(P,t) \; dD \qquad (2\text{-}10)$$

is the forcing term for mode r.

2.2.2 Practical Solution for a Real Problem.

To find the eigenvalues and eigenfunctions of the modes is usually very difficult and closed-form solutions only exist for very particular problems. Approximate solutions for a limited number of modes can however be found through finite element analysis for example. Approximate eigenfunctions $\underset{\sim}{\phi}_r^a$ associated with approximate eigenvalues λ_r^a are defined by a finite number of parameters or degrees of freedom, and thus only span a finite dimensional subspace of the solution space. The problem is discretized and can therefore be treated computationally, whereas the continuous problem cannot be treated at all.

Discretization preserves the orthonormality property and the $\underset{\sim}{\phi}_r^a$'s still constitute an orthonormal family on which the general solution can be projected.

The error of the approximate solution can be tuned by choosing an adequate number of degrees of freedom to describe each mode shape.

However, the number of degrees of freedom has to be increased if a better accuracy, and a larger number of modes, are wanted.

A practical solution will therefore be sought in the form ([4]):

$$\underset{\sim}{u}(P,t) = \sum_{r=1}^{r=n} u_r(t) \; \underset{\sim r}{\phi^a}(P) \qquad , \qquad (2\text{-}11)$$

where n is the number of selected modes.

The modal coordinates u_r's satisfy the following finite dimensional differential system:

$$\left\{ \; \ddot{u}_r + \omega_r^{a^2} u_r = f_r(t) \; , \; r=1\ldots n, \right. \qquad (2\text{-}12)$$

with: $\qquad f_r(t) = \int_D \underset{\sim r}{\phi^{a^T}}(P) \cdot \underset{\sim}{f}(P,t) \; dD,$

and: $\qquad \lambda_r^a = j \, \omega_r^a \qquad , \qquad j^2 = -1 \; .$

A lumped linear system can therefore approximate the dynamics of non-rigid bodies, simplifying tremendously the analysis, even though the dimension of the linear system must be very important for a satisfactory accuracy to be reached. Any solution to the dynamical problem for the body will be sought only in the form:

$$\underset{\sim}{u}(P,t) = \sum_{r=1}^{r=n} u_r(t) \; \underset{\sim r}{\phi}(P) \; , \qquad (2\text{-}13)$$

where $(\lambda_r, \underset{\sim r}{\phi})$ is a mode or an approximation we have of it.

2.3 Modeling of a Truss Structure with Nonlinear Joints.

2.3.1 General Approach.

Nonlinear systems with two distinct parts, one linear and one nonlinear, constitute a special class of nonlinear systems which have received a lot of attention already. Their general architecture is shown in figure 2-1 .

Extensive study of the behavior of this type of system with a SISO nonlinearity is made in Gelb and Vander Velde [5]. Extension to the MIMO case exists in [6,7].

A truss structure is essentially constituted of linear elements, the struts, connected by nonlinear elements, the joints, and it would be appealing to put the problem under the aforementioned form to make best use of its linear characteristics.

The most staightfoward approach would be to describe each strut with a linear model and cascade and feed these linear subsystems back through the nonlinear joints, but this would result in a maze of inextricable connections. Thus our approach is to first replace the real joints by linear equivalents. The resulting altered structure becomes linear, and modal analysis of the whole linearized truss is applied as described before. The linear model of the structure includes state variables for the joints which will be used to feedback the remaining nonlinear part as forcing terms.
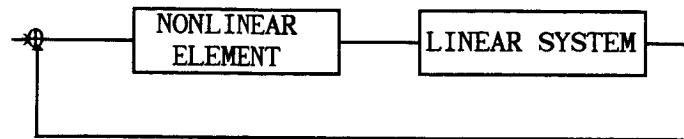
Figure 2-1a: SISO Nonlinear Feedback System.
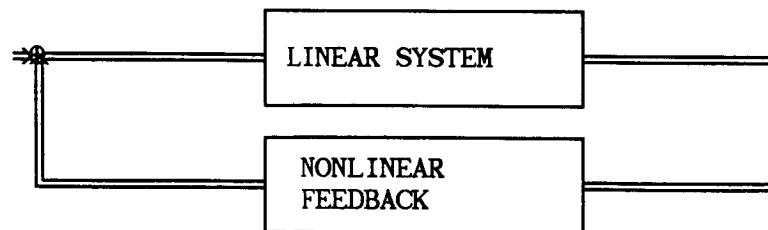
Figure 2-1b : MIMO Nonlinear Feedback System.

2.3.2 Mathematical Formulation.

Let $1, 2, \ldots, N_j$ be the indices of the joints in the structure.
The joints are assumed to be massless and each joint is described by
only two nodes at its ends located at P_{i1} and P_{i2}.
The efforts applied by joint i on the rest of the structure are
considered discrete, and can be written:

$$\underset{\sim}{F}_i(P, t) = \underset{\sim}{F}_i^L(P, t) + \underset{\sim}{F}_i^{NL}(P, t) \quad , \tag{2-14}$$

where $\underset{\sim}{F}_i^L$ is linear in the displacement of the joint and its rate of
displacement and $\underset{\sim}{F}_i^{NL}$ is the remaining nonlinear part.
The way the $\underset{\sim}{F}_i^L$'s are chosen is theoretically unimportant, as long as it
yields a linear model for the entire structure: the nonlinear feedback
will anyway cancel out any unrealistic dynamics assumed for the joints.

It would be much more satisfactory, however, if the linear
equivalent retained as much as possible of the real behavior for
principally two reasons:

First, it might allow to design the controller using only the linear
part, when the remaining nonlinearities are small enough, and to apply
therefore only linear system control design tools.

Secondly, and more importantly, the modal analysis fixes the subspace
where solutions will be sought. Thus, a main concern is that the
component of the complete solution obtained on this subspace may not be
preponderant. Perpendicular components may not be negligible, as it was

implicitly assumed, if the linear equivalents differ too much from the real joints.

Throughout the study, we will assume that such a close linear description of the joint exists as suggested by the test curve we have. (figure 1-4).

Since the linear part has been included to perform the modal analysis of the overall structure, the problem can be written as follows:

$$\ddot{u}_r + \omega_r^2 u_r = \sum_{i=1}^{i=N_j} \left[\phi_r^T(P_{i1}) \cdot F_i^{NL}(P_{i1}, t) + \phi_r^T(P_{i2}) \cdot F_i^{NL}(P_{i2}, t) \right] +$$

$$+ f_r^{ext}(t) \quad , \qquad r=1,2 \ldots n \quad . \tag{2-15}$$

where f_r^{ext} is an external forcing term, basically control forces and disturbances, and can be the result of either distributed or discrete loads.

The matrix formulation of the problem is the following:

$$\ddot{u} + \Lambda u = B_j F_{NL} + B_c F_c + L \cdot d \tag{2-16}$$

where u is the vector of modal coordinates
$$u = [u_1, u_2, \ldots, u_n]^T \quad ,$$

and

$$\Lambda = \text{diag}(\omega_1^2, \omega_2^2, \ldots, \omega_n^2) \quad ,$$

$\mathcal{F}_{NL}$ is the vector of nonlinear forcing terms,

$$\mathcal{F}_{NL} = [\ F_1^{NL^T}(P_{1_1},t) \ F_2^{NL^T}(P_{2_1},t) \ldots \ F_N^{NL^T}(P_{N_j 1},t)]^T , \qquad (2\text{-}17)$$

the B_j matrix is:

$$B_j = \begin{vmatrix} \phi_1^T(P_{1_1}) - \phi_1^T(P_{1_2}) & \cdots & \phi_1^T(P_{N_j 1}) - \phi_1^T(P_{N_j 2}) \\ \phi_2^T(P_{1_1}) - \phi_2^T(P_{1_2}) & & \phi_2^T(P_{N_j 1}) - \phi_2^T(P_{N_j 2}) \\ \vdots & & \vdots \\ \phi_n^T(P_{1_1}) - \phi_n^T(P_{1_2}) & \cdots & \phi_n^T(P_{N_j 1}) - \phi_n^T(P_{N_j 2}) \end{vmatrix} , \qquad (2\text{-}18)$$

$\mathcal{F}_c$ a vector of supposedly discrete control forces applied at different locations P_j^c's,

$$\mathcal{F}_c = [\ F_c^T(P_1^c,t) \ F_c^T(P_2^c,t) \ \ldots \ F_c^T(P_m^c,t) \ ]^T , \qquad (2\text{-}19)$$

$$B_c = \begin{vmatrix} \phi_1^T(P_1^c) & \phi_1^T(P_2^c) & \cdots & \phi_1^T(P_m^c) \\ \phi_2^T(P_1^c) & \phi_2^T(P_2^c) & & \phi_2^T(P_m^c) \\ \vdots & \vdots & & \vdots \\ \phi_n^T(P_1^c) & \phi_n^T(P_2^c) & \cdots & \phi_n^T(P_m^c) \end{vmatrix} , \qquad (2\text{-}20)$$

$\underset{\sim}{d}$ represents the disturbances and L the matrix through which they act on the system.

We implicitly took massless joints by assuming that the sum of the efforts on any joint is zero. Hence, the term $\underset{\sim}{\mathcal{F}}_{NL}$ contains only the forces applied at one end of each joint.

The nonlinear terms depend on the joint's state variables, and we can write $\underset{\sim}{\mathcal{F}}_{NL}$ as :

$$\underset{\sim}{\mathcal{F}}_{NL} = \underset{\sim}{\mathcal{F}}_{NL}(\underset{\sim}{\mathcal{U}}, \underset{\sim}{\dot{\mathcal{U}}}, \underset{\sim}{q}) \quad ,$$

where $\underset{\sim}{q}$ contains joints' history states which are necessary to completely describe the joints' behavior, and whose dynamics are usually nonlinear.

The block representation of figure 2-2 summarizes the way the open-loop system is described.

2.3.3 Dimensionality.

All vectors and matrices presented before have various dimensions, and it is important to know them to appreciate the size of the problem and later discuss the computational load and the size of memory required for its resolution.

The modal vector $\underset{\sim}{\mathcal{U}}$ is an n × 1 vector and the modal matrix Λ is therefore n × n .

Each eigenfunction $\underset{\sim}{\phi}_r$ is a 6 × 1 vector function, since it is necessary to include rotational deformation along with displacement in

the finite element representation.

The discrete forcing terms $\underset{\sim}{F}$ are also 6×1 and include a three dimensional force as well as a three dimensional torque.

Hence, $\underset{\sim NL}{\mathcal{F}}$ is a $(6 \ N_j) \times 1$ vector, and B_j is an $n \times (\ 6 \ N_j)$ matrix.

Similarly, $\underset{\sim c}{\mathcal{F}}$ is a $(6 \ m) \times 1$ vector, and B_c is an $n \times (6 \ m)$ matrix, where m represents the number of actuators.

Typically, the COFS I experimental mast has about 1200 joints, and we will take thereafter $N_j = 1000$ as the order of magnitude to discuss the size issue. The modal analysis should therefore include at least 1000 nodes and about 10,000 degrees of freedom. The number of modes to be retained should be in the range of 100. Hence, the model yielded by the modal analysis is considerably reduced compared to the one used to perform the analysis. However, it should still be meaningful if the modes are carefully selected.

2.3.4 Introducing the Control Laws.

As mentioned in the introduction, active control is required on most of the large flexible spacecraft to transform their dynamics and to obtain an acceptable behavior.

The type of control laws we will consider here are linear control feedback laws. It might be, for example, full state feedback control, or a LQG/LTR controller: the main purpose of this research is not, however, to study the design of controllers for linear descriptions of large space structures, and we do not include in this discussion the use of

reduced order dynamic controllers nor a wide variety of design methods which appears in the literature.

Thus, the control vector $\mathcal{F}_{\sim c}$ has the general form:

$$\mathcal{F}_{\sim c} = - G_1 \, \underset{\sim}{u} - G_2 \, \dot{\underset{\sim}{u}} \, , \tag{2-21}$$

where G_1 and G_2 are two (6 m) $\times$ n gain matrices. We can therefore rewrite the problem as follows:

$$\ddot{\underset{\sim}{u}} + B_c \, G_2 \, \dot{\underset{\sim}{u}} + (\Lambda + B_c \, G_1) \, \underset{\sim}{u} = B_j \, \mathcal{F}_{\sim NL} + L \, \underset{\sim}{d} \, . \tag{2-22}$$

The state vector can also be augmented if integrators are to be included in the control system, before the actuators' command inputs for example, in order to have a zero steady-state error in the presence of constant disturbances. This operation is classic in linear feedback control design ([8]), and the resulting form of the problem is similar but with an increased state vector.

As we can see in figure 2-3, the system still keeps a desired form with separate linear and nonlinear parts when the control loop is closed. Closing the loop only affects the linear part, and there is no need to repeat the modeling process for different control feedbacks.

In summary, only one very expensive modal analysis of a linear equivalent of the entire structure with no active control is required, yielding a linear model whose dynamics is modified by the introduction

of various feedbacks, one nonlinear corresponding to the remaining nonlinear characteristics of the joints, eventually a second nonlinear one corresponding to a possible nonlinear control feedback law, and a linear one corresponding to the linear control feedback law. As the control feedback loop is closed on the linear dynamics of the open-loop model, a new closed-loop linear system is formed, and this system becomes the linear part of the total system, to which the nonlinear part is fed back. The model of the system stays, therefore, in the form of a nonlinear feedback system, which allows simpler and further studies of its behavior.
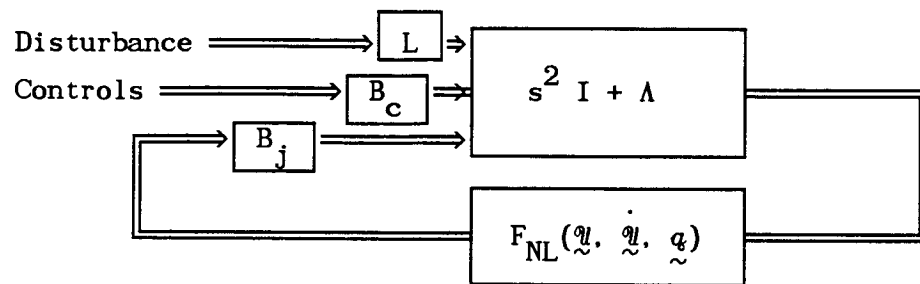
Figure 2-2: Block Diagram Representation of the Nonlinear System.
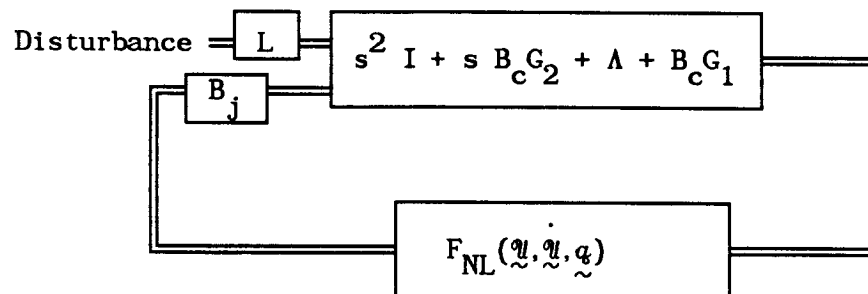
Figure 2-3 : Block Diagram Representation of the Closed-Loop System.

CHAPTER THREE

ANALYTICAL PREDICTION OF LIMIT CYCLE

IN LARGE TRUSS STRUCTURES

3.1 Foreseen Importance of Limit Cycle in Behavior of Large Truss Structure under Active Control.

Nonlinear systems can behave in a lot of different ways, and any designer should look for properties such as the presence of multiple equilibrium points, their stability, the possibility of jump phenomena and the occurrence of limit cycles and amplitude dependent behaviors in the closed-loop system. Everything is equally important for the performance of the design, but some assumptions made about the joints in the COFS I mast make some of them less critical.

3.1.1 Multiple Equilibrium Points.

Multiple equilibrium points means the possibility of having steady-state geometrical deformations of the structure and thus a loss of conformity in its shape. It could be very damaging if the geometry is a preponderant factor in the completion of the mission, as it is for large flexible antennas.

Even though the study does not address the issue directly, we will

show how to modify the limit cycle search technique to be able to determine the equilibrium points.

3.1.2 Stability about an Equilibrium Point.

Stability is always a major issue in any control problem, and if it is quite straightfoward to evaluate it for linear systems, special care has to be brought when it comes to nonlinear cases. The center manifold theory permits one to go further and extend linear system stability criteria to nonlinear systems to assess local stability, and Lyapunov's second method is a very powerful tool used to answer global stability questions. ([9] and [10]).

However, in the case of the joint dominated truss structure some heuristic arguments will easily convince one that stability can be guaranteed provided the joints possess certain properties. More precisely, we suppose the joints to be asymptotically linear, or if f represents the load at one end of a joint and x its displacement, we suppose that there exists a stiffness K such that:

$$\lim_{x \to \infty} (f(x) - K x)/f(x) = 0 . \qquad (3-1)$$

The range of x is naturally limited inside the region where the materials have a linear behavior, but it can be assumed that this region is wide enough, compared to the area where the nonlinear effects are predominant, so that (3-1) is satisfied. The property is illustrated in figure 3-1 .
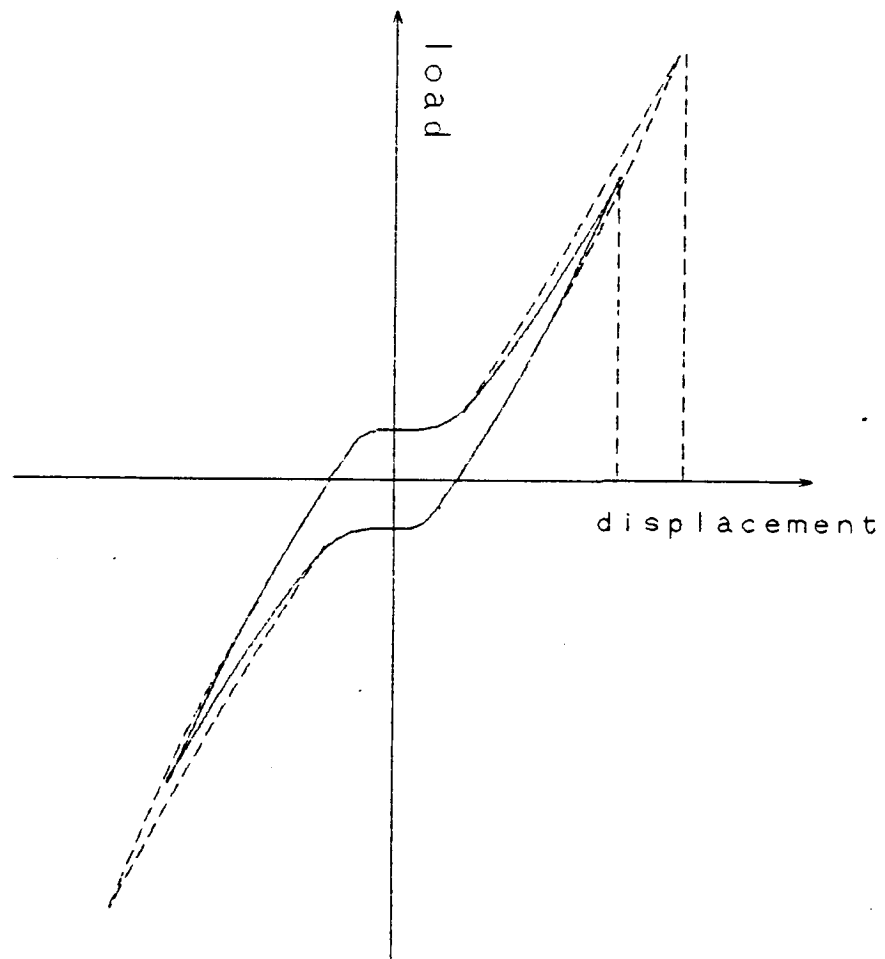
Figure 3-1: Asymptotic Linearity Property

Another underlying assumption made here is that the joints have no real dynamical characteristics, or that the restoring force depends mostly on the displacement x and not the rate of displacement $\dot{x}$, and that the energy dissipated per cycle depends on the amplitude of the excitation rather than its frequency. Otherwise, a viscous damping term must be added to the asymptotical linear model in (3-1).

The pinned-joints used in the COFS experiment seem to fall in this category of asymptotically linearly behaving elements because the main nonlinear phenomenon is thought to be the play at the pin connection and the Coulomb friction which opposes the backlash.

If the linear asymptotes are used to build the linear equivalent model of the structure, and a controller that stabilizes it is added, then the closed-loop nonlinear system will not blow up, since for large enough initial conditions the joints will behave like their asymptotical equivalents and the state variables will decay. Hence, bounded initial conditions result at least in bounded responses, which means that the system is stable.

3.1.3 Jump Phenomena.

Jump phenomena occur when the system switches from one equilibrium point to another for an infinitesimal change in one parameter. They are also referred to as catastrophe and are mostly studied in the very

powerful theory known as the catastrophe, or bifurcation theory ([9]). Buckling is an example of it, and it is the usual jump phenomenon found in structural problems.

Such things do not seem likely to happen in our system since the purpose of the structure is not to carry axial loads, and the presumed asymptotically linear behavior of the joints should guarantee continuity of the response of the structure. Hence, further study seems not important to this point.

3.1.4 Limit Cycles and Amplitude Dependent Behavior.

3.1.4.1 Limit Cycle Definition.

A limit cycle is a sustained, or self excited oscillation in a nonlinear system. Its representation in state space is an isolated closed path, and if the initial conditions are set on one point of the path, the trajectory of the system will remain on it.

A limit cycle is said to be stable if the trajectories originating in its vicinity tend toward it as time goes on. On the other hand, it is said to be unstable if the trajectories go away from it. Figures 3-2a and 3-2b illustrate the concept of stable and unstable limit cycles.

Unstable limit cycles are also called stability boundaries, limit cycle implying stability in that case.

Self excited oscillations might occur in the structure because of the nonlinear character of the joints: the nonlinearities may introduce

some delay in the transmission of the actions of the controller and they may change the phasing to such a point that the controller would add energy instead of dissipating it.

3.1.4.2 Amplitude Dependent Behavior.

Amplitude dependent behavior happens in the presence of two limit cycles and is best explained in figure 3-3:

The inner limit cycle is unstable, or is a so-called stability boundary, and the outer limit cycle is stable. Therefore, for initial conditions within the stability boundary, the system will come back to zero, and will be stable, whereas it will be trapped and will display a limit cycle if the initial conditions are anywhere outside this boundary. Hence, the behavior of the system depends on the amplitude of the initial conditions.

3.1.4.3 Consequences of Limit Cycle Occurrence.

Limit cycles in a structure can cause trouble of the same nature as free oscillations do when no active control is applied.

Their worst effect would be to interact with dynamics of modules or other systems connected to the truss and excite those dynamical systems periodically near their own resonant frequencies, thus forcing an amplified response or even causing instability.
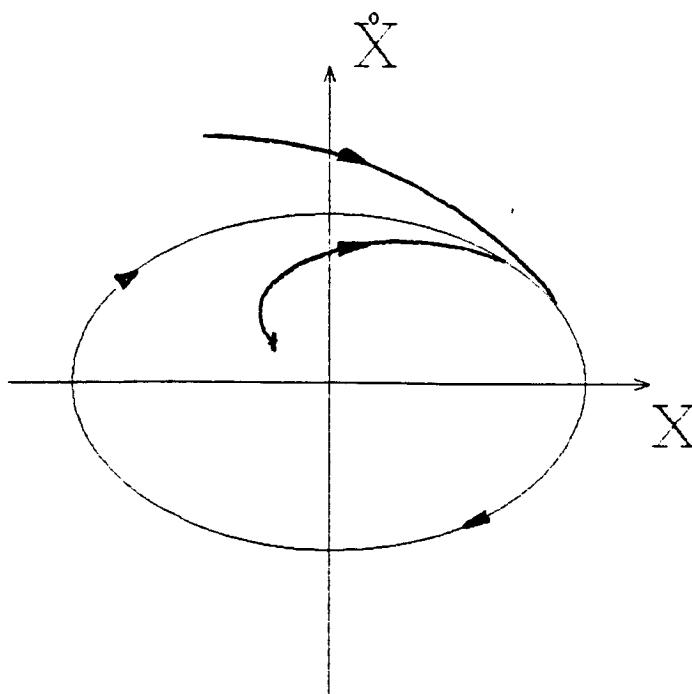
Figure 3-2a: Stable Limit Cycle
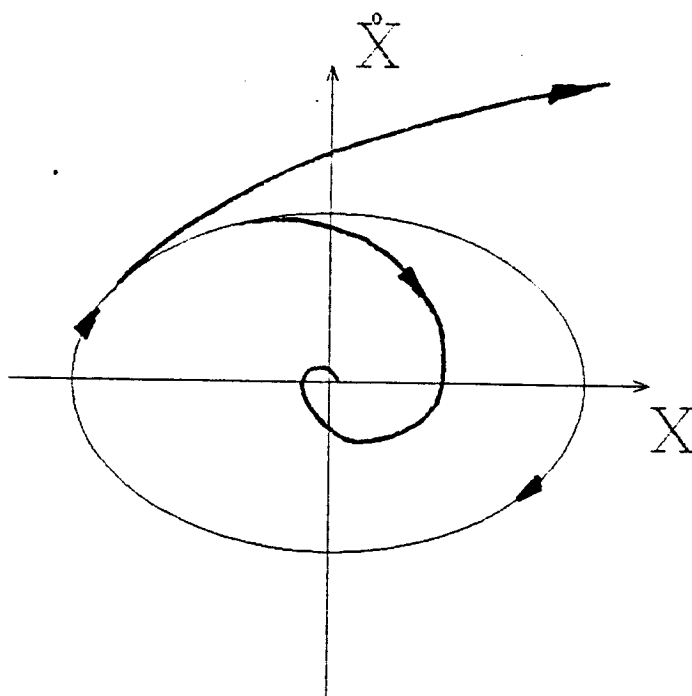
Figure 3-2b: Unstable Limit Cycle
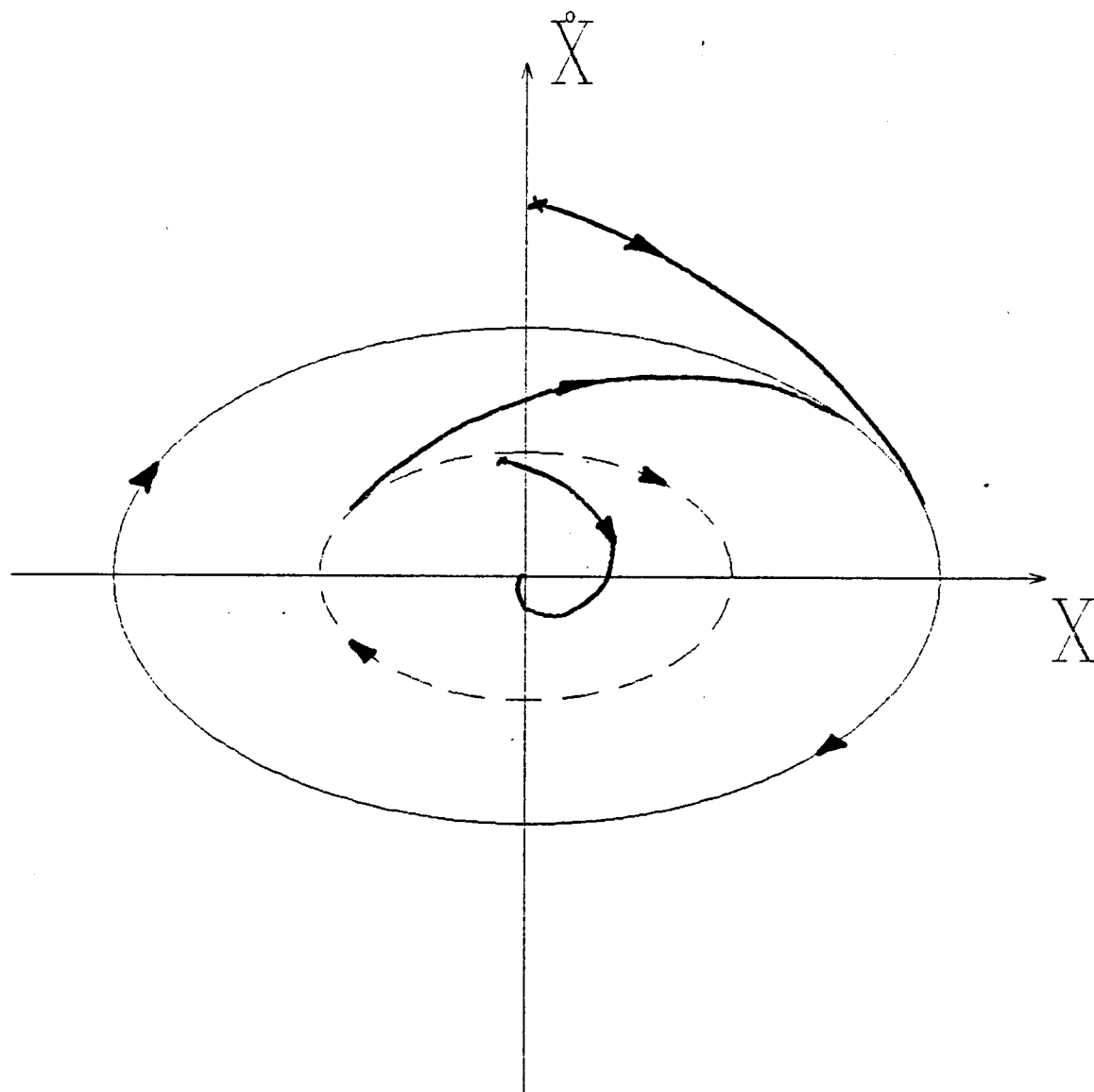
Figure 3-3:   Amplitude Dependent behavior

But even if unstability is not at stake, vibrations can be detrimental for the completion of the mission: loss of accuracy in the geometrical shape can result in a less efficient reception of solar power for solar arrays, or it can degrade the signals received and transmitted by flexible antennas. The vibrations can induce an unacceptable level of acceleration for microgravity experiments taking place in a lab facility of the Space Station.

Finally, it can be very damaging for the spacecraft itself, and it can reduce its reliability and its mission time by speeding the process of fatigue in the joints, in the electronics on-board and usually very sensitive to vibration, and also in the sensors and actuators of the control system which interact with the structure to produce the limit cycles and which are continuously sollicitated.

Therefore, the control system should be designed in such a way that no possible oscillation can occur, and searching for limit cycles must, hence, be of prime concern.

3.2 Analytical Determination of Limit Cycle: Problem Formulation.

3.2.1 General Approach.

A.A.Aderibigbe made a thorough study on how to predict limit cycles in multivariable nonlinear dynamic systems ([11]). He reviewed some already used techniques and he presented an alternate one based on a

particular Ritz–Galerkin method known as the Harmonic Balance Method.

From his work it appears that all applicable analytical techniques share some common features:

First they reduce the general multivariable nonlinear problem using quasi-linearization techniques in order to get a practical model to work with. As we will see later, quasi-linearization methods involve writing the dynamic equations as linear equations with coefficients that depend on certain properties of the state variables and which are chosen in order to reduce in some way the error made in the approximation.

Then a search technique is employed. It is usually an algorithm which will iterate until limit cycle conditions are reached. It also usually tries to make best use of the quasi-linearized form of the problem and track eigenvalues or characteristic equation roots.

The effectiveness of a technique can be appreciated by the degree of approximation reached in the process of getting a workable model and by the efficiency of the search algorithm in terms of memory and time.

3.2.2 Quasi-Linearization Methods.

Since a limit cycling behavior is essentially oscillatory, periodicity in the dynamical equations has to be considered; the quasi-linearization processes perform a sort of Fourier series expansion. However, there are different approaches to do it, involving global or local approximations and retaining only one or more harmonics in the model. Three basic methods can be used.

The first method uses a global statistical linearization. Assuming the system is in the form:

$$\dot{\underset{\sim}{x}} = \underset{\sim}{f}(\underset{\sim}{x}) + \Gamma \underset{\sim}{w} \qquad (3-2)$$

where $\underset{\sim}{x}$ is the state vector which contains a bias $\underset{\sim}{x}_b$, a sinusoidal component $\underset{\sim}{x}_s$, and a random component $\underset{\sim}{x}_r$:

$$\underset{\sim}{x} = \underset{\sim}{x}_b + \underset{\sim}{x}_s + \underset{\sim}{x}_r \qquad (3-3)$$

$\underset{\sim}{f}(\underset{\sim}{x})$ represents the system's nonlinear dynamics, and $\underset{\sim}{w}$ is the input with:

$$\underset{\sim}{w} = \underset{\sim}{w}_b + \underset{\sim}{w}_r \qquad (3-4)$$

where $\underset{\sim}{w}_b$ is a bias input and $\underset{\sim}{w}_r$ a random one.

$\underset{\sim}{f}(\underset{\sim}{x})$ can be approximated by the quasi-linear form

$$\underset{\sim}{f}(\underset{\sim}{x}) = N_b \underset{\sim}{x}_b + N_s \underset{\sim}{x}_s + N_r \underset{\sim}{x}_r \qquad . \qquad (3-5)$$

N_b, N_s and N_r are obtained by minimizing the mean square error of the difference $\underset{\sim}{\epsilon}$

$$\underset{\sim}{\epsilon} = \underset{\sim}{f}(\underset{\sim}{x}) - N_b \underset{\sim}{x}_b - N_s \underset{\sim}{x}_s - N_r \underset{\sim}{x}_r \qquad . \qquad (3-6)$$

The general form of the result is shown in Spanos and Iwan ([12]), and is the following:

$$N_b = (E[\underset{\sim}{f}\ x_b^T])\ (E[\underset{\sim}{x}_b\underset{\sim}{x}_b^T])^{-1} \qquad (3\text{-}7)$$

$$N_s = (E[\underset{\sim}{f}\ x_s^T])\ (E[\underset{\sim}{x}_s\underset{\sim}{x}_s^T])^{-1} \qquad (3\text{-}8)$$

$$N_r = (E[\underset{\sim}{f}\ x_r^T])\ (E[\underset{\sim}{x}_r\underset{\sim}{x}_r^T])^{-1} \qquad (3\text{-}9)$$

An alternate method consists in replacing individual constituting elements by their own quasi-linear representations. If $x(t)$ is the scalar input to the nonlinearity, it is assumed that it only contains a bias x_b, a sinusoidal term x_s, and a random one x_r:

$$x = x_b + x_s + x_r \qquad (3\text{-}10)$$

The output is also assumed to be the sum of a bias, a sinusoid and a random signal and is written as:

$$y(t) = n_b x_b + n_s x_s + n_r x_r \qquad (3\text{-}11)$$

The gains n_b n_s and n_r also minimize the mean square error of the difference between the real and the approximate signal and are called describing functions ([5]). It is shown in [12] that for systems consisting of isolated nonlinear elements connected between nodal points, the global and the element-by-element quasi-linearization yield the same model.

A third method uses the harmonic balance method and describes the nonlinear system as a proportional plus derivative system as a whole. Its main feature is that it involves more than one harmonic in the

assumed form of the state variables, as detailed in [11].

The assumed form of the state vector is:

$$\underset{\sim}{x} = \underset{\sim}{x}_b + \underset{\sim}{x}_{s_1} + \underset{\sim}{x}_{s_2} + \ldots + \underset{\sim}{x}_{s_h} ,$$

(3-12)

where the subscript b stands for bias, and the subscript s_k for the kth harmonic of the sinusoidal term.

The system :

$$\overset{..}{\underset{\sim}{x}} = \underset{\sim}{f}(\underset{\sim}{x} , \overset{.}{\underset{\sim}{x}})$$

is rewritten using:

$$\underset{\sim}{f}(\underset{\sim}{x} , \overset{.}{\underset{\sim}{x}}) = N_b \underset{\sim}{x}_b + N_{p1} \underset{\sim}{x}_{s_1} + \frac{1}{\omega} N_{d1} \overset{.}{\underset{\sim}{x}}_{s_1} + \ldots$$
$$+ N_{ph} \underset{\sim}{x}_{s_h} + \frac{1}{h\omega} N_{dh} \overset{.}{\underset{\sim}{x}}_{s_h} .$$

(3-13)

where each harmonic term N_{pk} and N_{dk} are again found to minimize a mean square error. For only one single harmonic, the solution yielded is the same for all three approaches.

3.2.3 The Single Harmonic Hypothesis.

In simulations performed in [2], a four bay plane truss structure excited by a sinusoidal input responded with a marked sinusoidal character and without any other apparent harmonic terms. In the presence of active control, it is also presumed that higher harmonic resonances will be damped enough so as not to appear in the response of the structure. We must emphasize here that the linear system to which the

nonlinear joint effects are applied is the closed-loop controlled structure. Therefore, the structural resonances within the bandwidth of the control system will be damped, and the bandwidth of the overall system will be limited. Hence, it is believed that a study of possible sustained oscillations involving only the first harmonic will be enough to predict whether or not limit cycles can occur. Anyhow, an analytical study involving higher harmonics would result in the multiplication of state variables and would rapidly make the problem untractable. Furthermore, no stability results can be derived if more than one harmonic is retained.

We shall mention however that an attempt to quantitatively evaluate the quality of the first harmonic approximation is presented by Chouldury and Atherton ([13]). It involves the computation of the distortion of the signal fed back after a sinusoidal input is sent in the open-loop. If the signal $x(t)$ has a Fourier series expansion of the form

$$x(t) = \sum_{k=1}^{\infty} a_k \cos(k\omega t) \tag{3-14}$$

the distortion is

$$\Delta = \left(\sum_{k=2}^{\infty} a_k^2 \right)^{1/2} / a_1 . \tag{3-15}$$

and it is claimed that if the distortion is less than 6%, one can expect an error no more than that amount. Hence there exists at least one test that can be performed to validate the approximation, but it requires mostly simulation techniques to be performed.

3.2.4 Quasi-Linearization of the Problem using Dual Input Describing Functions.

Because of the form of the problem, quasi-linearizing the nonlinear part of each joint is obviously the best way to operate. Dual Input Describing Functions (DIDF) are used under the single harmonic hypothesis.

3.2.4.1 Dual Input Describing Functions.

DIDF involves SISO nonlinearities. If x is the input and y the output of such an element, x is first assumed to be:

$$x = B + A \sin\omega t \qquad\qquad (3\text{-}16)$$

where A an B are real, and y is related to x in the most general case as follows:

$$y = n_B(A,B,\omega)\ B\ +\ n_A(A,B,\omega)\ A\ \sin\omega t\quad , \qquad\qquad (3\text{-}17)$$

where n_B is a real, and n_A is a complex, gain chosen so that the mean-square error of the difference between the true and the assumed signal is minimized.

As shown in [5], the general forms for the gains are:

$$n_B = \frac{1}{2\pi\ B} \int_0^{2\pi} y(\ B + A\sin\theta,\ A\omega\cos\theta\ )d\theta \qquad (3\text{-}18)$$

$$n_A = n_p + j\ n_q\ ,$$

$$n_p = \frac{1}{\pi\ A} \int_0^{2\pi} y(\ B + A\sin\theta,\ A\omega\cos\theta\ )\ \sin\theta\ d\theta \qquad (3\text{-}19)$$

$$n_q = \frac{1}{\pi\ A} \int_0^{2\pi} y(\ B + A\sin\theta,\ A\omega\cos\theta\ )\ \cos\theta\ d\theta \qquad (3\text{-}20)$$

A simplification occurs when it is supposed that the output y only depends on the input and not its first time derivative. If

$$y = y(\ x,\ \dot{x}) = y(\ x) \qquad (3\text{-}21)$$

then there is no term in $A\omega\cos\theta$ in the expressions 3-18 to 3-20. The same simplification occurs when, as it is assumed for the joints of the COFS I Mast problem, the nonlinear function is symmetrical, even though not necessarily single-valued.

3.2.4.2 General Quasi-Linearized Form.

The inputs to the global nonlinear part of the system are the modal coordinates u_r's contained in the modal vector $\underset{\sim}{u}$. The outputs are the forcing terms applied at one end of each joint, i.e. the $\underset{\sim}{F}_{i_1}^{NL}$'s. The

global representation of the nonlinear part has the following form:

$$\underset{\sim}{\mathcal{F}}_{NL} = \mathcal{N}_B(\underset{\sim}{\mathcal{U}}_0, \underset{\sim}{\mathcal{U}}_1) \underset{\sim}{\mathcal{U}}_0 + \mathcal{N}_A(\underset{\sim}{\mathcal{U}}_0, \underset{\sim}{\mathcal{U}}_1) \underset{\sim}{\mathcal{U}}_1 \exp(j\omega t) \qquad (3\text{-}22)$$

where the modal vector is supposed to have the form

$$\underset{\sim}{\mathcal{U}} = \underset{\sim}{\mathcal{U}}_0 + \underset{\sim}{\mathcal{U}}_1 \exp(j\omega t) \qquad (3\text{-}23)$$

where: $\underset{\sim}{\mathcal{U}}_0$ is a n × 1 real vector representing bias

$\underset{\sim}{\mathcal{U}}_1$ is a n × 1 complex vector representing the amplitudes as

well as the phases of the oscillations of the state variables.

$\mathcal{N}_A$ and $\mathcal{N}_B$ are both $(6N_j)$ × n matrix functions.

3.2.4.3 Quasi-Linearization Process for One Single Joint.

The first step in getting the global model is to find the quasi-linearized model that gives for one joint i the forces $\underset{\sim}{F}_i^{NL}$ in terms of $\underset{\sim}{\mathcal{U}}_0$ and $\underset{\sim}{\mathcal{U}}_1$.

The use of DIDF implies a SISO relation between an excitation term and an output from the nonlinear device. However a joint is described by 6 parameters: 3 displacement parameters and 3 rotational parameters, and the efforts it transmits are also 6 dimensional, consisting of a 3 dimensional force and a 3 dimensional torque. This indicates that 36 coefficients should be found to fully describe the behavior of the joint in the most general case.

Hopefully however, there should not be too many nonlinear effects and they should be decomposed into simple SISO nonlinear relations such as the one relating the axial load to the axial displacement in figure 1-4. Hence, the decomposition of the problem will have the following steps.

First, consider the vector of parameters called $\underset{\sim}{q}^i$ that defines the deformation of the ith joint:

$$\underset{\sim}{q}^i = [\ v_x\ v_y\ v_z\ \theta_x\ \theta_y\ \theta_z]^T \tag{3-24}$$

v_x, v_y and v_z are the components of the deformation of the joint measured at its end P_{i1}, along the reference coordinate frame axes Oxyz, and θ_x, θ_y and θ_z account for the rotational distortion of the joint's body. The deformation components in a two dimensional case are shown in figure 3-4.
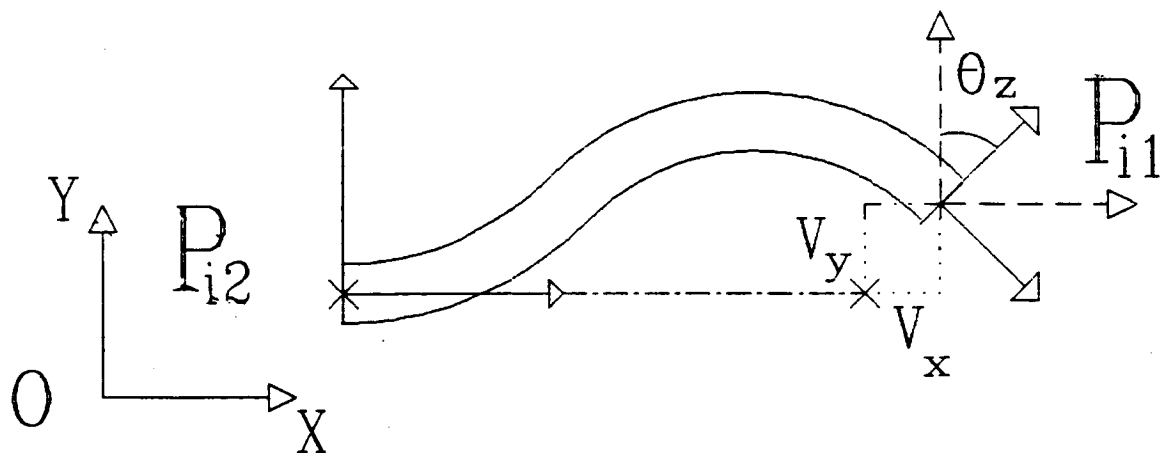
Figure 3-4: Joint's Deformation Parameters

q^i is obtained by a linear transformation of the state vector $\underset{\sim}{u}$, and it can be written as:

$$\underset{\sim}{q}^i = C_i \underset{\sim}{u} \qquad (3\text{-}25)$$

where C_i is the following matrix:

$$C_i = [\ \underset{\sim}{\phi}_1(P_{i_1}) - \underset{\sim}{\phi}_1(P_{i_2}) \ \cdot \ \cdot \ \cdot \ \cdot \ \underset{\sim}{\phi}_n(P_{i_1}) - \underset{\sim}{\phi}_n(P_{i_2})\ ] \qquad (3\text{-}26)$$

Now suppose that one particular nonlinear effect has been retained, which depends on a one dimensional quantity which is linearly related to q^i, and whose output is also one dimensional. The direction along which the input and the output respectively occur are $\underset{\sim i}{P}^I$ and $\underset{\sim i}{P}^O$. The input to the nonlinear element is therefore:

$$x = \underset{\sim i}{P}^{I^T} \underset{\sim}{q}^i$$

$$x = \underset{\sim i}{P}^{I^T} C_i \underset{\sim}{u} \qquad (3\text{-}27)$$

x can be separated as the sum of a bias B and a sinusoidal term of amplitude A and phase ϕ which are directly related to the bias and sinusoidal components assumed for the modal variables as shown:

$$x = \underset{\sim}{P_i^I}^T C_i \left(\underset{\sim}{u_0} + \underset{\sim}{u_1} \exp(j\omega t) \right)$$

$$x = \underset{\sim}{P_i^I}^T C_i \underset{\sim}{u_0} + \underset{\sim}{P_i^I}^T C_i \underset{\sim}{u_1} \exp(j\omega t) \tag{3-28}$$

$$= B + A \exp\left(j(\omega t + \phi) \right)$$

The one dimensional output y is approximated using DIDF by:

$$y = n_B(A,B) B + n_A(A,B) A \exp\left(j(\omega t + \phi) \right) \tag{3-29}$$

$$= n_B\left(\left| \underset{\sim}{P_i^I}^T C_i \underset{\sim}{u_1} \right|, \underset{\sim}{P_i^I}^T C_i \underset{\sim}{u_0} \right) \underset{\sim}{P_i^I}^T C_i \underset{\sim}{u_0} +$$

$$+ n_A\left(\left| \underset{\sim}{P_i^I}^T C_i \underset{\sim}{u_1} \right|, \underset{\sim}{P_i^I}^T C_i \underset{\sim}{u_0} \right) \underset{\sim}{P_i^I}^T C_i \underset{\sim}{u_1} \exp(j\omega t) \tag{3-30}$$

where $\mid z \mid$ represents the magnitude of the complex number z. The phase term ϕ does not appear explicitly in (3-30) since $\underset{\sim}{u_1}$ is already expressed as a complex vector, and the sinusoidal term in x is therefore described with a complex amplitude.

The resulting forcing term is:

$$\underset{\sim}{F}_i^{NL} = y \underset{\sim}{P}_i^O \tag{3-31}$$

Hence, for one given SISO effect recognized in the joint, the load-displacement law can be written as follows:

$$\underset{\sim}{F}_i^{NL} = N_B^i(\underset{\sim}{u}_0, \underset{\sim}{u}_1) \underset{\sim}{u}_0 + N_A^i(\underset{\sim}{u}_0, \underset{\sim}{u}_1) \underset{\sim}{u}_1 \exp(j\omega t) \qquad (3-32)$$

where:

$$N_B^i = \underset{\sim}{P}_i^O n_B(| \underset{\sim}{P}_i^{I^T} C_i \underset{\sim}{u}_1 |, \underset{\sim}{P}_i^{I^T} C_i \underset{\sim}{u}_0) \underset{\sim}{P}_i^{I^T} C_i \qquad (3-33)$$

and

$$N_A^i = \underset{\sim}{P}_i^O n_A(| \underset{\sim}{P}_i^{I^T} C_i \underset{\sim}{u}_1 |, \underset{\sim}{P}_i^{I^T} C_i \underset{\sim}{u}_0) \underset{\sim}{P}_i^{I^T} C_i \qquad (3-34)$$

N_A^i and N_B^i are two 6 × n matrices that depend on the characteristics of the joint through the direction of the main exciting variable, the direction of its action, the nature of the SISO nonlinearity summarized by a describing function and the way the exciting deformation of the joint is related to the state variables.

It is possible to consider that more than one nonlinear effect exists, but in that case the process shall be repeated and the matrices N_A^i as well as N_B^i found for each process summed up, provided all the nonlinear effects are SISO with a good approximation.

3.2.4.4 Quasi-Linearization Process for the Whole Structure.

The general model is obtained by assembling the different models found for each joint. Since the general forcing term $\underset{\sim}{\mathscr{F}}_{NL}$ has the form

shown in (2-17), it can be rewritten in the form (3-22) with:

$$
\mathcal{N}_B(\underset{\sim}{\mathcal{U}}_0, \underset{\sim}{\mathcal{U}}_1) = \left| \begin{array}{c} N_B^1(\underset{\sim}{\mathcal{U}}_0, \underset{\sim}{\mathcal{U}}_1) \\ N_B^2(\underset{\sim}{\mathcal{U}}_0, \underset{\sim}{\mathcal{U}}_1) \\ \vdots \\ N_B^{Nj}(\underset{\sim}{\mathcal{U}}_0, \underset{\sim}{\mathcal{U}}_1) \end{array} \right| \tag{3-35}
$$

$$
\mathcal{N}_A(\underset{\sim}{\mathcal{U}}_0, \underset{\sim}{\mathcal{U}}_1) = \left| \begin{array}{c} N_A^1(\underset{\sim}{\mathcal{U}}_0, \underset{\sim}{\mathcal{U}}_1) \\ N_A^2(\underset{\sim}{\mathcal{U}}_0, \underset{\sim}{\mathcal{U}}_1) \\ \vdots \\ N_A^{Nj}(\underset{\sim}{\mathcal{U}}_0, \underset{\sim}{\mathcal{U}}_1) \end{array} \right| \tag{3-36}
$$

3.3 Limit Cycle Conditions.

3.3.1 Closed-Form Conditions.

A limit cycle occurs when an oscillatory regime is established in the system and when both the nonlinear forcing terms and the modal variables are sinusoidal functions of time.

In steady-state, the state vector $\underset{\sim}{\mathcal{U}}$ is related to the forcing term $\underset{\sim}{\mathcal{F}}_{NL}$ through a linear matrix transfer function we call G, which can be derived from equation (2-22). Equation (3-22) on the other hand shows the relation between the forcing term $\underset{\sim}{\mathcal{F}}_{NL}$ and the modal vector $\underset{\sim}{\mathcal{U}}$. Combining the two equations, and balancing the harmonic terms, leads to

a system of $2n$ equations, with n of them on $\mathbb{R}$, when the bias terms are considered, and n of them on $\mathbb{C}$ when the sinusoidal terms are treated:

$$
\begin{cases}
[\, I - G(0) \; N_B(\underset{\sim}{\mathcal{U}}_0, \underset{\sim}{\mathcal{U}}_1) \,]\, \underset{\sim}{\mathcal{U}}_0 = \underset{\sim}{0} \\
\\
[\, I - G(j\omega) \; N_A(\underset{\sim}{\mathcal{U}}_0, \underset{\sim}{\mathcal{U}}_1) \,]\, \underset{\sim}{\mathcal{U}}_1 = \underset{\sim}{0}
\end{cases}
\qquad \underset{\sim}{\mathcal{U}}_0 \in \mathbb{R}^n , \; \underset{\sim}{\mathcal{U}}_1 \in \mathbb{C}^n \qquad (3\text{-}37)
$$

where I is the n dimensional identity matrix and where $\underset{\sim}{0}$ is the n dimensional null vector.

The unknowns in (3-37) are $\underset{\sim}{\mathcal{U}}_0$, $\underset{\sim}{\mathcal{U}}_1$ and the frequency ω. If a limit cycle exists, the system must admit a solution with $\underset{\sim}{\mathcal{U}}_1$ different from $\underset{\sim}{0}$, which means that there must be at least one modal coordinate that displays a sinusoidal oscillation of non zero amplitude.

It must be mentioned here that an alternate system can result from the combination of equation (2-22) and equation (3-22) which results from the elimination of the state variables between the two expressions:

$$
\begin{cases}
[\, I - N_B(\underset{\sim}{\mathcal{U}}_0, \underset{\sim}{\mathcal{U}}_1) \; G(0) \,]\, \underset{\sim}{\mathcal{Z}}_0 = \underset{\sim}{0} \\
\\
[\, I - N_A(\underset{\sim}{\mathcal{U}}_0, \underset{\sim}{\mathcal{U}}_1) \; G(j\omega) \,]\, \underset{\sim}{\mathcal{Z}}_1 = \underset{\sim}{0}
\end{cases}
\qquad (3\text{-}38)
$$

where I is the N_j dimensional identity matrix and $\underset{\sim}{0}$ is the N_j dimensional null vector.

Since it is supposed that N_j is much greater than n, it is obvious

that the system (3-38) must contain redundant equations, and in any case, the system of the smallest dimension must be retained.

3.3.2 Expansion of the Equations on ℝ.

Handling complex variables is not a natural operation for computers. Therefore, in view of a numerical resolution of the system (3-37), and in order to be able to evaluate the computing task, it is relevant at this point to develop the equations on ℝ. This requires first to express the variables on ℝ as

$$\underset{\sim}{\mathcal{U}}_0 = [\ u_1^0,\ u_2^0,\ .\ .\ .\ u_n^0]^T$$

$$\underset{\sim}{\mathcal{U}}_1 = [\ u_1^1,\ u_2^1\ e^{j\phi_2},\ .\ .\ .\ .\ ,\ u_n^1\ e^{j\phi_n}\ ]^T$$

(3-39)

where the u_i^k's are all real variables and where the ϕ_i's represent the phases between the sinusoids coming into each mode. The phases of the different signals are defined to an arbitrary constant, and the phase of the first sinusoidal component has been taken as zero without loss of generality. In a vector form, we can regroup the u_i^k's in

$$\underset{\sim}{U}_0 = [\ u_1^0,\ u_2^0,\ .\ .\ .\ .\ ,\ u_n^0]^T$$

$$\underset{\sim}{U}_1^r = [\ u_1^{1r},\ u_2^{1r},\ .\ .\ .\ .\ ,\ u_n^{1r}]^T$$

$$\underset{\sim}{U}_1^i = [\ 0\ \ ,\ u_2^{1i},\ .\ .\ .\ .\ ,\ u_n^{1i}]^T$$

(3-40)

where for any i:

$$u_i^1 \, e^{j\phi_i} = u_i^{1r} + j \, u_i^{1i} \tag{3-41}$$

The transfer matrix G as well as the DIDF matrix $\mathcal{N}_A$ shall also be separated into their real and imaginary parts. $\mathcal{N}_A$ can be written as

$$\mathcal{N}_A = \mathcal{N}_p + j\mathcal{N}_q \tag{3-42}$$

where $\mathcal{N}_p$ and $\mathcal{N}_q$ are functions of $\mathcal{U}_0$, $\mathcal{U}_1$ and the frequency ω. A simplification appears when partitioning G that can also save an expensive matrix inversion if we recall (2-22). Expecting a sinusoidal solution in (2-22), the equation can be rewritten as:

$$(-\omega^2 I + \Lambda + B_c G_1 + j\omega B_c G_2) \, \mathcal{U} = B_j \, \mathcal{Z}_{NL} \tag{3-43}$$

Therefore, (3-37) can be expressed as the following system of three subsystems of n simultaneous nonlinear equations

$$[\Lambda + B_c G_1 - B_j \mathcal{N}_B(\mathcal{U}_0, \mathcal{U}_1^r, \mathcal{U}_1^i)]\mathcal{U}_0 = \mathcal{0} \tag{3-44a}$$

$$[\Lambda - \omega^2 I + B_c G_1 - B_j \mathcal{N}_p(\mathcal{U}_0, \mathcal{U}_1^r, \mathcal{U}_1^i)]\mathcal{U}_1^r - [\omega B_c G_2 - B_j \mathcal{N}_q(\mathcal{U}_0, \mathcal{U}_1^r, \mathcal{U}_1^i)]\mathcal{U}_1^i = \mathcal{0} \tag{3-44b}$$

$$[\Lambda - \omega^2 I + B_c G_1 - B_j \mathcal{N}_p(\mathcal{U}_0, \mathcal{U}_1^r, \mathcal{U}_1^i)]\mathcal{U}_1^i + [\omega B_c G_2 - B_j \mathcal{N}_q(\mathcal{U}_0, \mathcal{U}_1^r, \mathcal{U}_1^i)]\mathcal{U}_1^r = \mathcal{0} \tag{3-44c}$$

The system can be solved in $\mathcal{U}_0$, $\mathcal{U}_1^r$, $\mathcal{U}_1^i$ and ω, knowing that u_1^{1i} is null, or it can be solved in $\mathcal{U}_0$, the u_i^1's and the phase variables, but the latter case requires the use of sines and cosines functions to further express the real and imaginary parts of the complex amplitude vector $\mathcal{U}_1$.

3.4 Limit Cycle Stability.

3.4.1 Introduction.

Stability of limit cycles is an important issue since it can determine important stability properties for the system as seen in section 3.1.4. Simulation techniques are mostly used to assess stability by perturbing the system around a limit cycle. However an analytical determination can be made under the single harmonic hypothesis([11]).

The trajectory of a limit cycle is approximately an ellipse in the n dimensional state space, and may not be centered at $\underset{\sim}{0}$ (figure 3-5):

$$\underset{\sim}{u} - \underset{\sim}{u}_0 = \text{Re}(\underset{\sim}{u}_1 \, \exp^{j\omega t})$$

$$\underset{\sim}{u} - \underset{\sim}{u}_0 = \text{Re}(\underset{\sim}{u}_1)\cos\omega t - \text{Im}(\underset{\sim}{u}_1)\sin\omega t \qquad (3\text{-}45)$$

In the subspace orthogonal to the plane Π_ϵ of the ellipse, the system is believed to be <u>asymptotically stable</u>. The assumption is similar to the one used in the Hopf bifurcation theory ([9]), and it states that the tangent linear model found about $\underset{\sim}{u}_0$ should have all but two eigenvalues strictly stable and only two on the imaginary axis for formerly reviewed nonlinear phenomena such as a limit cycle to exist. The study of the nonlinear part is then carried in the 2 dimensional manifold ϵ_c tangent to Π_ϵ at the limit cycle conditions. Therefore, the stability of the system in the subspace orthogonal to this plane does not affect the question of the limit cycle stability, and perturbation of the limit cycle for the purpose of testing stability should occur in ϵ_c to be consistent.
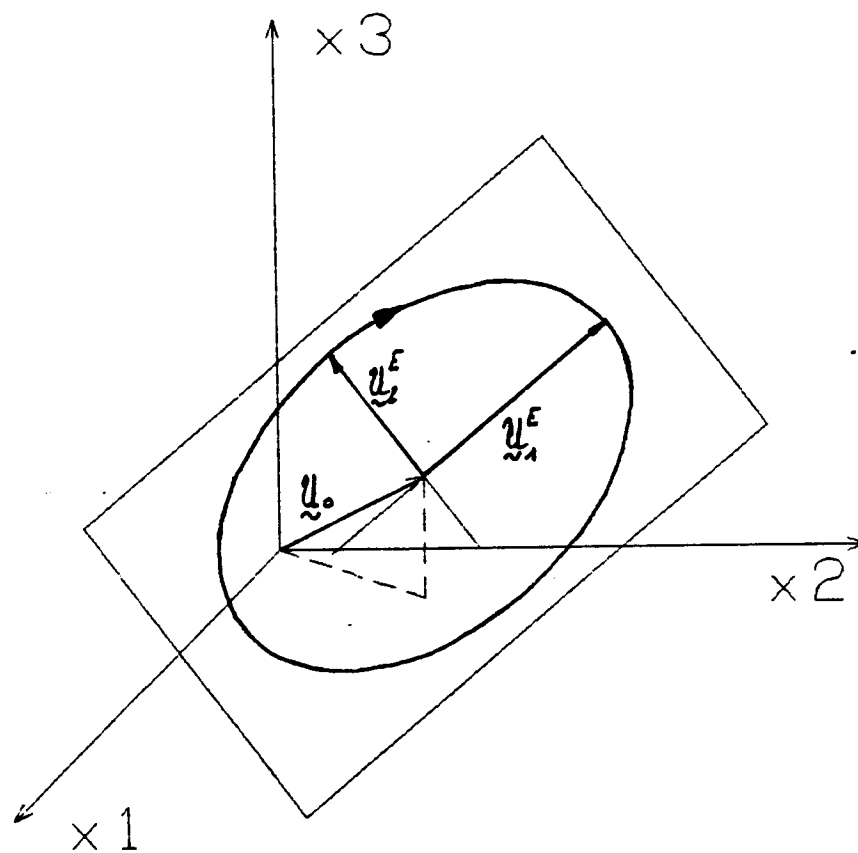
Figure 3-5: Example of Limit Cycle in 3 Dimensional State Space

3.4.2 Consistent Perturbation Conditions.

The parameters of system (3-37) are perturbed around the limit cycle conditions in terms of amplitude, phase and frequency. More precisely, if ω^{lc}, $\underset{\sim}{u}_0^{lc}$ and $\underset{\sim}{u}_1^{lc}$ define the limit cycle conditions, the perturbed terms will be

$$\underset{\sim}{u}_0 = \underset{\sim}{u}_0^{lc} + \delta\underset{\sim}{u}_0$$

$$\underset{\sim}{u}_1 = \underset{\sim}{u}_1^{lc} + \delta\underset{\sim}{u}_1 \tag{3-46}$$

$$\lambda = j\omega^{lc} + \delta\sigma + j\delta\omega$$

If we rewrite the system (3-37) under the generic form

$$\begin{cases} f_0(\underset{\sim}{u}_0, \underset{\sim}{u}_1, \omega) = \underset{\sim}{0} \\ \\ f_1(\underset{\sim}{u}_0, \underset{\sim}{u}_1, \omega) = \underset{\sim}{0} \end{cases} \tag{3-47}$$

the consistency conditions become

$$\begin{cases} \delta f_0 = \underset{\sim}{0} \\ \\ \delta f_1 = \underset{\sim}{0} \end{cases} \tag{3-48}$$

Furthermore, if the vectors of parameters are expressed in terms of their amplitudes and phases as in (3-39), then the condition (3-48) can be developed by linearizing (3-47) about the limit cycle condition.

$$\delta f_0 = \sum_{i=1}^{n} \frac{\delta f_0}{\delta u_i^0}\bigg|_{lc} \delta u_i^0 + \sum_{i=1}^{n} \frac{\delta f_0}{\delta u_i^1}\bigg|_{lc} \delta u_i^1 +$$

$$+ \sum_{i=2}^{n} \frac{\delta f_0}{\delta \phi_i}\bigg|_{lc} \delta \phi_i + \frac{\delta f_0}{\delta \omega}\bigg|_{lc} (\delta \omega - j\delta\sigma) \qquad (3\text{-}49a)$$

$$\delta f_1 = \sum_{i=1}^{n} \frac{\delta f_1}{\delta u_i^0}\bigg|_{lc} \delta u_i^0 + \sum_{i=1}^{n} \frac{\delta f_1}{\delta u_i^1}\bigg|_{lc} \delta u_i^1 +$$

$$+ \sum_{i=2}^{n} \frac{\delta f_1}{\delta \phi_i}\bigg|_{lc} \delta \phi_i + \frac{\delta f_1}{\delta \omega}\bigg|_{lc} (\delta \omega - j\delta\sigma) \qquad (3\text{-}49b)$$

Regrouping the equations (3-49a) and (3-49b) in a matrix form, the condition (3-48) can be written as:

$$M \, \delta \underset{\sim}{V} = -\underset{\sim}{P} \, \delta\sigma \qquad (3\text{-}50)$$

where:

$$\delta \underset{\sim}{V} = [\delta u_1^0, \delta u_2^0, \ldots, \delta u_n^0, \delta u_1^1, \delta u_2^1, \ldots, \delta u_n^1, \delta \phi_2, \delta \phi_3, \ldots$$

$$\ldots, \delta \phi_n, \delta \omega]^T \qquad (3\text{-}51)$$

and where the matrix M and the vector $\underset{\sim}{P}$ depend on the parameters at the limit cycle conditions.

Therefore ([11]), a consistent perturbation can be put in the form:

$$\delta \underset{\sim}{V} = -M^{-1} \underset{\sim}{P} \, \delta\sigma \qquad (3\text{-}52)$$

3.4.3 Stability Conditions.

The method to determine the stability of a limit cycle involves first some geometric transformations: basically one which transforms the coordinates so that the equation of the plane Π_ϵ of the ellipse be in a canonical form, and that in the new coordinate frame n-2 states remain zero for any point of Π_ϵ. A scaling of the coordinates then brings the ellipse back to a circle. Details can be found in [11].

Stability can then be assessed by applying a consistent perturbation which is also put in the new coordinate frame. Figure 3-6 gives an illustration of the transformation and shows how stability can be checked after that, as it is explained in the following:
The distance to the origin of the point of initial conditions defined by the perturbation can be measured to see if it is inside or outside the circle representing the limit cycle. The position is next compared to the sign of the parameter $\delta\sigma$ which governs the size of the perturbation through the consistency condition (3-52): a stable limit cycle will require a positive $\delta\sigma$ to place the perturbation inside the circle, and a negative one outside, whereas the correspondency is inverted for an unstable limit cycle. In other words, the sign of

$$\frac{\delta\sigma}{\delta r} = \frac{\delta\sigma}{r - r_o} \tag{3-53}$$

is determined, where r is the distance of the perturbed point to the origin and r_o the radius of the transformed limit cycle. The sign must be negative for a limit cycle to be stable.
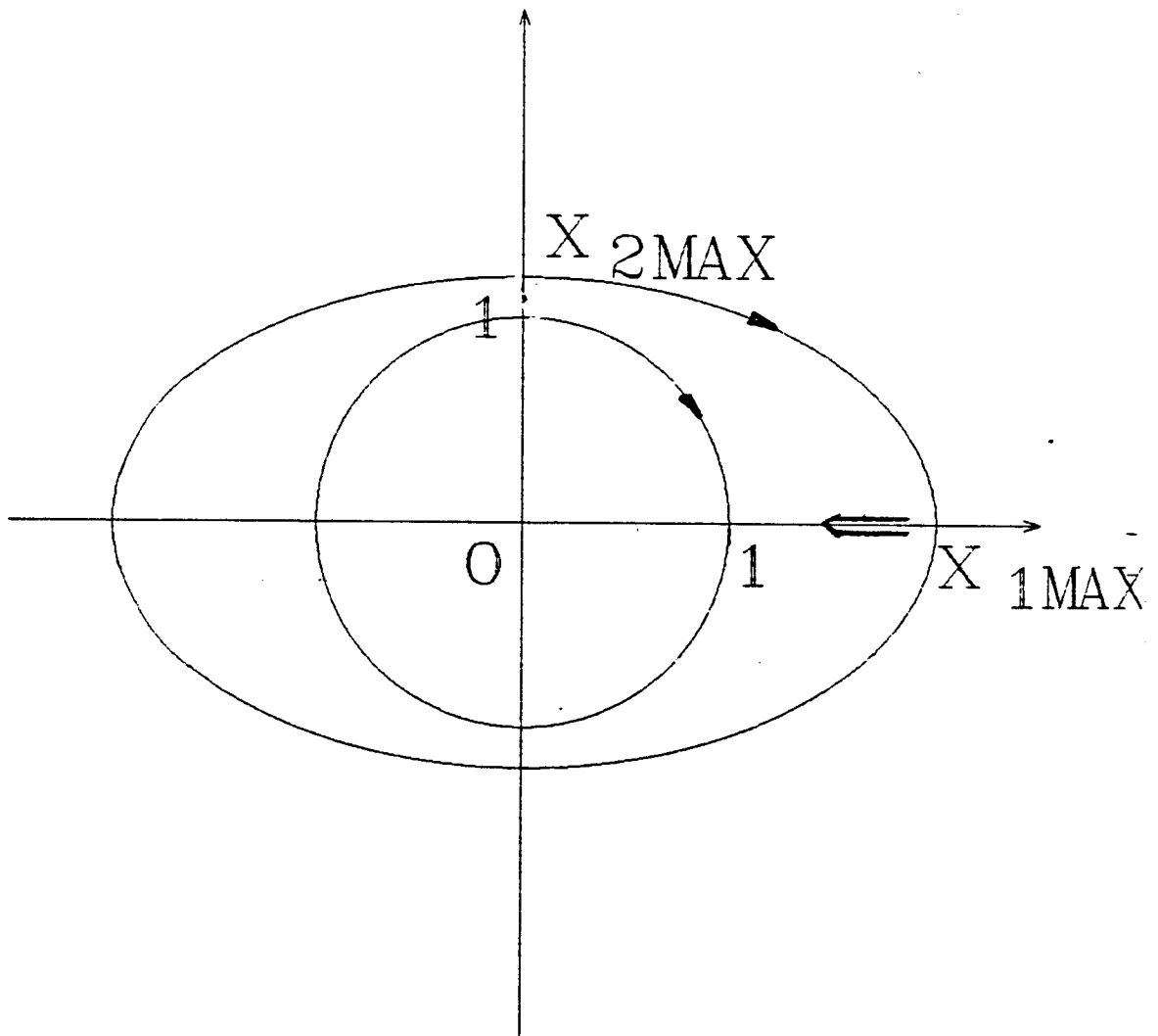
Figure 3-6: Geometrical Transformation for Stability Assessment

CHAPTER FOUR

NUMERICAL DETERMINATION OF LIMIT CYCLES

4.1 Choice of a Resolution Method.

4.1.1 Possible Approaches.

The system (3-37) is a set of $3 \times n$ simultaneous nonlinear equations. It is generally advised to approach the resolution of such systems by keeping their multidimensional vectorial form, using techniques based on the Jacobian of the sytem of equations. Numerous algorithms have been developed, the best of which being reported to be one based on a hybrid Newton-Raphson method [14]. A ready-to-use code, MINPACK-1 [15], is available and applies this method. The code is limited to problems with less than 20 variables.

Dealing with the Jacobian becomes very expensive beyond that range of variables, and since the present problem is very similar to a singular value decomposition problem, it can be soved at least as efficiently with a function minimization approach. The methodology used here is therefore to try to minimize the square of the norm of the

residual vector $\underset{\sim}{\epsilon}$, where

$$\underset{\sim}{\epsilon} = \left| \begin{array}{c} f_0(\underset{\sim}{V}) \\ f_1(\underset{\sim}{V}) \end{array} \right| \tag{4-1}$$

and where f_0, f_1 and $\underset{\sim}{V}$ are the notations used in 3-46 through 3-51.

4.1.2 Residual Functions.

A limit cycle condition is reached if and only if the set of variables satisfying (3-37), or its equivalent form (3-44), is such that $\underset{\sim}{\mathcal{U}}_1$ is not the zero vector. Hence, using the variables as defined in chapter 3, and using the system of equations (3-44) rewritten in closed-form, the following residual function can be derived as

$$R(\underset{\sim}{V}) = \frac{\| [\Psi(0) - B_j \mathcal{N}_B(\underset{\sim}{V})] \underset{\sim}{\mathcal{U}}_0 \|^2}{\| \underset{\sim}{\mathcal{U}}_1 \|^2} +$$

$$+ \frac{\| [\Psi(\omega) - B_j \mathcal{N}_A(\underset{\sim}{V})] \underset{\sim}{\mathcal{U}}_1 \|^2}{\| \underset{\sim}{\mathcal{U}}_1 \|^2} \tag{4-2}$$

where the matrix function Ψ is defined as:

$$\Psi(\omega) = -\omega^2 I + j\omega\, B_c G_2 + \Lambda + B_c\, G_1 \quad , \quad \omega \in \mathbb{R} \tag{4-3}$$

and where the rest of the parameters are defined in chapter 2. Dividing the square of the norm of the residual vector by the square of the norm

of the complex amplitude vector ensures that any solution will have at least one non zero sinusoidal signal.

Similarly, a residual function can be built to search for multiple equilibrium points. Since the origin is an equilibrium point, the residual function is straightfoward and is

$$R_0(\underset{\sim}{u}_0) = \| [\Psi(0) - B_j \mathcal{N}_B(\underset{\sim}{u}_0, \underset{\sim}{Q})] \underset{\sim}{u}_0 \|^2 \qquad (4\text{-}4)$$

A set of limit cycle conditions equivalently satisfies (3-37) or sets the residual function R to zero. A limit cycle will therefore occur whenever the function reaches zero, and the parameters of the limit cycle are the ones for which this value is taken. Since R is always positive or null, it is also theoretically possible to infer the nonexistence of limit cycles by checking the absolute minimum of the function over the whole range of values the variables can take. If the absolute minimum is strictly greater than zero, no limit cycle can occur. On the other hand, if it is zero, limit cycles will occur whenever the residual function reaches its absolute minimum.

It is clear, however, that restrictions apply, and a practical solution can only rely effectively on finding a limited number of limit cycles, if some exist, since the computational task is the major limiting factor in the application of the theory.

4.2 Adapted Minimization Algorithms.

4.2.1 Presentation of Unconstrained Minimization Techniques.

Unconstrained minimization can be achieved with various degrees of complexity which goes along with various effectiveness. It is obvious that the more information is known on the function behavior -i.e. the more derivatives we consider- the faster the convergence can be.

However, the derivatives may not exist, but if they do, their computation can be very time consuming, and can require a lot of extra memory. Not only shall the methods with the highest rate of convergence be therefore considered to solve problems with a great number of variables.

Almost all the minimization algorithms share the following features: from a current point, the algorithm finds a direction in the state space where the function is most likely to decrease. An univariate minimization, or line search, is then performed along this direction to locate the local minimum which becomes the new current point for the next iteration.

The way those operations are performed separates the techniques, and it is possible to classify them into three main types:
The first type is constituted by nongradient techniques which do not require any derivatives, but only grope toward the solution by evaluating the function at many locations, and make use of these computed values to determine the search directions. Their only advantage

is that they save the computation of the derivatives, but they suffer a very low rate of convergence and require many function evaluations.

The second type is constituted by gradient methods which make use of the first derivatives to create a search pattern which yields search directions better distributed to find the solution more rapidly. Their rate of convergence is higher, but the line search is still blind.

Finally, Newton and Quasi-Newton methods go one step further, and by using the Hessian or by approximating it, they allow the forecast of the location of the local minimum along a line search direction. Their rate of convergence is quadratic, but their main drawback is the necessity to update the Hessian matrix which can be a very large matrix.

4.2.2 Possible Algorithms for the Determination of Limit Cycles.

According to Scales [16] who reviews a great number of existing unconstrained minimization techniques along with their advantages and their disadvantages, the <u>Conjugate Gradient method</u> is the most appropriate when the number of variables becomes very large, above 250 variables. The main reason is that the method requires much less function evaluations than nongradient methods, even if the gradient is derived numerically, but it does not require the computation of the Hessian matrix which is square with dimension equal to the number of variables.

However it is also reported in Scales that <u>Quasi-Newton methods</u> are very superior in terms of execution time and convergence rate. Among

those methods, the one suggested independently by Broyden, Fletcher, Golfarb and Shanno ([17,18,19,20]), and also referred to as the BFGS method is more specifically reported to be the most effective. The claim is also confirmed by Himmelblau [21], who conducted a uniform evaluation of the performance of different types of unconstrained optimization techniques. Even though the size needed to store the Hessian is a major problem when the function depends on a great number of variables, an other positive point is that the BFGS method suffers rather rough line searches, thus saving many function evaluations which appear to be one of the computationally most important burdens, as shown later on. Therefore, the BFGS method is another candidate to consider for the determination of limit cycles.

4.2.3 Polak Ribière Conjugate Gradient Method.

The main feature of a conjugate gradient method is that the search lines are conjugate. For a non-degenerate quadratic function, this property means that the search directions form an orthogonal base, the dot product taken being the one induced by the Hessian of the function which is a constant positive definite symmetric matrix in that case. If

$$f(\underset{\sim}{X}) = \underset{\sim}{X}^T G \underset{\sim}{X} \qquad , \underset{\sim}{X} \in \mathbb{R}^m \qquad (4\text{-}5)$$

is the generic function to minimize, where G is a positive definite symmetric matrix and m an integer representing the number of variables,

then the search directions p_i's satisfy:

$$p_j^T G p_i = p_i^T G p_i \, \delta_{ij} \qquad (4\text{-}6)$$

where δ_{ij} is the Kroenecker symbol. Furthermore in the quadratic case the minimum of the function is reached in exactly m iterations. Things change in the nonlinear case since the Hessian is not constant. If m still represents the number of variables, the algorithm will perform major iterations, which are groups of m minor iterations, or computations of a search direction p_k and an univariate minimization along the line. During a major iteration the directions are generated so that they satisfy the conjugacy property. It is proven, [16], that if g_k represents the gradient of the function f at a current point X_k, the direction p_k along which to find the next point X_{k+1} should be of the form

$$p_k = -g_k + \beta_k p_{k-1} \qquad (4\text{-}7)$$

to ensure conjugacy between the search directions in a major iteration. β_k is a scalar which can be chosen according to the particular form of conjugate gradient method wished to be used ([16]). The choice of β_k due to Polak and Ribière [22] reportedly succeeds more often and should

be therefore preferred to other choices. Its form is

$$\beta_k = \frac{(g_k - g_{k-1})^T g_k}{g_{k-1}^T g_{k-1}} \qquad (4\text{-}8)$$

The update of the search direction p_k requires the knowledge of the previous search direction p_{k-1}, the gradient at the previous iteration g_{k-1} as well as the gradient at the current point g_k.

When m minor iterations have been performed, the search direction is reset equal to the gradient at the current point: this reset has been reportedly very successful to prevent the search directions from drifting and lie in a subspace of $\mathbb{R}^m$ because of rounding errors in the update formula.

Hence, only four m × 1 vectors have to be stored to update the search direction and this constitutes the main advantage of the method for large systems. Also, when close to the minimum, the Hessian matrix is approximately constant and a quadratic termination can be expected.

The gradient can be found by finite difference as well as analytically without influencing the convergence properties of the method. However the method requires a very precise univariate search, and each updated point coming from each minor iteration has to be very close to the true local minimum in order to get an acceptable convergence speed. This can be one of the major problems in applying the conjugate gradient method since the evaluation of the function can be very time consuming, and that is why other methods might be considered.

4.2.4 The BFGS Quasi-Newton Method.

The Newton method uses Taylor series expansion of the function up to the quadratic term to find the next step, or equivalently a Taylor series expansion of the gradient to the first order. If the next point X_{k+1} is related to the current point X_k as follows

$$X_{k+1} = X_k + P_k \qquad (4\text{-}9)$$

then the Taylor series expansion of the gradient $g(X)$ is:

$$g(X_k + P_k) = g(X_k) + G_k P_k \qquad (4\text{-}10)$$

where G_k is the Hessian matrix of f at X_k. A successful step is one which sets the next gradient $g(X_{k+1})$ to zero. Using the first order approximation for the gradient, this step is found to be

$$P_k = - G_k^{-1} g(X_k) \ , \qquad (4\text{-}11)$$

which gives not only the direction, but also the step to take in that direction, at each iteration.

The pure Newton method however suffers from multiple problems among which is the necessity to compute the Hessian G at each iteration and to invert it, which is expensive and not always possible. Quasi-Newton

methods have therefore been developed: they avoid the computation of the Hessian, and they carry and update instead an approximation of its inverse.

As seen in [16], there exists families of Quasi-Newton methods, but the most successful seems to be the one referred to as the BFGS method. If H_k represents the approximate of the inverse of the Hessian at the kth iteration, it is updated as follows:

$$H_{k+1} = [I - \frac{\Delta X_k \, \Delta g_k^T}{\Delta X_k^T \Delta g_k}] \, H_k \, [I - \frac{\Delta X_k \, \Delta g_k^T}{\Delta X_k^T \Delta g_k}]^T + \frac{\Delta X_k \, \Delta X_k^T}{\Delta X_k^T \Delta g_k} \qquad (4\text{-}12)$$

where ΔX_k is the step taken in the iteration, Δg_k the vector difference between the gradient at point X_k and X_{k+1}, I the m dimensional identity matrix and H_k the current approximation of the inverted Hessian.
The step p_k is given by

$$p_k = - H_k \, g_k \qquad (4\text{-}13)$$

p_k represents the step in a real Newton method. However the Quasi-Newton method starts only with an approximate Hessian, and therefore the method only considers p_k as a search direction and still performs an univariate

minimization. But it must be noticed that if the step is

$$\Delta \underset{\sim}{X}_k = \alpha_k \underset{\sim}{p}_k \quad , \quad \alpha_k \in \mathbb{R} \tag{4-14}$$

the sequence of α_k tends rapidly toward 1. It therefore provides a good initial guess in the univariate minimization and the line search can eventually be abandoned in the final steps.

The search directions are still better distributed in quasi-Newton methods than in first order methods. It is proven in [16] that they too satisfy the conjugacy property. It is also reported there, and in Dixon, [23], that the method suffers an imprecise line search, and that not reaching the local minimum at each iteration can indeed improve the convergence.

Since updating the matrix H is not a much more expensive task than evaluating the residual function, as it will be seen later, the method appears potentially better than the conjugate gradient method, whose advantage lies principally in the small cost associated with the computation of the search directions.

4.3 Evaluation of the Computational Task.

4.3.1 General Purpose.

It is necessary to estimate the computational task of any analytical limit cycle prediction method in order to be able to comment

on its effectiveness. Determining the most applicable minimization method shall then be possible, as well as comparing alternate methods that can be used to study the nonlinear dynamics, such as simulation. Hence, the following sections will be devoted to finding rough estimates of the calculations undertaken in the different parts of the limit cycle determination process. The most general case is studied, and the estimates can be taken as upper bounds, but they shall however be considered as significant results.

4.3.2 Residual Function Calculation.

The way to compute the residual function is to first evaluate the residual vector as in (4-1) using (3-44), then compute the square of its norm and divide it by the square of the norm of the complex amplitude vector. The main chore of the computation is to evaluate the forcing terms through the matrices N_B and N_A. Following the steps of section 3.2.4 to build the nonlinear terms, and referring to the expression (3-44), the computation of one forcing term can be summarized as detailed in figure 4-1. Following the calculation shown there, the number of required operations can be estimated to the order of $O(21\ N_j n)$ multiplications, when all the joints are taken into account, and not accounting for the $3\ N_j$ evaluations of describing function terms.

If the describing functions are evaluated on line and computed through a numerical integration of some available test functions, then
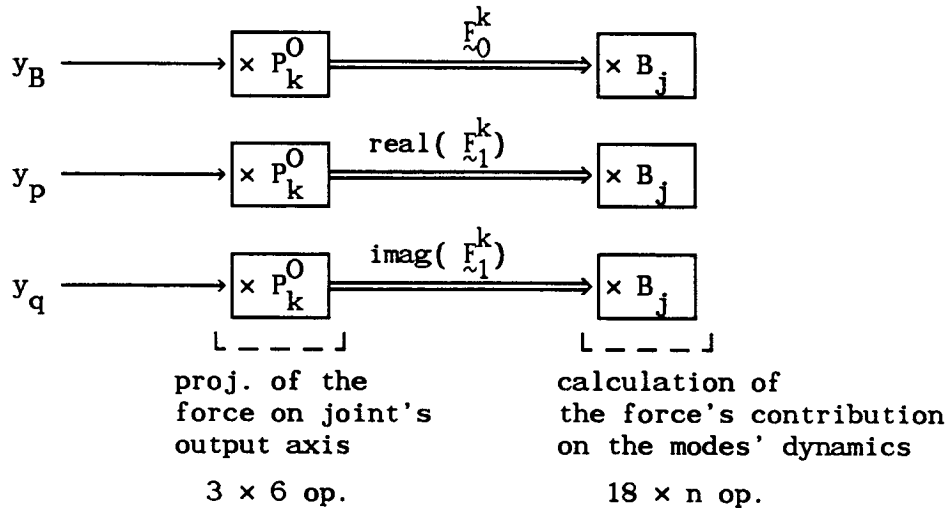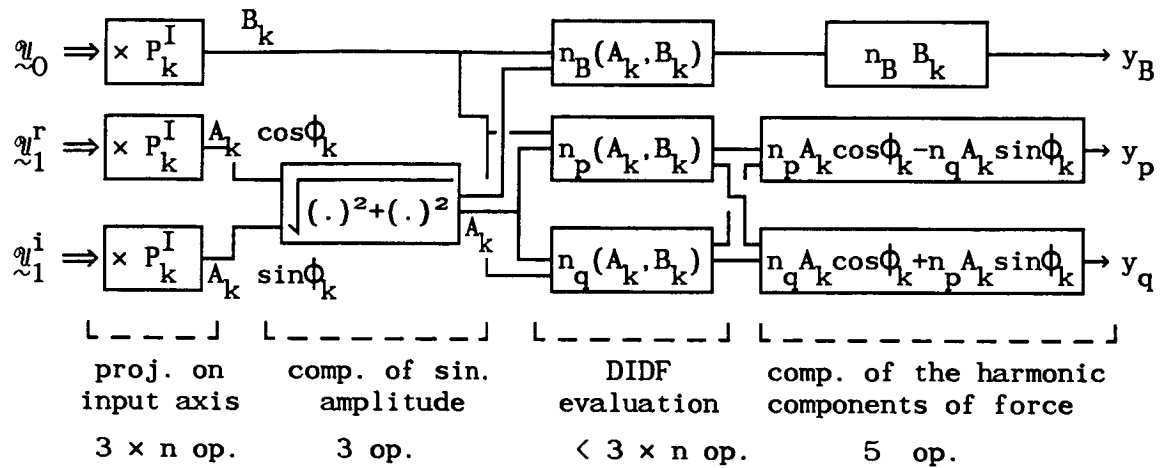
Figure 4-1: Steps of the Computation of the Forcing Term

due to One Single Joint

the extra task can be evaluated on the order of $O(3\ N_j n)$ operations, assuming that about n points are taken to perform the numerical integration. The choice seems reasonable if n is about 100 as we have implicitly assumed.

On the other hand, models can be available that simply describe the shape of the envelope of the load-displacement test curves ([24,25]). In that case, closed-forms may exist that give the values of the describing functions taken for each joint, and the task then would be reduced to $O(3N_j)$.

The rest of the residual function evaluation requires $O(5n^2)$ operations, as shown in figure 4-1 . Therefore, we can evaluate the chore to be of the order of $O(\ 24\ N_j n\ +\ 5\ n^2)$ multiplications, which represents about 2.5 million operations for one function evaluation if n and N_j are 100 and 1000 respectively. Hence, it is clear that minimizing the number of function evaluations is of prime concern, and that the fastest method should be considered.

4.3.3 Gradient Evaluation.

The gradient can be evaluated numerically by perturbing one variable at a time. However two main problems arise:

first the size of the perturbation must be chosen small enough so that the step taken lies in the linear domain, but also large enough so that rounding errors do not dominate the variations. Unfortunately, the choice is made blindly since the necessary information is contained in

the second derivative of the function.

The second and more crucial problem is that given the number of operations required to evaluate the function, repeating the process 3n times appears unacceptable from an execution time viewpoint.

If an analytical calculation of the gradient is undertaken, it would proceed as follows.

Since:

$$r(\underset{\sim}{V}) = \frac{\underset{\sim}{\epsilon}(\underset{\sim}{V})^T \underset{\sim}{\epsilon}(\underset{\sim}{V})}{\underset{\sim 1}{U}^{rT}\underset{\sim 1}{U}^r + \underset{\sim 1}{U}^{iT}\underset{\sim 1}{U}^i} \qquad (4\text{-}15)$$

we have:

$$\frac{\partial r}{\partial u_i^0} = 2\, \frac{\underset{\sim}{\epsilon}(\underset{\sim}{V})^T}{\underset{\sim 1}{U}^{rT}\underset{\sim 1}{U}^r + \underset{\sim 1}{U}^{iT}\underset{\sim 1}{U}^i}\, \frac{\partial\underset{\sim}{\epsilon}}{\partial u_i^0} \qquad , \qquad (4\text{-}16)$$

where

$$\partial\underset{\sim}{\epsilon}\,/\,\partial u_i^0 = \begin{vmatrix} [A + B_c G_1 - B_j \mathcal{N}_B]\,\underset{\sim}{E}_i - B_j \partial \mathcal{N}_B / \partial u_i^0\,\underset{\sim 0}{U} \\[2mm] -B_j \partial \mathcal{N}_p / \partial u_i^0\,\underset{\sim 1}{U}^r + B_j \partial \mathcal{N}_q / \partial u_i^0\,\underset{\sim 1}{U}^i \\[2mm] -B_j \partial \mathcal{N}_p / \partial u_i^0\,\underset{\sim 1}{U}^i - B_j \partial \mathcal{N}_q / \partial u_i^0\,\underset{\sim 1}{U}^r \end{vmatrix} \qquad (4\text{-}17)$$

with $\underset{\sim}{E}_i = [0, \ldots, 0, 1, \ldots, 0]^T$, the 1 component being the ith element.

$$\frac{\partial r}{\partial u_i^{1r}} = 2 \; \frac{\underset{\sim}{\epsilon}(\underset{\sim}{v})^T}{\underset{\sim}{U}_1^{rT}\underset{\sim}{U}_1^r + \underset{\sim}{U}_1^{iT}\underset{\sim}{U}_1^i} \; \frac{\partial \underset{\sim}{\epsilon}}{\partial u_i^{1r}} - 2 \; \frac{r(\underset{\sim}{v}) \; u_i^{1r}}{\underset{\sim}{U}_1^{rT}\underset{\sim}{U}_1^r + \underset{\sim}{U}_1^{iT}\underset{\sim}{U}_1^i} \; , \tag{4-18}$$

where:

$$\partial \underset{\sim}{\epsilon} \; / \; \partial u_i^{1r} = \left| \begin{array}{l} -B_j \partial N_B / \partial u_i^{1r} \underset{\sim}{U}_0 \\[2mm] [\Lambda - \omega^2 I + B_c G_1 - B_j N_p] \; \underset{\sim}{E}_i \; -B_j [\partial N_p / \partial u_i^{1r} \underset{\sim}{U}_1^r - \partial N_q / \partial u_i^{1r} \underset{\sim}{U}_1^i] \\[2mm] [\omega B_c G_2 - B_j N_q] \; \underset{\sim}{E}_i \; -B_j [\partial N_p / \partial u_i^{1r} \underset{\sim}{U}_1^i + \partial N_q / \partial u_i^{1r} \underset{\sim}{U}_1^r] \end{array} \right. \tag{4-19}$$

$$\frac{\partial r}{\partial u_i^{1i}} = 2 \; \frac{\underset{\sim}{\epsilon}(\underset{\sim}{v})^T}{\underset{\sim}{U}_1^{rT}\underset{\sim}{U}_1^r + \underset{\sim}{U}_1^{iT}\underset{\sim}{U}_1^i} \; \frac{\partial \underset{\sim}{\epsilon}}{\partial u_i^{1i}} - 2 \; \frac{r(\underset{\sim}{v}) \; u_i^{1i}}{\underset{\sim}{U}_1^{rT}\underset{\sim}{U}_1^r + \underset{\sim}{U}_1^{iT}\underset{\sim}{U}_1^i} \; , \tag{4-20}$$

where

$$\partial \underset{\sim}{\epsilon} \; / \; \partial u_i^{1i} = \left| \begin{array}{l} -B_j \partial N_B / \partial u_i^{1i} \underset{\sim}{U}_0 \\[2mm] -[\omega B_c G_2 - B_j N_q] \; \underset{\sim}{E}_i \; -B_j [\partial N_p / \partial u_i^{1i} \underset{\sim}{U}_1^r - \partial N_q / \partial u_i^{1i} \underset{\sim}{U}_1^i] \\[2mm] [\Lambda - \omega^2 I + B_c G_1 - B_j N_p] \; \underset{\sim}{E}_i \; -B_j [\partial N_p / \partial u_i^{1i} \underset{\sim}{U}_1^i + \partial N_q / \partial u_i^{1i} \; \underset{\sim}{U}_1^r] \end{array} \right. \tag{4-21}$$

and finally

$$\frac{\partial r}{\partial \omega} = 2 \; \frac{\underset{\sim}{\epsilon}(\underset{\sim}{v})^T}{\underset{\sim}{U}_1^{rT}\underset{\sim}{U}_1^r + \underset{\sim}{U}_1^{iT}\underset{\sim}{U}_1^i} \; \frac{\partial \underset{\sim}{\epsilon}}{\partial \omega} \tag{4-22}$$

where

$$\partial \underset{\sim}{\epsilon} \, / \, \partial \omega = \begin{vmatrix} \underset{\sim}{0} \\[1em] -2\omega \, \underset{\sim 1}{U^r} \; - \; B_c G_2 \, \underset{\sim 1}{U^i} \\[1em] -2\omega \, \underset{\sim 1}{U^i} \; + \; B_c G_2 \, \underset{\sim 1}{U^r} \end{vmatrix} \qquad (4\text{-}23)$$

Assuming the residual vector has been stored, each element of the gradient can be computed using (4-16) through (4-23), recalling there is no u_1^{1i} variable. Again, the evaluation of the partial derivatives of the matrices N_B, N_p and N_q are the longest operations. Assuming the state of each joint is available from the computation of the function, figure 4-2 shows that still $O(\ 18 \ N_j n)$ operations are required to get only one partial derivative of the function. The cost of computation of the derivatives of the describing functions can be assumed similar to the cost of the computation of the describing function, especially if a model is available. The analytical evaluation of the gradient might therefore be marginally less expensive, but accuracy is much likely to be gained over the numerical evaluation.

In summary, computation of the gradient needs approximately 3n times the number of operations needed to compute the function, whether it is evaluated numerically or analytically. The latter method may be however faster and probably more accurate. And even though the gradient is expensive to get, it is still believed, based on [16] and [21], that gradient and Quasi-Newton methods are still more efficient than

$$A_u' = P_k^I(j)\cos\phi_j, \quad A_{p_u}' = P_k^I(j), \quad A_{q_u}' = 0, \quad B_u' = 0 \qquad \text{if } u = u_j^{1r}$$

$$A_u' = P_k^I(j)\sin\phi_j, \quad A_{p_u}' = 0, \quad A_{q_u}' = P_k^I(j), \quad B_u' = 0 \qquad \text{if } u = u_j^{1i}$$

$$A_u' = 0, \quad A_{p_u}' = 0, \quad A_{q_u}' = 0, \quad B_u' = P_k^I(j) \qquad \text{if } u = u_j^O$$
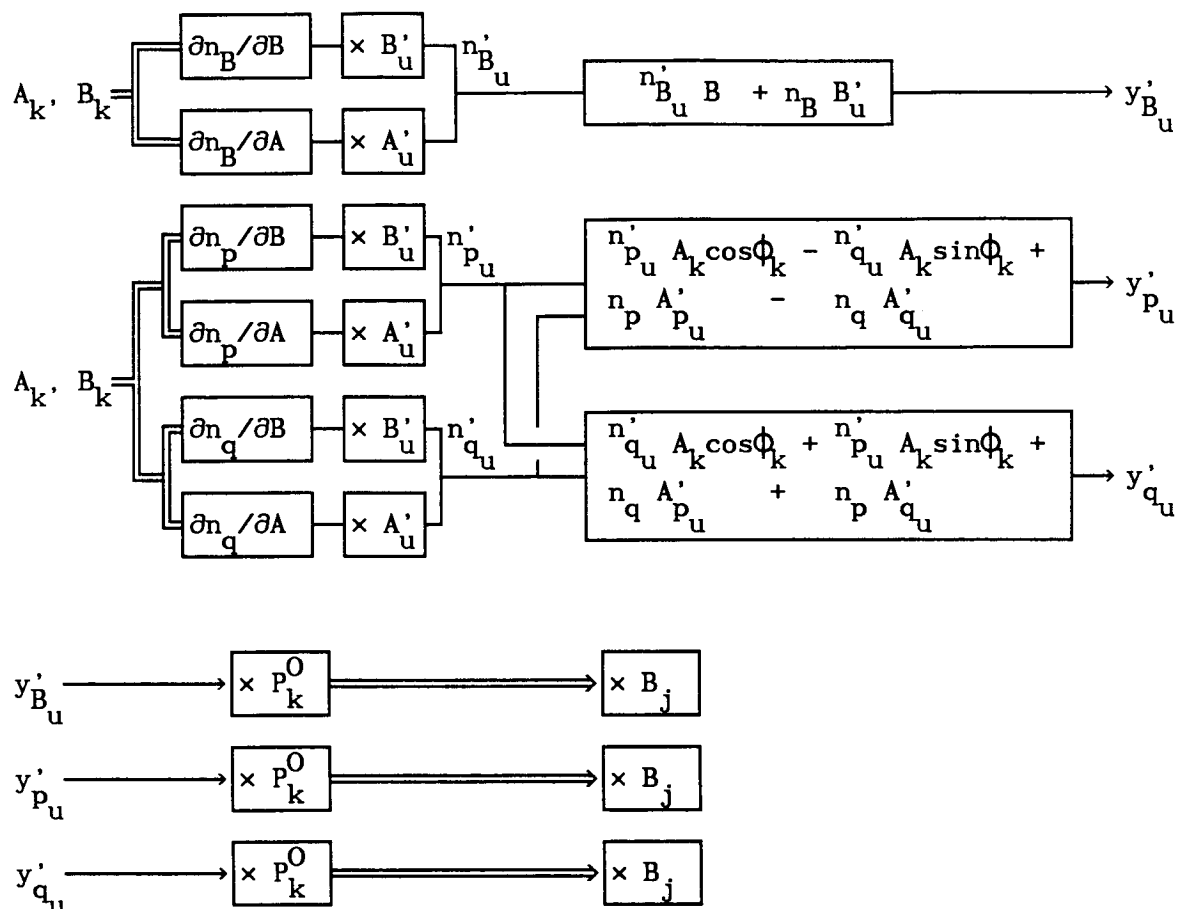
u is the generic variable relatively to which the derivation is performed. We use the following notation: $z_u' = \partial z / \partial u$

Figure 4-2: Steps of the Computation of the Derivative of the

Forcing Term due to One Single Joint relative to One Variable

nongradient methods.

4.3.4 Univariate Minimization Scheme.

The univariate search scheme is important, since multivariate minimization needs rather precise line searches, and since the technique used should provide the required precision in as few steps as possible.

An efficient univariate minimization scheme is used by Dixon in [23], based on a bracketing technique and quadratic fit to improve the bracket. The bracketing technique consists in having the local minimum of a scalar function h(α) enclosed between a lower and an upper bound called L and M to respect Dixon's notation. A third point α_m is the current estimate of the minimum location, and the exact values of the function h(α) are known at those three points. In order to improve the bracket, a parabola is fitted using those points and its minimum estimated at $\alpha^{(E)}$. If the prediction $\alpha^{(E)} = L + E (M - L)$ is such that $0.25 < E < 0.75$, the prediction is accepted, otherwise E is replaced by 0.25 or 0.75 in order to have the length of the bracket decrease by at least one quarter. The exact value of the scalar function h is then computed at $\alpha = \alpha^{(E)}$, and a new bracket is formed using the four points at L, M, α_m and $\alpha^{(E)}$, by enclosing the one giving the smallest value for h between the two nearest points.

The first bracket is obtained by taking a unit step $\alpha^{(1)}$ downhill from the first current point $\alpha = 0$. The exact value of h is computed and a parabola is fitted using the two points and the slope at $\alpha=0$. If a

bracket is not formed, the process is repeated with $\alpha^{(2)} = 5 \times \alpha^{(1)}$ if the absolute value of the estimate of the minimum $\alpha^{(E)}$ is bigger than $\alpha^{(1)}$, or with $\alpha^{(2)} = \alpha^{(E)}$ if it is smaller.

The acceptance criterion stops the process whenever the new predicted value $\alpha^{(E)}$ agrees with α_m within $\epsilon |\alpha_m|$, or the bracket has its size less than $\epsilon |\alpha_m|$, where ϵ is the accuracy parameter.

The univariate scalar function used to execute a line search from the current point $\underset{\sim}{X}_k$ in the direction $\underset{\sim}{p}_k$ is

$$h(\alpha) = f(\underset{\sim}{X}_k + \alpha \, \underset{\sim}{p}_k) \tag{4-24}$$

and its derivative relative to α used to give the downhill direction and to fit the first parabola is

$$\frac{dh}{d\alpha} = \underset{\sim}{g}_k^T \cdot \underset{\sim}{p}_k = g \tag{4-25}$$

where f is a generic scalar multivariate function, $\underset{\sim}{g}_k$ the gradient at point $\underset{\sim}{X}_k$, and $\underset{\sim}{p}_k$ the line search direction.

The accuracy of the line search given in [16] for the different multivariate minimization techniques is given in terms of gradient discrepancy: it states that a step should be accepted if

$$|\underset{\sim}{g}(\underset{\sim}{X}_{k+1})^T \underset{\sim}{p}_k| < \eta |\underset{\sim}{g}(\underset{\sim}{X}_k)^T \underset{\sim}{p}_k| \tag{4-26}$$

η can be as large as 0.9 in the BFGS method, but it has to be at least equal to 0.001 in the conjugate gradient method. The search termination test has to be converted in terms of the precision parameter ϵ, since the computation of the gradient is too expensive. Nevertheless, the value of the parameter η provides a meaningful idea on what accuracy is required in the two methods.

Two factors should make the line search process in the BFGS method faster than in the conjugate gradient method. The first factor is the precision of the local minimum prediction, which has to be high only in the Conjugate Gradient method. The second factor is the a priori knowledge of the location of the minimum, which is contained in the value of the second derivative of the function, and which is only derived in the BFGS method. This latter technique should therefore have much faster line searches.

4.3.5 Update of the Search Direction.

According to formula (4-7) and (4-8), the update of the search direction in the conjugate gradient method only requires $3 \times (3n)$ multiplications, which is very low. On the other hand, the update of the matrix H_k and the computation of the new direction can be estimated as requiring at least $5 \times (3n)^2$ multiplications if intermediate vectors are being used in the update formula (4-12) and if best advantage is taken of the symmetry of the H_k's. It is therefore obvious that if the number of joints is much greater than the number of retained states, the

computational task of updating the matrix H_k is negligible compared to the task of computing the function itself.

4.3.6 Stability Determination.

Recalling section 3.4, the trajectory of the limit cycle is an ellipse, and perturbations in the ellipse plane are the only consistent disturbances to apply in order to check stability. Using (3-45), the principal axes of the ellipse have to be computed. If ϕ_u is

$$\phi_u = \cos^{-1}(\underset{\sim}{U_1^{rT}}\underset{\sim}{U_1^i}/\|\underset{\sim}{U_1^r}\|.\|\underset{\sim}{U_1^i}\|) \qquad (4\text{-}27)$$

or in other words the angle between the vectors $\underset{\sim}{U_1^r}$ and $\underset{\sim}{U_1^i}$, and if the following vectors are defined with

$$\varphi_\iota = 1/2 \ \text{atan} \ \left(\ \frac{2.\|\underset{\sim}{U_1^r}\|.\|\underset{\sim}{U_1^i}\| \ \cos\phi_u}{\|\underset{\sim}{U_1^r}\|^2 - \|\underset{\sim}{U_1^i}\|^2} \ \right) \ + \iota\frac{\pi}{2} \ , \ \iota = 0,1 \quad (4\text{-}28a)$$

$$\underset{\sim}{U_\iota^E} = \underset{\sim}{U_1^r} \cos\varphi_\iota + \underset{\sim}{U_1^i} \sin\varphi_\iota \ , \ \iota = 0,1 \qquad (4\text{-}28b)$$

the equation of the ellipse becomes

$$\underset{\sim}{U} - \underset{\sim}{U_0} = \underset{\sim}{U_1^E} \cos\theta + \underset{\sim}{U_2^E} \sin\theta \qquad (4\text{-}29)$$

where θ is a dummy variable, and where $\underset{\sim}{U_1^E}$ and $\underset{\sim}{U_2^E}$, as defined before, are

orthogonal, thus lying along the principal axes, and with norms equal respectively to the maximum and minimum distance from the ellipse to its center.

In order to check for stability, consistent perturbations have to be found. Recalling (3-52), a matrix M and a vector $\underset{\sim}{P}$ must be computed. M is the Jacobian of the residual vector $\underset{\sim}{\epsilon}(\underset{\sim}{V})$; $\underset{\sim}{P}$ can be expressed as

$$
\underset{\sim}{P} = \left|
\begin{array}{l}
\underset{\sim}{0} \\[2ex]
-2\omega\,\underset{\sim}{U}_1^i - B_c G_2\,\underset{\sim}{U}_1^r \\[2ex]
2\omega\,\underset{\sim}{U}_1^r - B_c G_2\,\underset{\sim}{U}_1^i
\end{array}
\right. \qquad (4\text{-}30)
$$

and is closely related to the last column of the Jacobian, as can be seen from (4-23).

The main task is therefore to compute the Jacobian at the limit cycle conditions, which takes $O(21N_j n)$ operations, and to invert it. The Jacobian is not hollow, thus its inversion should be performed using for example a QR decomposition algorithm.

Once $\partial\underset{\sim}{V} = -M^{-1}\underset{\sim}{P}$ is found, the corresponding initial point of the perturbed trajectory $\underset{\sim}{\mathcal{U}}'$ must be determined in the modal space. Recalling (3-45), which is the equation of the limit cycle trajectory, and using the notation as in (3-46) for the perturbed point in state space, $\underset{\sim}{\mathcal{U}}'$ is:

$$
\underset{\sim}{\mathcal{U}}' = \underset{\sim}{\mathcal{U}}_0^{lc} + \delta\underset{\sim}{\mathcal{U}}_0 + \mathrm{Re}(\,\underset{\sim}{\mathcal{U}}_1^{lc} + \delta\underset{\sim}{\mathcal{U}}_1\,) \qquad (4\text{-}31)
$$

This represents some projections and some other $O(n)$ operations.

The final step involves comparing the perturbed point to the ellipse, which is done by comparing the expression

$$\rho = \left[\frac{\underset{\sim}{q}'^T \underset{\sim}{U}_1^E}{\| \underset{\sim}{U}_1^E \|^2} \right]^2 + \left[\frac{(\underset{\sim}{q}'^T \underset{\sim}{U}_2^E)}{\| \underset{\sim}{U}_2^E \|^2} \right]^2 - 1 \qquad (4\text{-}32)$$

to 0. Hence, once the consistency condition has been found, the remaining operations cost only an $O(n)$ and they are not therefore the principal source of computation.

In summary, the stability determination consists mostly in inverting a large $3n \times 3n$ matrix, and this is a computationally very important calculation since the matrix is not hollow.

4.4 The Singular Value Test.

We are concerned in this last section about finding a more global type of test which could yield some information on the size of the different limit cycle parameters, in order to determine some region where they should lie, and to be able to pick initial guesses to start the limit cycle determination process.

The system (3-37), or any of its alternate expressions, states that two complex matrices M_0 and M_1 are singular, where

$$M_0 = I - G(0) \mathcal{N}_B(\underset{\sim}{V}) \qquad (4\text{-}33)$$

$$M_1 = I - G(j\omega) \mathcal{N}_A(\underset{\sim}{V}) \qquad (4\text{-}34)$$

The system also states some properties for the eigenvectors of M_0 and M_1 associated with the zero eigenvalue, more specifically that they must be respectively $\underset{\sim}{u}_0$ and $\underset{\sim}{u}_1$. A very conservative test, however, is to check only for the possible singularity of the matrices without any regard to the eigenvectors' directions.

In order to perform the test, we use a general property of matrices of the form

$$M = I - H N \qquad (4-35)$$

where M, N and H are here only generic matrices.

The property is the following ([8]):

The matrix M is not singular if the matrices H and N satisfy

$$S_{max}(H) < \frac{1}{S_{max}(N)} \qquad (4-36)$$

where $S_{max}(P)$ represents the maximum singular value of a matrix P.

If the test is applied to the matrices M_0 and M_1, which depend on the limit cycle parameters, it is theoretically possible to determine values of $\underset{\sim}{V}$ and ω where the test stands and where it is violated.

If the test is true for all values of the parameters, then no limit cycle can occur. However, the test is very conservative and it is very likely that it will not stand if any performance has been sought in the design of the controller. On the other hand, the test can provide a

region in the variables space where a singularity can occur, and thus where limit cycles can occur. Hence, it provides bounds for the variables, and it may help choose an initial point to start the iteration in the limit cycle search process.

CHAPTER FIVE

EXAMPLE OF ANALYTICAL DETERMINATION
OF LIMIT CYCLES AND THEIR STABILITY

5.1 Scope and Means of the Section.

Examples of analytical determination of limit cycles are derived in this section for simple dynamical systems. They are constituted of a series of one or two masses connected by nonlinear springs, and they are under active dynamical control through full state feedback.

The number of nonlinearities is much smaller in these examples than what occurs in the case of large truss structures. However, very complex examples are likely to complicate the understanding of the problems arising in the implementation of the analytical search methods. Furthermore, the chore associated with their derivation would be considerable since no actual controlled truss model is yet available, and extended computer capabilities would be necessary. Hence, the study is limited to simple problems, but this only forbids the addressing and the analyzing of the size issue, and still provides valuable results on the performances of the analytical methods.

The simplicity of the examples limited the need for computing power, and an IBM PC/AT personal computer was used to implement the search algorithms. The software package MATLAB, [26], was extensively

used for its capability to handle vectors and matrices and its ability to manipulate real as well as complex numbers. The complex formulation of the limit cycle conditions, as expressed in (3-37), was therefore conveniently used. The software was also utilized for simulation. It provided graphic outputs, and the plots and tables of results relative to the examples derived can be found at the end of this section.

5.2 Presentation of Tested Systems.

5.2.1 General Architecture.

Two systems were used, one with only one SISO nonlinear joint, the other one with two joints. Their general architecture is similar: they are constituted of masses assembled in series by the nonlinear joints and clamped to a fixed wall.
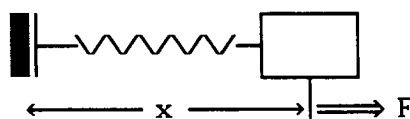
Figure 5-1a: Single Joint System.
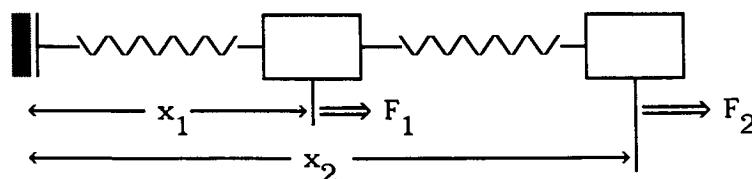
Figure 5-1b: Two Joint System.

The masses were taken unitary. It was supposed that full state was available, and that each mass could be independently driven by an actuator. Those last hypotheses gave complete freedom in the design of the linear feedback controllers and thus allowed controllers that induced limit cycles. The joints are represented as springs in figure 5-1, but they are nonlinear types of spring, and they were chosen to be identical in case 2.

5.2.2 Idealized Joints' Characteristics.

A simple idealized model of a joint that fits in the hypotheses made in Chapter 3 was chosen. Each joint is constituted of a linear spring of unitary stiffness attached to a simple Coulomb friction element with threshold F_c. The displacement of the Coulomb element is limited to a bound S. The joints were supposed massless.

Figure 5-2: Model of Nonlinear Joint.

This type of joint can be modeled with two states, one giving the total deformation, x, and one giving the sliding of the friction element, s. The load, F, required at one end to produce the displacement

is the following

$$F = K (x - s) , \qquad K = 1 \qquad\qquad (5-1)$$

and the dynamics of the joint is

$$\left|\begin{array}{l} \dot{s} = \dot{x} \quad , \; \text{if} \; | \, s \, | < S, \; | \, F \, | = F_c \; \text{and} \; \text{sgn}(\dot{x}) = \text{sgn}(\, F). \\[2ex] \dot{s} = 0 \end{array}\right. \qquad (5-2)$$
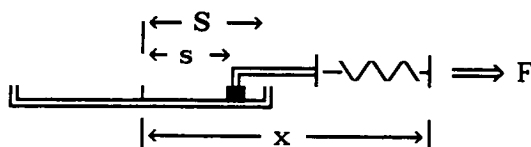
Such a model of a joint is a very simplified version of what are believed to be the true elements, and it more particularly displays the two properties we assumed in Chapter 3, which are, that it is "asymptotically linear", and that it has a hysteresis whose size does not depend on the frequency of the excitation.

Starting from $x = 0$ and $s = 0$, the joint is truly linear and s stays constant as long as F does not cross the threshold F_c. This corresponds to the linear behavior in figure 5-3a. If s is not initially zero, and if the load does not cross the threshold, the joint will still behave linearly, but around an other operating point: because of the Coulomb element, there is a loss of static accuracy.

When the load crosses the threshold, the Coulomb element "gives way" and starts to slide. The sliding will not stop until the maximum play is reached, and the spring will then be streched again. When the load is released, the spring will start to shrink back and may be compressed, but the Coulomb element will not slide back toward $s = 0$ until the compression force reaches $-F_c$: hence the load-displacement curve displays a hysteresis, as shown in figure 5-3b.
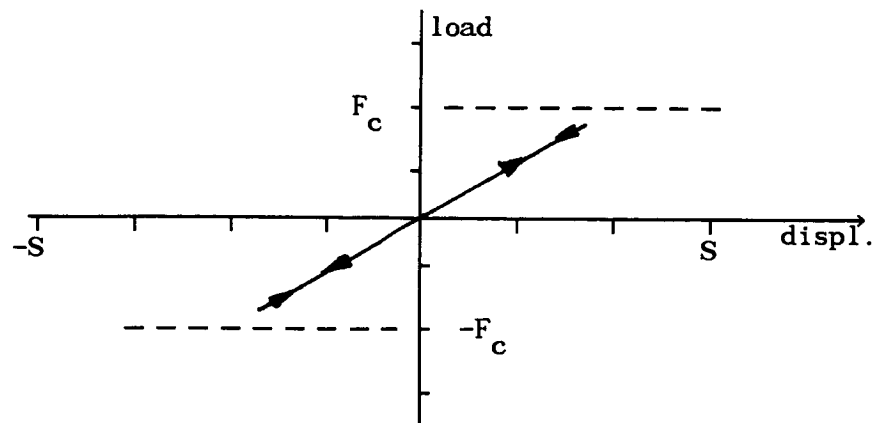
Figure 5-3a: **Restoring Force for Small Displacements**
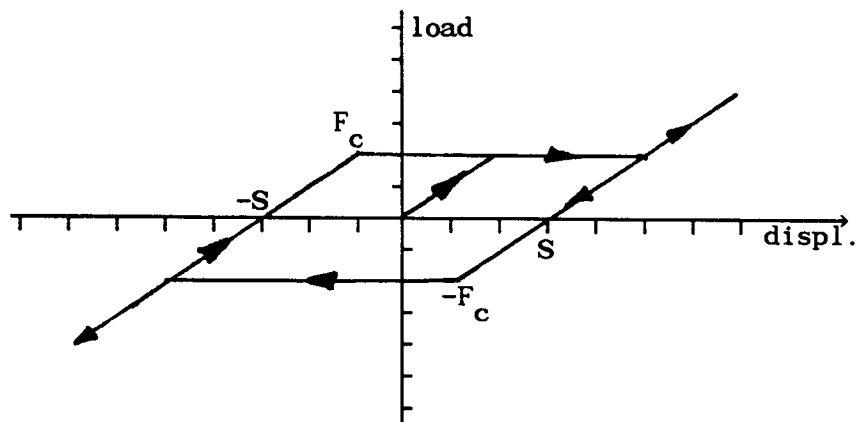
figure 5-3b: **Hysteretic Behavior for Large Displacements**

C - 2

5.2.3 Describing Function for Idealized Joints.

The use of integrators in the control design prevents, in all cases, any non zero steady state errors when a static disturbance is applied. This implies that the gain n_B need not be calculated, and that the gain n_A only needs to be evaluated for B = 0, since, as it will be shown later, the controller forces the biases to zero. In other words, Sinusoidal Input Describing Functions can be used here, rather than Dual Input Decribing Functions.

A closed-form expression can be found for the describing functions of the remaining nonlinear part of the joints. If F^{NL} is defined as:

$$F^{NL} = F^{load} - K\,x, \tag{5-3}$$

where F^{load} is the total load as in (5-1), and F = K x is the linear spring model taken to replace it, then we have the following expressions for n_A:

$$n_A(\,A,\,0) = n_p(\,A,\,0) + j\,n_q(\,A,\,0)$$

$$\left[\begin{array}{l} n_p(\,A,\,0) = 0 \\[2mm] n_q(\,A,\,0) = 0 \end{array}\right. \qquad \text{if } A < F_c \tag{5-4a}$$

$$\left[\begin{array}{l} n_p(\,A,\,0) = \dfrac{1}{2}\left[\,-1 + f\left(\dfrac{2Fc - A}{A}\right)\,\right] \\[4mm] n_q(\,A,\,0) = \dfrac{A^2 - (\,2Fc - A)^2}{\Pi\,A^2} \end{array}\right. \qquad \text{if } F_c < A < F_c + S \tag{5-4b}$$

$$\begin{bmatrix} n_p(A, 0) = \frac{1}{2} \left[f\left[\frac{Fc - S}{A} \right] - f\left[\frac{Fc + S}{A} \right] \right] \\[2em] n_q(A, 0) = \frac{4 \, Fc \, S}{\Pi \, A^2} \end{bmatrix} \quad \text{if } A > F_c + S \quad (5\text{-}4c)$$

where the function f is given by:

$$f(z) \begin{bmatrix} = -1, \ z < -1 \\[1em] = \frac{2}{\Pi} \left[\sin^{-1}z + \sqrt{1 - z^2} \right], \ -1 < z < 1 \\[1em] = +1, \ z > 1 \end{bmatrix} \quad (5\text{-}5)$$

5.2.4 Closed-loop Linear Models.

The linear model for the joints is obviously a simple linear spring of unitary stiffness, $F = K \, x$, where F is specified in figure 5-2.

The controllers implemented are multivariable PID feedback control systems. The integrators were found necessary for two reasons: first, they keep the system from settling down in a steady state that shows constant biases, which otherwise occured due to the loss of static accuracy implied by the Coulomb friction. Second, they provide the necessary phase lag to lead the systems to limit cycle.

It must be noticed that the examples differ somehow from the large systems presented in the previous chapters, since the number of states is superior to the number of nonlinearities in these examples. Nevertheless, this only requires minor changes in the implementation of the method, as it will be shown later, and it does not change the way the problem is approached.

The state variables taken are the displacement x_i, the rate of displacement $\dot{x}_i$ and the integral of the displacement $\int x_i dt$ of each mass. Once chosen, the feedback systems yielded respectively the following dynamics for the closed-loop systems:

System 1:

$$\dot{\underset{\sim}{X}} = A_1 \underset{\sim}{X} - B_{c_1} K_1 \underset{\sim}{X} + B_{j_1} F^{NL} \qquad (5\text{-}6)$$

where:

$$A_1 = \begin{bmatrix} 0 & 1 & 0 \\ 0 & 0 & 1 \\ 0 & -1 & 0 \end{bmatrix}$$

$$B_{c_1} = [\ 0 \quad 0 \quad 1\ ]^T \ ; \ B_{j_1} = -B_{c_1}$$

$$K_1 = [\ -0.5 \quad 0 \quad -1\ ]\ ,$$

and where

$$F^{NL} = F^{load} - K x$$

where F^{load} is the total force to be applied at one end of the joint to produce a displacement x.

The displacement of the joint d is:

$$d = C_1 \underset{\sim}{X} \qquad (5\text{-}7)$$

where:

$$C_1 = [\ 0 \quad 1 \quad 0\ ]\ .$$

The poles of the closed-loop linear system are the following:

$$\lambda_{1/2} = -0.1761 \pm j\ 0.8607$$

$$\lambda_3 = -0.6478$$

The damping ratio of the oscillatory mode is only 0.2.

System 2:

$$\dot{\underset{\sim}{X}} = A_2 \underset{\sim}{X} - B_{c_2} K_2 \underset{\sim}{X} + B_{j_2} \begin{bmatrix} F_1^{NL} \\ F_2^{NL} \end{bmatrix} \tag{5-8}$$

where:

$$A_2 = \begin{bmatrix} 0 & 1 & 0 & 0 & 0 & 0 \\ 0 & 0 & 1 & 0 & 0 & 0 \\ 0 & -2 & 0 & 0 & 1 & 0 \\ 0 & 0 & 0 & 0 & 1 & 0 \\ 0 & 0 & 0 & 0 & 0 & 1 \\ 0 & 1 & 0 & 0 & -1 & 0 \end{bmatrix}$$

$$B_{c_2} = \begin{bmatrix} 0 & 0 & 1 & 0 & 0 & 0 \\ 0 & 0 & 0 & 0 & 0 & 1 \end{bmatrix}^T \; ; \; B_{j_2} = \begin{bmatrix} 0 & 0 & -1 & 0 & 0 & 0 \\ 0 & 0 & 1 & 0 & 0 & -1 \end{bmatrix}^T$$

$$K_2 = \begin{bmatrix} 6.3156 & 4.4587 & 4.7650 & 5.4444 & 6.8613 & 1.1250 \\ 5.3056 & 6.8062 & 0.5750 & 6.4544 & 5.5138 & 5.2250 \end{bmatrix}$$

The F_i^{NL}'s are the remaining nonlinear parts of each joint.

The displacement of the joints, called d_i's, are:

$$\begin{vmatrix} d_1 \\ d_2 \end{vmatrix} = C_2 \underset{\sim}{X} \tag{5-9}$$

where:

$$C_2 = \begin{bmatrix} 0 & 1 & 0 & 0 & 0 & 0 \\ 0 & -1 & 0 & 0 & 1 & 0 \end{bmatrix}$$

The poles of the closed-loop linear system are:

$$\lambda_{1/2} = -0.05 \pm j\, 0.5$$

$$\lambda_{3/4} = -1.4 \pm j\, 1.4$$

$$\lambda_5 = -3.0$$

$$\lambda_6 = -4.0$$

The damping ratio of the first oscillatory mode is only 0.1. The damping ratio of the second mode is 0.707, and therefore, only one closed-loop resonant mode really appears.

The eigenvectors associated with the first oscillatory mode are:

$$\underset{\sim 1}{V} = [1.0000 \quad -0.0500 \quad -0.2475 \quad -1.0000 \quad 0.0500 \quad 0.2475]^T \quad (5\text{-}10\text{a})$$

$$\underset{\sim 2}{V} = [0.0000 \quad 0.5000 \quad -0.0500 \quad 0.0000 \quad -0.5000 \quad 0.0500]^T \quad (5\text{-}10\text{b})$$

The controller was designed using eigenstructure assignment techniques, ([8]), in order to have a resonant mode where $x_1 = -x_2$ when the system is oscillating along this mode, as one can check on $\underset{\sim 1}{V}$ and $\underset{\sim 2}{V}$.

The linear transfer functions can be readily derived from the state representations of the closed-loop systems. The transfer functions to be used go from each forcing term F^{NL}_k to each joint's displacement d_i. In case 1, the transfer function G_1 is defined as:

$$G_1 = \frac{d}{F^{NL}} = C_1(pI - A_1 + B_{c_1}K_1)^{-1} B_{j_1} \quad (5\text{-}11)$$

In case 2, the matrix transfer function G_2 is defined as:

$$G_2 = \begin{bmatrix} d_1/ F^{NL}_1 & d_1/ F^{NL}_2 \\ d_2/ F^{NL}_1 & d_2/ F^{NL}_2 \end{bmatrix} = C_2(pI - A_2 + B_{c_2}K_2)^{-1} B_{j_2} \quad (5\text{-}12)$$

5.3 Residual Functions.

The set of equations (3-37) can be rebuilt for those simple examples by writing the following generic relations that stand for both cases, when the indices i, k and l are specified:

Displacement and forcing terms:

$$d_i = B_i + A_i \exp^{j\omega t}$$

$$F_k^{NL} = F_k^0 + F_k^1 \exp^{j\omega t} \tag{5-13}$$

Relationship between forcing terms and displacement:

$$F_k^{NL} = n_B B_k + n_A(A_k, B_k) A_k \exp^{j\omega t}$$

$$d_i = \sum_k G_{1_{ik}}(0) F_k^0 + \sum_k G_{1_{ik}}(\omega) F_k^1 \quad , \tag{5-14}$$

Equating the different harmonics, the sytem of equations becomes in the single joint case:

$$\left[\begin{array}{l} [\ 1 - n_B G_1(\ 0)\ ]\ B = 0 \\ \\ [\ 1 - n_A(\ A,B) G_1(j\omega)]\ A = 0 \end{array} \right. \tag{5-15}$$

and in the two joint case:

$$
\begin{bmatrix}
\left[\begin{bmatrix} 1 & 0 \\ 0 & 1 \end{bmatrix} - G_2(0) \times \begin{bmatrix} n_B & 0 \\ 0 & n_B \end{bmatrix}\right] \begin{vmatrix} B_1 \\ B_2 \end{vmatrix} = \underset{\sim}{0} \\[2em]
\left[\begin{bmatrix} 1 & 0 \\ 0 & 1 \end{bmatrix} - G_2(j\omega) \times \begin{bmatrix} n_A(A_1,B_1) & 0 \\ 0 & n_A(A_2,B_2) \end{bmatrix}\right] \begin{vmatrix} A_1 \\ A_2 \end{vmatrix} e^{j\phi} = \underset{\sim}{0}
\end{bmatrix}
\tag{5-16}
$$

In both applications, the bias terms B, B_1 and B_2 are zero, since both $G_1(0) = 0$ and $G_2(0) = \begin{bmatrix} 0 & 0 \\ 0 & 0 \end{bmatrix}$. The problems therefore decouple, and the residual function becomes, in the single joint case

$$
R(A,\omega) = \left| 1 - n_A(A)G_1(j\omega) \right|
\tag{5-17}
$$

and in the two joint case

$$
R(A_1, A_2, \phi, \omega) = \frac{\left\| \begin{bmatrix} -G_{2_{11}}(\omega)n_A(A_1)+1 & -G_{2_{12}}(w)n_A(A_2) \\ -G_{2_{21}}(\omega)n_A(A_1) & -G_{2_{22}}(\omega)n_A(A_2)+1 \end{bmatrix} \begin{vmatrix} A_1 \\ A_2 e^{j\phi} \end{vmatrix} \right\|^2}{A_1^2 + A_2^2}
\tag{5-18}
$$

5.4 Limit Cycle Regions.

It is simple here to find the maximum singular value of the matrix $\mathcal{N}_A$, where $\mathcal{N}_A$ is defined as in section 3.2, since the matrix is diagonal, equal to $\mathrm{diag}(n_A(A_i))$ for both examples. Therefore, $S_{max}(\mathcal{N}_A)$

is bounded by $M_A = \max\limits_{A} (\; n_A(A))$. Figure 5-4 represents the values of $1/n_A$ for the values of parameters $F_c = 0.1$ and $S = 0.5$. Figures 5-5 and 5-6 show respectively the maximum singular value of the respective transfer function of case 1 and 2. Regions where limit cycles might occur can therefore be determined in both examples, and the limit cycles parameters will verify

<u>System 1:</u>

$$0.5143 \text{ rad/s} < \omega < 1.2397 \text{ rad/s}$$

$$0.1556 < A < 1.7333 \tag{5-19}$$

<u>System 2:</u>

$$0.3082 \text{ rad/s} < \omega < 0.8577 \text{ rad/s}$$

$$0.0889 < A_1 < 3.3778 \text{ or } 0.0889 < A_2 < 3.3778 \tag{5-20}$$

It must be noticed, however, that the mathematics only requires one of the variables A_1 or A_2 to be within the indicated range, and not both of them simultaneously. The information is, however, still valuable, particularly for the frequency.

Furthermore, the nonlinearities are only perturbation terms, and it can be seen that the limit cycle areas are defined by values of the frequency for which the input forcing terms are amplified, or in other words, where the linear system displays a resonant peak.
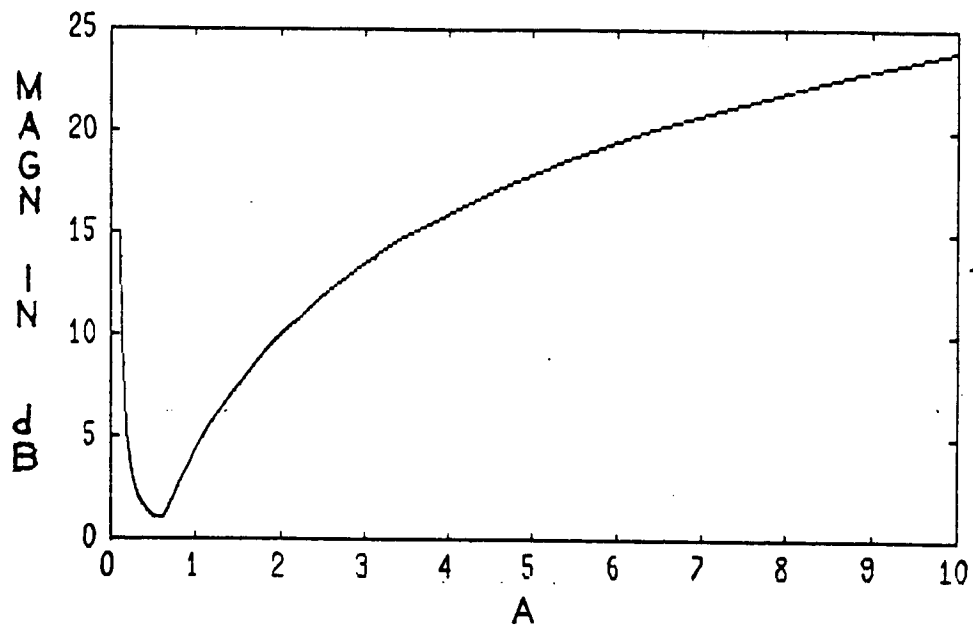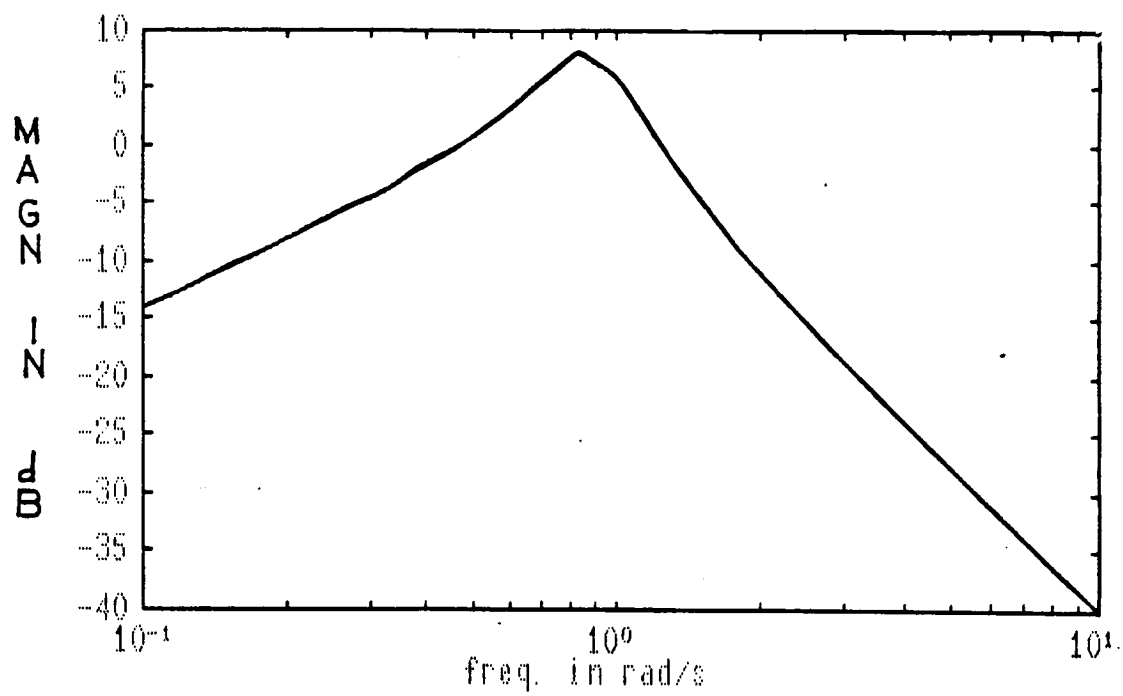
Figure 5-4: $1/n_A(A, 0)$
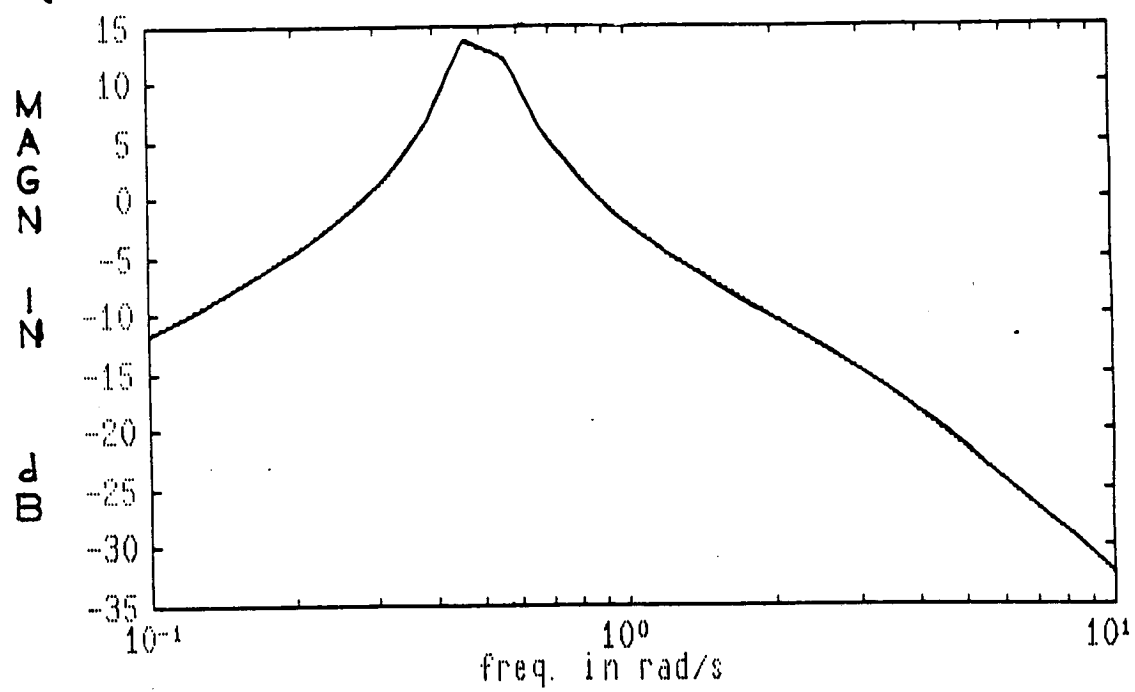
Figure 5-5: $G_1(j\omega)$ Magnitude

Figure 5-6: $G_2(j\omega)$ Maximum Singular Value

5.5 Shape of the Residual Function.

In order to get some insight, the log of the residual function in case 1 was plotted on figure 5-7 on a 3 dimensional mesh representation. The scale on the frequency is logarithmic.

Particular features of the residual function include two plateaux, one occuring when $A \to \infty$ or $\omega \to \infty$, the second one when $A \to 0$ or $\omega \to 0$. The value of the residual on the plateaux tends toward 1. In fact, in both cases, either n_A or $G_1(\omega)$ goes to 0, and the value of the limit can be directly checked from the equations.

The importance of the linear system's resonant mode is again underlined. A valley appears for ω below the resonant peak frequency, at $\omega_r = 0.8785$ rad/s, and there is a ridge around $\omega = \omega_r$. The ridge seems to keep any search starting with ω greater than ω_r from being successful, and such an attempt will end up in the plateau region.

It appears, therefore, from the general shape of the residual function, that the initial conditions should be around the lower bounds given by the Singular Value Test, in order to reach the valley region during the search process and not to be trapped in the plateau area where the search can drift toward points located at infinity. Caution should also be taken during the search process so that a step does not lead to frequencies well above the resonant frequency.
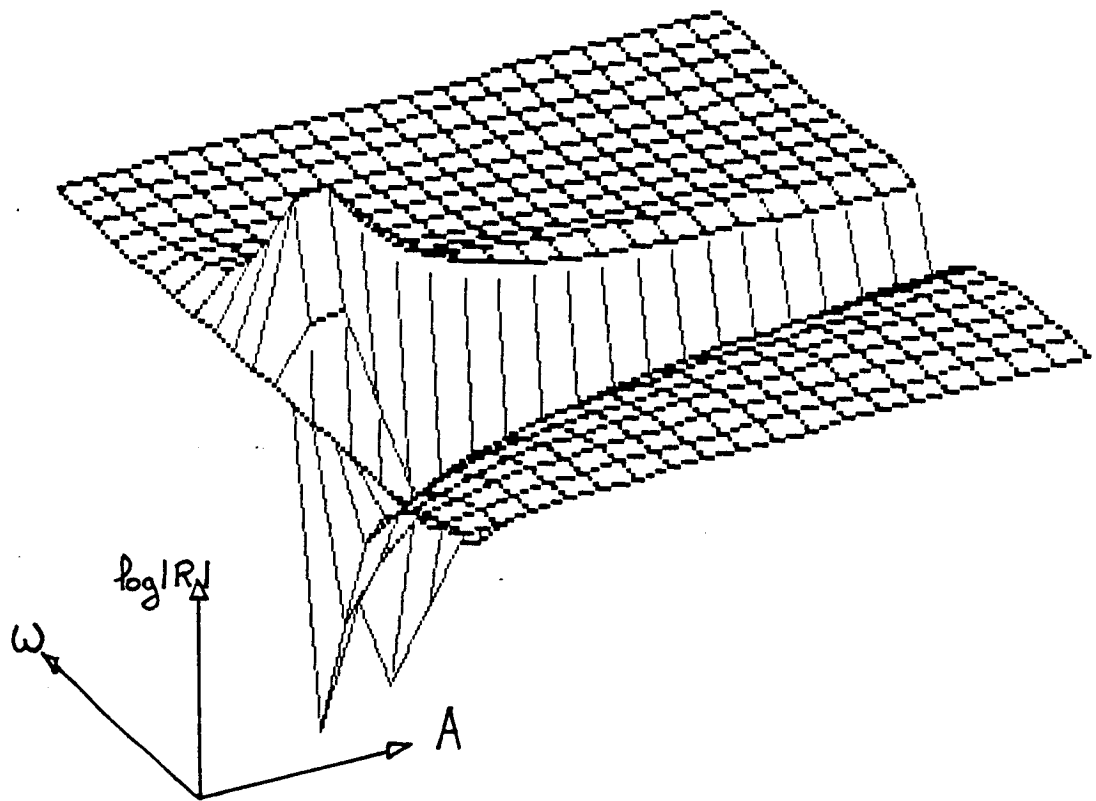
Figure 5-7: Three Dimensional Plot of Single Mass Case's

Residual Function

5.6 Evaluation of the Limit Cycle Prediction Method Based on The BFGS Algorithm.

5.6.1 General.

Two limit cycles were found in the first system, using the BFGS based limit cycle prediction method. The first one was located at:

$$A = 0.2739 \ , \ \omega = 0.5748 \ rad/s$$

and the second one at:

$$A = 1.1510 \ , \ \omega = 0.6835 \ rad/s.$$

Simulations were performed to confirm the existence of such limit cycles, but only one was found, corresponding to the second set of conditions. The results of the simulations are shown in figure 5-8 through 5-10 . As it can be checked there, the characteristics of the limit cycle found by simulation were accurately predicted by the analytical method: the measured frequency is at $\omega \simeq 0.68$ rad/s, and the measured amplitude is $A \simeq 1.14$.

Two limit cycles were also found in the second system, corresponding to the following conditions:

$$A_1 = 0.0698 \ , \ A_2 = 0.1391 \ , \ \phi = 3.1410 \ rad \ , \ \omega = 0.4375 \ rad/s,$$

for the first limit cycle, and,

$$A_1 = 2.3441 \ , \ A_2 = 4.6675 \ , \ \phi = 3.1351 \ rad \ , \ \omega = 0.4950 \ rad/s$$

for the second one.

Simulations shown in figures 5-11 through 5-13 confirmed the existence of the second limit cycle. It can be seen in the phase plane representation of figures 5-11 and 5-12 that the expected elliptic form of the trajectory suffers some distortion that shrinks it in its middle. However, only the first harmonic is really present in the displacement of the masses, as it can be checked in figure 5-13. The parameters of the limit cycle measured from the simulation results correspond to

$$A_1 \simeq 2.30 \; , \; A_2 \simeq 4.63 \; , \; \phi \simeq 3.11 \; , \; \omega \simeq 0.49 \; rad/s$$

and are therefore very close to their predicted values.

Interestingly, the limit cycles are closely related to the resonant mode of the linear part the systems. The frequencies of the limit cycles are only slightly smaller than $\omega_r = 0.8785$ rad/s in the first case, and again slightly below $\omega_r = 0.5025$ rad/s in the second case.

Also, calculating the displacements of the masses from the characteristics of the joints' deformations in the two joint system case, one can find that, for the first limit cycle:

$$x_1 = 0.0698 \cos(0.4375t)$$
$$x_2 = -0.0693 \cos(0.4375t) + 0.0001 \sin(0.4375t)$$

(5-21)

and for the second limit cycle:

$$x_1 = 2.3441 \cos(0.4950t)$$
$$x_2 = -2.3233 \cos(0.4950t) + 0.0303 \sin(0.4950t)$$

(5-22)

Hence, it is very interesting to note that, in both cases, x_1 is almost equal to $-x_2$, and therefore, that the oscillations strongly resemble the oscillations of the resonant mode of the second system,

where x_1 always equals $-x_2$, as one can find from the expressions (5-10a) and (5-10b).

5.6.2 Effects of the Line Search Accuracy.

5.6.2.1 Tests Performed.

Searches were undertaken, for both systems, with various values of the line search accuracy parameter ϵ in order to verify that the BFGS method suffered rough univariate minimizations.

With the single joint system, all searches were started at

$$A = 0.11 \ , \ \omega = 0.25 \ \text{rad/s}, \tag{5-23}$$

and ϵ was set successively to 10^{-1}, 10^{-3}, 10^{-5} and 10^{-7}. The convergence criterion compared the value of the gradient at each iteration to 10^{-10}, and terminated the search as soon at it was below the threshold. The number of iterations, as well as the number of function evaluations, the converged point and the residual are recorded in table 5.1, and figure 5-14 shows the residual values during the different searches.

With the two joint system, three sets of initial conditions were taken. The first two sets corresponded to starting points far from a zero of the residual function. The first set was located at

$$A_1 = 0.11 \ ; \ A_2 = 0.11 \ ; \ \phi = \Pi \ ; \ \omega = 0.3 \ \text{rad/s}. \tag{5-24}$$

and the second at:

$$A_1 = 0.11 \ ; \ A_2 = 0.11 \ ; \ \phi = \Pi/2; \ \omega = 0.3 \ \text{rad/s}. \tag{5-25}$$

ϵ was set to 0.5, 0.1 and 10^{-3}. The features of the searches are gathered in tables 5.2 and 5.3. The residual values during the searches with the first set of initial conditions are displayed in figure 5-15. Figure 5-16 shows the values taken by the amplitude parameters for the different searches, and figure 5-17 shows the frequencies. The residual values during the searches, started with the second set of initial conditions, are plotted in figure 5-18.

The last set of initial conditions was:

$$A_1 = 0.6 \ , \ A_2 = 0.14 \ , \ \varphi = \Pi \ , \ \omega = 0.4 \ rad/s \tag{5-26}$$

and searches were made with ϵ equal successively to 0.5, 10^{-1}, 10^{-2}, down to 10^{-5}. The results were gathered in table 5.4, and the residual values were plotted in figure 5-19.

The convergence criterion in the two joint case was unchanged.

5.6.2.2 Discussion.

The increase of the line search accuracy appears to have little, or unfavorable effect on the number of iterations. It can be seen from the results of the single joint model that the accuracy fixes the sequence of points in the search process: the first trial converges to a different limit cycle than the three last trials (table 5.1). On the other hand, figure 5-14 shows that the sequences of points become similar after ϵ has been chosen small enough.

Results obtained on the second system show that a rough line search with $\epsilon = 0.5$ is always more successful when the search is started far

from a minimum (tables 5.2 and 5.3), and this same value of ϵ only implies one more iteration when the search is started close to a limit cycle (table 5.4). Also, figures 5-16 and 5-17 indicate that the sequences of points generated by the various line search accuracies are different. However, figure 5-19 indicates that all the sequences of points converge toward a similar bound as ϵ tends to 0. Hence, it can be concluded that the BFGS method might be more successful when the sequence of points generated in the search process is not close to the sequence of exact local minima which should theoretically be used: this conclusion meets what is reported in the literature.

The value of ϵ for which the method is the most efficient appears to depend on the problem, and is for example 10^{-3} in the first case, and 0.5 in the second case.

5.6.3 Influence of the Initial Conditions.

Some assessments were already made about the values of the initial parameters: the singular value test provided some limits for the amplitudes and the frequency, and the shape of the residual function indicated that the search should be started with parameters equal to their lower bounds.

It was also noted that the characteristics of a limit cycle were close to the characteristics of the first resonant mode. This can help fix the initial phases, as well as the relative amplitudes of the modal variables.

Information about the relative amplitudes appeared not to be really relevant, since searches can start far away from a minimum, and the values of the amplitudes can be considerably modified. Some trials, where the inverse of the limit cycle relative amplitude was taken initially, where $A_1 = 0.2$ and $A_2 = 0.1$, were even found to converge faster than others, started with the right relative amplitude values, where $A_1 = 0.1$ and $A_2 = 0.2$.

On the other hand, phase initial conditions appeared to strongly affect the length of the search. Various trials were made, to assess the influence of the initial phase conditions. The searches were started successively with $\phi = -\pi/2$, 0 , $\pi/2$ and π, and the remaining variables were kept to

$$A_1 = 0.11 \ ; \ A_2 = 0.11 \ ; \ \omega = 0.3 \text{ rad/s}. \tag{5-27}$$

The line search accuracy was set to 0.5, and the convergence threshold to 10^{-10}. Results of the searches can be found in table 5.5, and the residual values were plotted in figure 5-20.

It appears clearly from the results that the fastest search occurs for $\phi = \pi$, that is, for the initial phase condition corresponding to the phase between the oscillations of the masses in the resonant mode. For $\phi = \pi/2$, the search even converges toward the second limit cycle, which, in term of magnitude of the defining paramaters, seems to be more distant from the chosen initial conditions than the first limit cycle (table 5.5). For the other phase initial conditions, the relative increase in the number of iterations compared to the one required when

$\varphi = \Pi$, is 33%. Hence, the phase information provided by the study of the eigenvectors of the resonant mode appears extremely valuable, and should enable the search to converge in a minimum amount of steps.

5.7   Evaluation of the Limit Cycle Prediction Method Based on the Conjugate Gradient Algorithm.

5.7.1   General.

The evaluation of the limit cycle prediction method, using the conjugate gradient algorithm, was conducted in the same manner as in the previous section. The exact same limit cycles were found for both systems. The influence of the line search accuracy, as well as the importance of the choice of the initial phase conditions were studied, as in the previous case.

5.7.2   Effects of the Line Search Accuracy.

5.7.2.1   Tests Performed.

The same evaluations as in section 5.6.2.1. were conducted on the first system with the conjugate gradient based search method. Results were gathered in table 5.6, and the residual values during the searches plotted in figure 5-21.

With the second system, only the set of initial conditions (5-27) was used to evaluate the performance of the method when started far from

a minimum. The line search accuracy parameter ϵ was set to 0.5, 0.1 and 10^{-4}. Table 5.7 and figure 5-22 show the interesting features of those trials.

For the evaluation of the convergence properties of the search when started close to a minimum, the set of initial conditions used was:

$$A_1 = 0.065 \; ; \; A_2 = 0.140 \; ; \; \phi = \pi \; ; \; \omega = 0.45 \text{ rad/s.}$$

ϵ was decreased from 10^{-1} to 10^{-5}. The results are shown in table 5.8, and the residual values generated during the searches plotted in figure 5-23.

Throughout the trials, the number of iterations was limited to 50.

5.7.2.2 Discussion.

The different tests proved that the line search accuracy is a crucial factor in the success of the search processes based on the conjugate gradient method, and that, in order to be efficient, any of these algorithms should produce a sequence of points as close as possible to the sequence of exact local minima generated by the univariate minimizations along the line search directions. Even for this case with as few as four variables, the search began to be admissibly successful for ϵ less than 10^{-4}, as one can check in table 5.7 . Figure 5-22 accentuates the failure of search processes using a rough line search.

Another interesting result is indicated in table 5.8, and is confirmed by the plots of figure 5-23: there appears to be a threshold

for the accuracy parameter ϵ. For ϵ above 10^{-4}, the search fails to converge, or is very slow. For ϵ below 10^{-4}, however, the sequences of points generated by the algorithm are close to the exact sequence of local minima, and the total number of iterations does not noticeably change. Decreasing ϵ below 10^{-4} therefore implies only more function evaluations. The threshold is the same for the two different systems studied, but it cannot be concluded at this point, that it would not change when other systems are considered.

5.7.3 Influence of the Initial Conditions.

The influence of the initial phase conditions was investigated as in section 5.6.3. The initial phase was set successively to $-\Pi/2$, 0, $\Pi/2$ and Π and the remaining variables were as in (5-27). ϵ was taken to be 10^{-4}. The convergence test was relaxed, and a search was terminated whenever one of these two events occured first, the gradient became less than 10^{-8}, or 50 iterations were completed. Table 5.9 summarizes the features of the searches, and figure 5-24 shows the values of the residuals during the different attempts.

$\phi = \Pi$ does not lead, here, to the fastest search. Interestingly, when $\Pi = 0$, the search converges toward the second limit cycle in the smallest number of iterations. In that case, the initial phase is not close to the value of the phase corresponding to the limit cycle. However, to ensure continuity, we allowed a point to have different formulations in polar coordinates. Hence, as seen in table 5.9, the

limit cycle found by the search started with $\Pi = 0$, is defined by $A_1 = -2.3441$, $A_2 = 4.6675$, and $\phi = -0.0065$, but can otherwise be defined by $A_1 = 2.3441$, $A_2 = 4.6675$ and $\phi = \Pi - 0.0065$. Therefore, it can still be claimed that the fastest search occured when the initial phase condition was close to the phase derived from the resonant mode direction.

Thus, with the conjugate gradient method too, the phase information brought by the resonant mode characteristics appears to be very valuable, and allows the search to converge more rapidly.

5.8 Evaluation of the Limit Cycle Stability in the Two Joint Case.

5.8.1 Stability of Limit Cycle 1.

The state variables considered in the following are $\int x_1 dt$, x_1, $\dot{x}_1$, $\int x_2 dt$, x_2 and $\dot{x}_2$, where x_1 is the displacement of the first mass, and x_2 the displacement of the second mass.

$$\underset{\sim}{X} = [\ \int x_1 dt \ , \ x_1, \ \dot{x}_1 \ , \ \int x_2 dt, \ x_2, \ \dot{x}_2 \ ]^T$$

The limit cycle trajectory expressed in the state space is:

$$\underset{\sim}{X} = \underset{\sim}{U}_1^r \cos(0.4375t) + \underset{\sim}{U}_1^i \sin(0.4375t) \tag{5-28}$$

where, $\underset{\sim}{U}_1^r$ and $\underset{\sim}{U}_1^i$ can be found from the expressions of $x_1(t)$ and $x_2(t)$ in formulas (5-21), and are:

$$\underset{\sim}{U}_1^r = [\ 0, \ A_1, \ 0, \ A_2\sin\phi/\omega, \ A_1 + A_2\cos\phi, -A_2\sin\phi \ \omega \ ]^T \tag{5-29}$$

$$\underset{\sim}{U}_1^i = [\ A_1/\omega, \ 0, -A_1 \ \omega, \ (A_1 + A_2\cos\phi)/\omega, -A_2\sin\phi, -(A_1 + A_2\cos\phi) \ \omega \ ]^T \tag{5-30}$$

Using the values defining the first limit cycle, one finds:

$$\underset{\sim}{U}_1^r = [\ 0,\ 6.9795\ 10^{-2},\ 0,\ 1.7461\ 10^{-4}, -6.9318\ 10^{-2}, -3.6\ 10^{-5}]^T$$

$$\underset{\sim}{U}_1^i = [1.5953\ 10^{-1},\ 0, -3.0537\ 10^{-2}, -1.5844\ 10^{-1}, -7.64\ 10^{-5},\ 3.0328\ 10^{-2}]^T$$

The transformation into principal axes indicated in section 4.3.6 yields the following vectors:

$$\underset{\sim}{U}_1^E = [2.85\ 10^{-6}, 6.9795\ 10^{-2}, -5.4\ 10^{-7}, 1.7178\ 10^{-4}, -6.9318\ 10^{-2}, -3.25\ 10^{-5}]^T$$

$$\underset{\sim}{U}_2^E = [1.5953\ 10^{-1}, -1.2\ 10^{-6}, -3.0537\ 10^{-2}, -1.5844\ 10^{-1}, 7.76\ 10^{-5}, 3.0328\ 10^{-2}]^T$$

The matrix M and vector $\underset{\sim}{P}$ are respectively found to be

$$M = \begin{vmatrix} 1.0000 & -1.7324 & 0.0000 & -0.7620 \\ 0.0000 & -0.5019 & -0.0698 & 0.5648 \\ 0.0000 & 2.4534 & 0.0000 & 1.5229 \\ 0.0000 & 0.9991 & 0.0000 & -1.1292 \end{vmatrix} \tag{5-31}$$

$$\underset{\sim}{P} = \begin{vmatrix} 0.5648 \\ 0.7620 \\ -1.1292 \\ -1.5229 \end{vmatrix} \tag{5-32}$$

Perturbation parameters were found using (3-52), and expression (5-29) was used to generate an initial point in the state space corresponding to these perturbed values. The stability index ρ derived in expression (4-32) was computed, and was found to be: $\rho = +12.04\ \delta\sigma$. The positive sign of ρ indicates that the limit cycle is <u>unstable</u>. It is not surprising, therefore, that it could not be found through simulation, since infinitesimal perturbations make the system drift away

from the limit cycle trajectory.

5.8.2 Stability of Limit Cycle 2.

The parameters of the second limit cycle yield the following directions for the ellipse:

$$\underset{\sim}{U}_1^r=[\ 0,\ 2.3441,\ 0,\ 6.1518\ 10^{-2},\ -2.3233,\ -1.5074\ 10^{-2}]^T$$

$$\underset{\sim}{U}_1^i=[\ 4.7355,\ 0,\ -1.1604,\ -4.6934,\ -3.0453\ 10^{-2},\ 1.1501]^T$$

The transformation into principal axes indicated in section 4.3.6 yields the following vectors:

$$\underset{\sim}{U}_1^E=[\ 3.076\ 10^{-2},\ 2.3441,\ -7.54\ 10^{-3},\ 3.103\ 10^{-2},\ -2.3234,\ -7.60\ 10^{-3}]^T$$

$$\underset{\sim}{U}_2^E=[\ 4.7354,\ -1.523\ 10^{-2},\ -1.1604,\ -4.6937,\ -1.536\ 10^{-2},\ 1.1501]^T$$

The matrix M and vector $\underset{\sim}{P}$ are respectively found to be

$$M = \begin{vmatrix} 0.9948 & -0.0013 & 0.0004 & -6.6431 \\ -0.0146 & -0.0072 & -1.5611 & 46.9348 \\ 0.0108 & -0.9974 & -0.0566 & 13.2108 \\ 0.0287 & 0.0209 & -7.7851 & -93.9046 \end{vmatrix} \qquad (5-33)$$

$$\underset{\sim}{P} = \begin{vmatrix} 46.9348 \\ 6.6431 \\ -93.9046 \\ -13.2108 \end{vmatrix} \qquad (5-34)$$

As before, the stability index was computed for the new values of amplitudes, phase and frequency generated through (3-52). The stability index was found to be: $\rho = -41.50\ \delta\sigma$.

The negative sign of ρ indicates that the limit cycle is <u>stable</u>.

The second system has, therefore, a stable, and an unstable limit cycle, which, recalling section 3.1.4, leads to amplitude dependent behaviors. These results should not, however, be surprising, since the system is truly linear for small amplitudes, and the linear controller ensures asymptotic stability in that range, and since the system is also "asymptotically linear", which implies that very large initial conditions result in bounded responses. Hence, if limit cycles exist, there must be one stable, since the system is stable, and there must also be a stability boundary that separates the truly linear behavior around the origin from the more nonlinear behaviors that appear for larger values of the state variables.

5.9 Conclusion.

Examples of analytical determination of limit cycles in nonlinear dynamical systems were derived in this chapter, and they proved that the analytical techniques previously derived could successfully locate the conditions of sustained oscillations.

The two different techniques presented in Chapter 4 were used. The influence of the line search accuracy was investigated: as reported in [16] or [23], the BFGS method was found to perform better with a poor line search accuracy. The process seems, however, always successful, whatever level of accuracy is used in the univariate searches. On the other hand, the conjugate gradient method seems to require very accurate

line searches. It can fail to succeed if the local minima along the search directions are not closely approached, and thus, appears to be very sensitive to changes in the accuracy parameter.

The influence of the initial conditions was also investigated. Very valuable results were found in the Singular Value Test. The shape of the residual function, for the single joint case, showed that the amplitudes as well as the initial frequency should be chosen around the lower bounds yielded by the Singular Value Test in order for the search to be successful. The limit cycles were also found to be very close to the first resonant mode of the linear parts of the systems, and this might provide valuable initial phase information. It was shown that starting with a phase in accordance with the one yielded by the resonant mode direction resulted in the fastest searches, with either one of the minimization techniques. However, the conjugate gradient method appeared, again, to be very sensitive to the initial phase condition, whereas the BFGS method was found more robust.

Generally, the BFGS method always appeared to be noticeably more successful than the conjugate gradient method. When the line search accuracy parameters were taken to be the optimal values for both methods, the BFGS method consistently required less iterations. In fact, looking back at the results found in table 5.5, the BFGS method could complete a search in about 4 to 6 major iterations with the two joint model, whereas table 5.9 shows that, with the conjugate gradient method, 6 major iterations correspond to the most favorable case with a relaxed convergence test, and that the number of major iterations is spread

between 6 and more than 12, depending on the initial condition chosen. Furthermore, more function evaluations are required in the conjugate gradient method, since a better line search must be performed, increasing accordingly the length of the process.

Being faster, and being much more robust, the BFGS method appears to be, therefore, very superior to the conjugate gradient method, and should be retained to perform the analytical determination of limit cycles in dynamical systems.

A = 0.11 ; ω = 0.25 rad/s

Line Search Accuracy Parameter ϵ	Number of Iterations	Number of function Evaluations	Converged Point A ; ω	Residual Function value
10^{-1}	12	66	A = 1.1510 ω = 0.6835	$2.6 \ 10^{-29}$
10^{-3}	9	93	A = 0.2739 ω = 0.5748	$7.6 \ 10^{-31}$
10^{-5}	7	84	A = 0.2739 ω = 0.5748	$6.7 \ 10^{-26}$
10^{-7}	7	95	A = 0.2739 ω = 0.5748	$7.4 \ 10^{-26}$

Table 5.1:   BFGS Method's Performances for Different Line Search

Accuracies in Single Mass Case

$\underline{A}_1 = 0.11$; $A_2 = 0.11$; $\phi = \pi$; $\omega = 0.3$ rad/s

Line Search Accuracy Parameter ϵ	Number of Iterations	Number of function Evaluations	Converged Point A's, ϕ, ω	Residual Function value
0.5	15	64	$A_1 = 0.0698$ $A_2 = 0.1391$ $\phi = 3.1410$ $\omega = 0.4375$	$2.1\ 10^{-26}$
0.1	18	112	$A_1 = 0.0698$ $A_2 = 0.1391$ $\phi = 3.1410$ $\omega = 0.4375$	$1.9\ 10^{-27}$
10^{-3}	17	154	$A_1 = 0.0698$ $A_2 = 0.1391$ $\phi = 3.1410$ $\omega = 0.4375$	$2.1\ 10^{-27}$

Table 5.2: BFGS Method's Performances for Different Line Search

Accuracies in Two Mass Case with Remote Starting Point

$\underline{A}_1 = 0.11$; $A_2 = 0.11$; $\phi = \pi/2$; $\omega = 0.3$ rad/s

Line Search Accuracy Parameter ϵ	Number of Iterations	Number of function Evaluations	Converged Point A's, ϕ, ω	Residual Function value
0.5	25	107	$A_1 = 2.3441$ $A_2 = 4.6675$ $\phi = 3.1351$ $\omega = 0.4950$	$9.9\ 10^{-25}$
0.1	26	121	$A_1 = 2.3441$ $A_2 = 4.6675$ $\phi = 3.1351$ $\omega = 0.4950$	$1.3\ 10^{-29}$
10^{-3}	25	215	$A_1 = 2.3441$ $A_2 = 4.6675$ $\phi = 3.1351$ $\omega = 0.4950$	$4.8\ 10^{-25}$

Table 5.3: BFGS Method's Performances for Different Line Search

Accuracies in Two Mass Case with Remote Starting Point

$\underline{A}_1 = 0.06$; $\underline{A}_2 = 0.14$; $\phi = \Pi$; $\omega = 0.4$ rad/s

Line Search Accuracy Parameter ϵ	Number of Iterations	Number of function Evaluations	Converged Point A's, ϕ, ω	Residual Function value
0.5	13	58	$A_1 = 0.0698$ $A_2 = 0.1391$ $\phi = 3.1410$ $\omega = 0.4375$	$2.0\ 10^{-29}$
10^{-1}	12	61	$A_1 = 0.0698$ $A_2 = 0.1391$ $\phi = 3.1410$ $\omega = 0.4375$	$2.9\ 10^{-28}$
10^{-2}	12	82	$A_1 = 0.0698$ $A_2 = 0.1391$ $\phi = 3.1410$ $\omega = 0.4375$	$2.4\ 10^{-29}$
10^{-3}	12	100	$A_1 = 0.0698$ $A_2 = 0.1391$ $\phi = 3.1410$ $\omega = 0.4375$	$8.1\ 10^{-30}$
10^{-4}	12	104	$A_1 = 0.0698$ $A_2 = 0.1391$ $\phi = 3.1410$ $\omega = 0.4375$	$1.5\ 10^{-29}$
10^{-5}	12	140	$A_1 = 0.0698$ $A_2 = 0.1391$ $\phi = 3.1410$ $\omega = 0.4375$	$1.0\ 10^{-29}$

Table 5.4:   BFGS Method's Performances for Different Line Search

Accuracies in Two Mass Case with Accurate Start

$A_1= 0.11$; $A_2= 0.11$; $\omega = 0.3$ rad/s; $\epsilon = 0.5$

Initial Phase Condition	Number of Iterations	Number of Function Evaluations	Converged Point	Residual Function Value
$\phi = -\Pi/2$	20	89	$A_1 = 0.0698$ $A_2 = 0.1391$ $\phi = -3.1421$ $\omega = 0.4375$	$2.9 \ 10^{-26}$
$\phi = 0$	20	70	$A_1 = -0.0698$ $A_2 = 0.1391$ $\phi = 0.0005$ $\omega = 0.4375$	$1.6 \ 10^{-28}$
$\phi = \Pi/2$	25	107	$A_1 = 2.3441$ $A_2 = 4.6675$ $\phi = 3.1351$ $\omega = 0.4950$	$9.9 \ 10^{-25}$
$\phi = \Pi$	15	64	$A_1 = 0.0698$ $A_2 = 0.1391$ $\phi = 3.1410$ $\omega = 0.4375$	$2.1 \ 10^{-26}$

Table 5.5:   BFGS Method Performances for Different Initial Phase

Conditions in Two Mass Case

$\underline{A = 0.11 \; ; \; \omega = 0.25 \; rad/s}$

Line Search Accuracy Parameter ϵ	Number of Iterations	Number of function Evaluations	Converged Point A ; ω	Residual Function value
10^{-1}	24	121	A = 1.1510 ω = 0.6835	$2.6 \; 10^{-21}$
10^{-3}	10	82	A = 0.2739 ω = 0.5748	$6.9 \; 10^{-26}$
10^{-5}	9	115	A = 0.2739 ω = 0.5748	$1.8 \; 10^{-24}$
10^{-7}	9	141	A = 0.2739 ω = 0.5748	$1.8 \; 10^{-24}$

Table 5.6: Conjugate Gradient Method's Performances for Different

Line Search Accuracies in the Single Mass Case

$A_1 = 0.11$; $A_2 = 0.11$; $\phi = \Pi$; $\omega = 0.3$ rad/s

Line Search Accuracy Parameter ϵ	Number of Iterations	Number of function Evaluations	Converged Point A's, ϕ, ω	Residual Function value
0.5	50	307	$A_1 = -0.0698$ $A_2 = -0.1391$ $\phi = 3.1378$ $\omega = 0.4375$	$1.8 \ 10^{-6}$
0.1	50	327	$A_1 = 0.0698$ $A_2 = 0.1391$ $\phi = 3.1400$ $\omega = 0.4375$	$1.9 \ 10^{-7}$
10^{-4}	42	397	$A_1 = 0.0698$ $A_2 = 0.1391$ $\phi = 3.1410$ $\omega = 0.4375$	$1.1 \ 10^{-20}$

Table 5.7 : CG Method's Performances for Different Line Search

Accuracies in Two Mass Case with Remote Starting Point

$\underline{A}_1 = 0.065;\ A_2 = 0.14;\ \varphi = \pi;\ \omega = 0.45\ rad/s$

Line Search Accuracy Parameter ϵ	Number of Iterations	Number of function Evaluations	Converged Point A's, φ, ω	Residual Function value
10^{-1}	50	297	$A_1 = 0.0698$ $A_2 = 0.1391$ $\varphi = 3.1411$ $\omega = 0.4375$	$1.6\ 10^{-10}$
10^{-2}	31	211	$A_1 = 0.0698$ $A_2 = 0.1391$ $\varphi = 3.1410$ $\omega = 0.4375$	$4.1\ 10^{-26}$
10^{-3}	24	193	$A_1 = 0.0698$ $A_2 = 0.1391$ $\varphi = 3.1410$ $\omega = 0.4375$	$1.8\ 10^{-23}$
10^{-4}	23	208	$A_1 = 0.0698$ $A_2 = 0.1391$ $\varphi = 3.1410$ $\omega = 0.4375$	$1.1\ 10^{-27}$
10^{-5}	25	307	$A_1 = 0.0698$ $A_2 = 0.1391$ $\varphi = 3.1410$ $\omega = 0.4375$	$1.9\ 10^{-24}$

Table 5.8:   CG Method's Performances for Different Line Search

Accuracies in Two Mass Case with Accurate Start

$\underline{A}_1= 0.11;\ \underline{A}_2= 0.11;\ \omega = 0.3\ rad/s;\ \epsilon=10^{-4}$

Initial Phase Condition	Number of Iterations	Number of Function Evaluations	Converged Point	Residual Function Value
$\phi =-\Pi/2$	50 $(grad>10^{-8})$	610	$A_1= 0.0631$ $A_2= 0.1341$ $\phi =-2.6755$ $\omega = 0.4432$	0.0337
$\phi = 0$	28	293	$A_1=-2.3441$ $A_2= 4.6675$ $\phi =-0.0065$ $\omega = 0.4950$	$9.9\ 10^{-17}$
$\phi = \Pi/2$	50 $(grad>10^{-8})$	684	$A_1= 2.3441$ $A_2= 4.6676$ $\phi = 3.1531$ $\omega = 0.4950$	$8.1\ 10^{-11}$
$\phi = \Pi$	38	373	$A_1= 0.0698$ $A_2= 0.1391$ $\phi = 3.1410$ $\omega = 0.4375$	$3.3\ 10^{-20}$

Table 5.9: CG Method's Performances for Different Initial Phase

Conditions in Two Mass Case
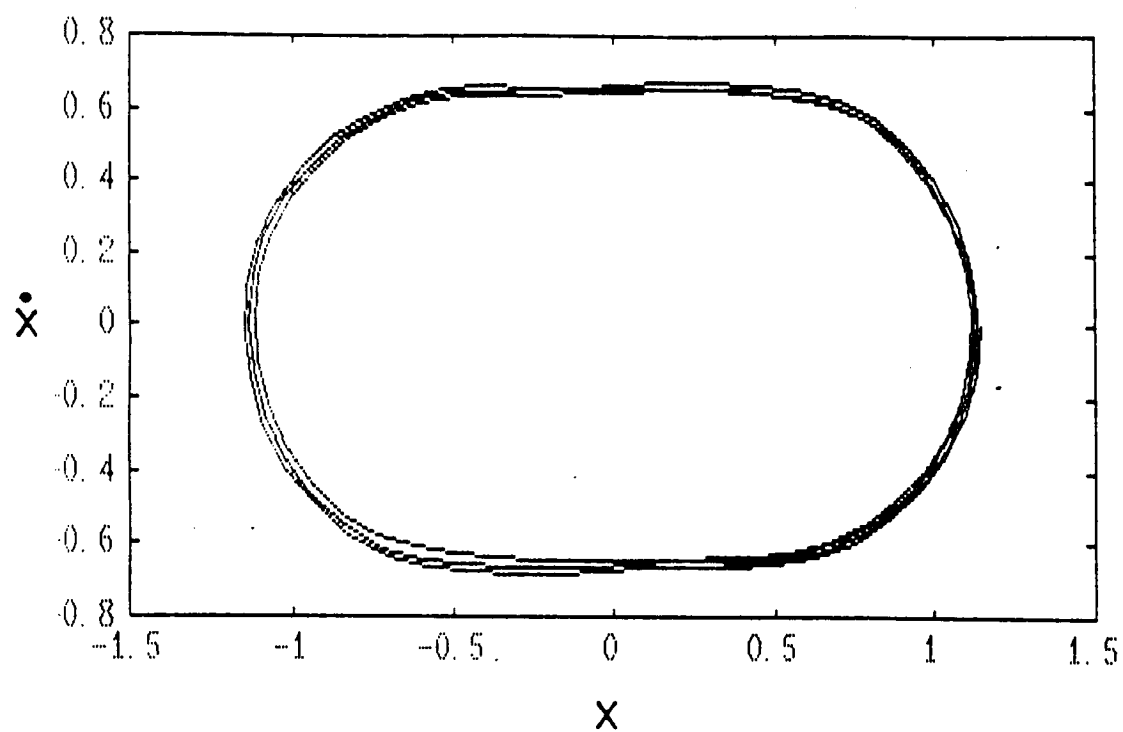
Figure 5-8:   Single Mass Case: x(t) and ẋ(t) in Phase Plane
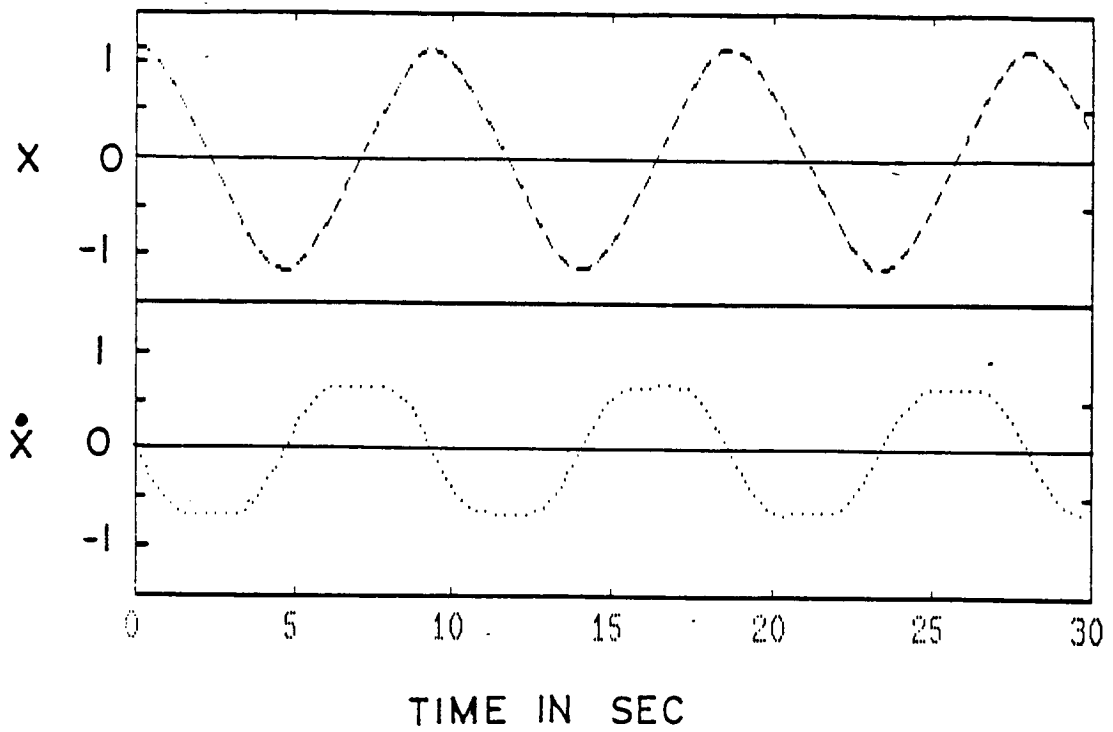
Figure 5-9: Single Mass Case: x(t) and ẋ(t) versus Time
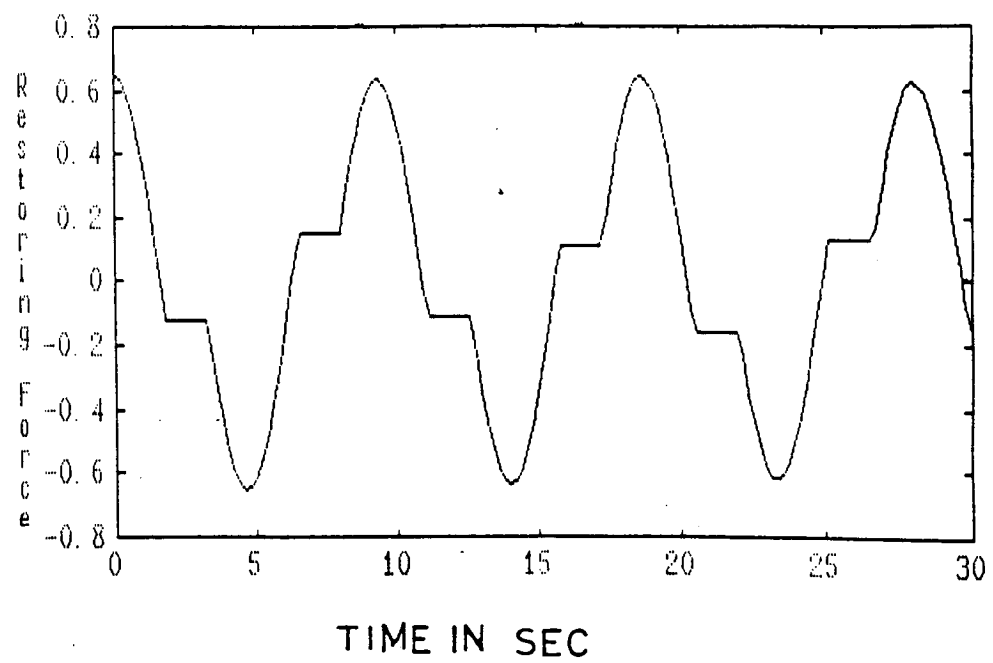
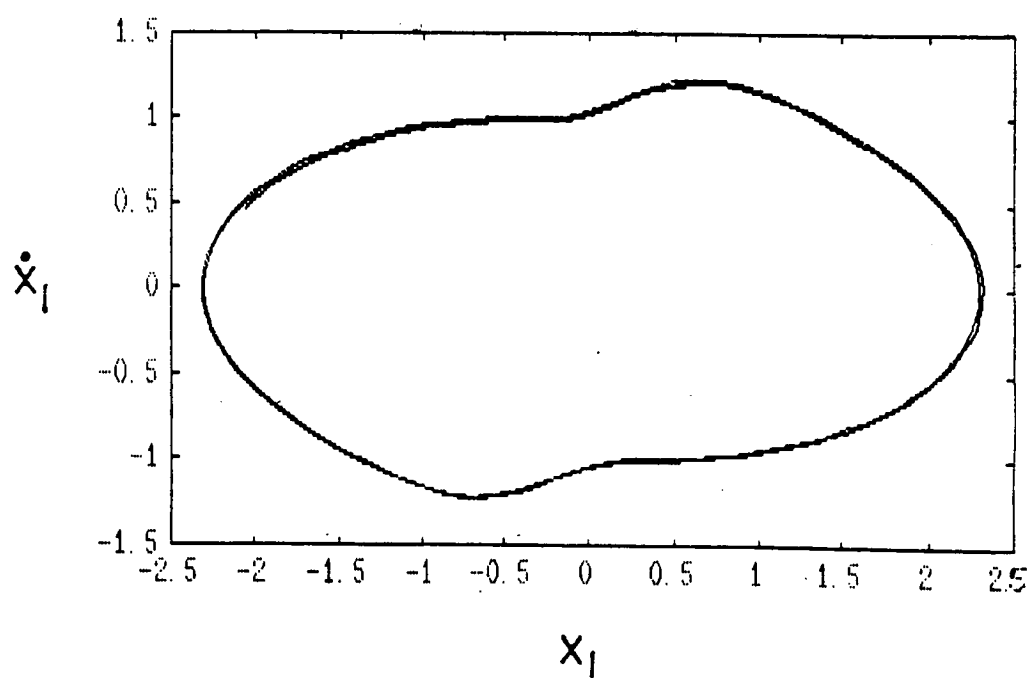Figure 5-10: Single Mass Case: Restoring Force versus Time

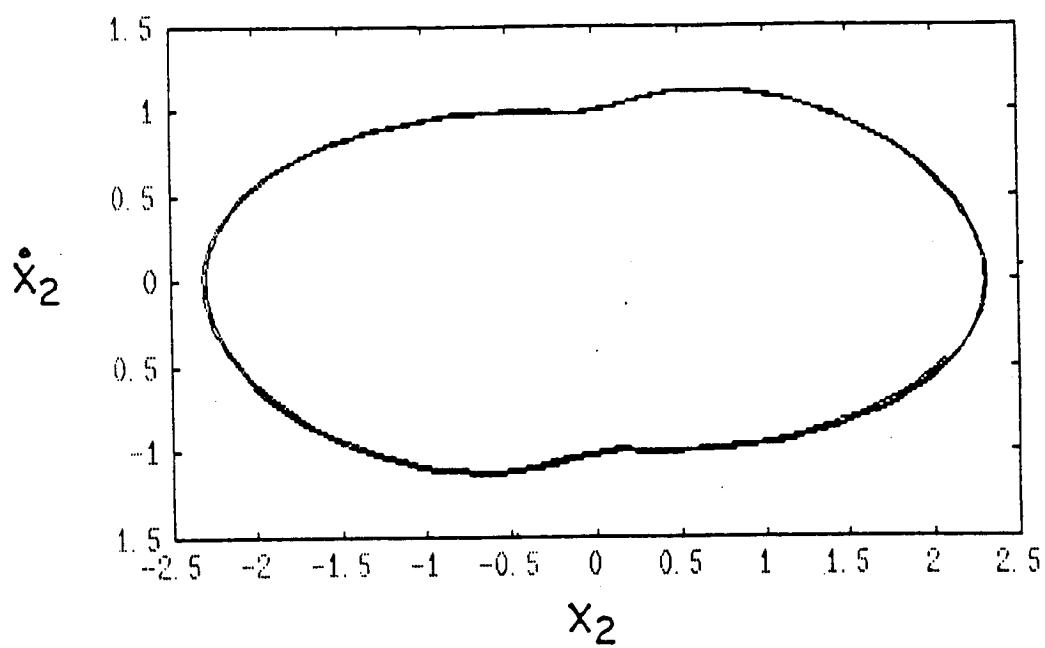Figure 5-11: Two Mass Case: x_1 and $\dot{x}_1$ in Phase Plane

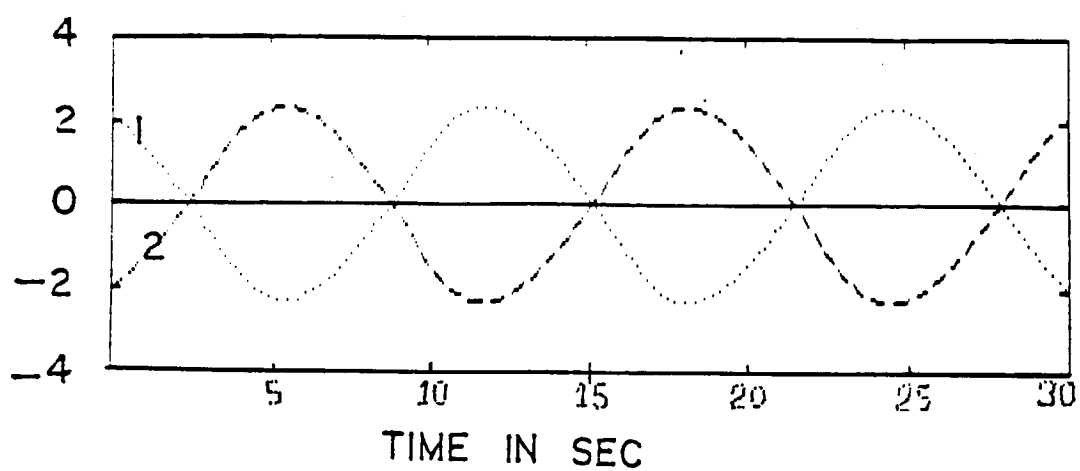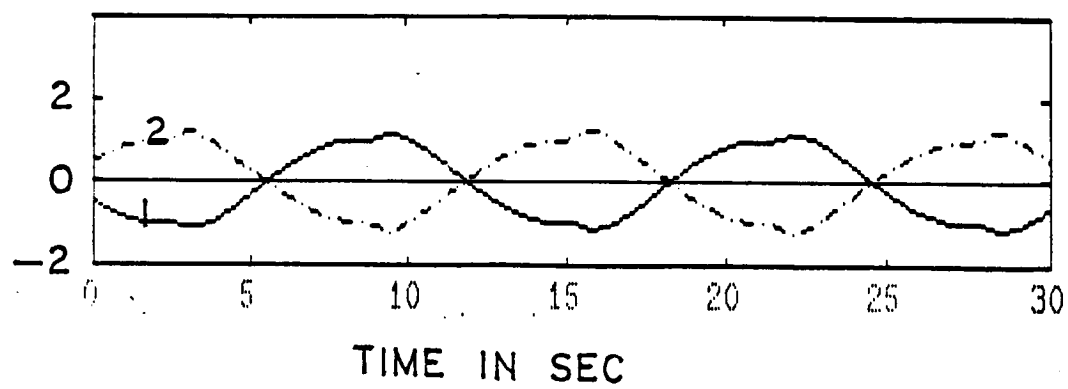Figure 5-12: Two Mass Case: x_2 and $\dot{x}_2$ in Phase Plane

$$x_1(t) \text{ and } x_2(t)$$

$$\dot{x}_1(t) \text{ and } \dot{x}_2(t)$$

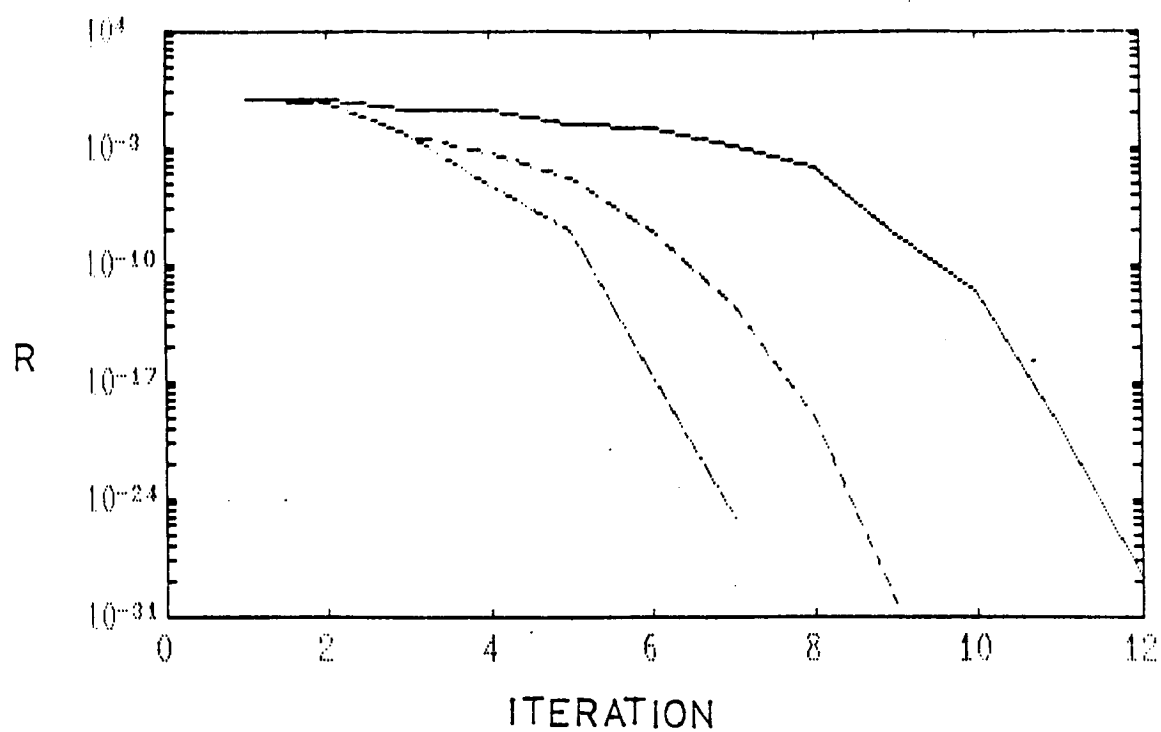Figure 5-13:   Two Mass case: $x_1(t)$, $x_2(t)$, $\dot{x}_1(t)$ and $\dot{x}_2(t)$

Figure 5-14: BFGS Method: Values of the Residual during Minimization with $\epsilon = 10^{-1}$, 10^{-3}, 10^{-5}, 10^{-7}, One Mass
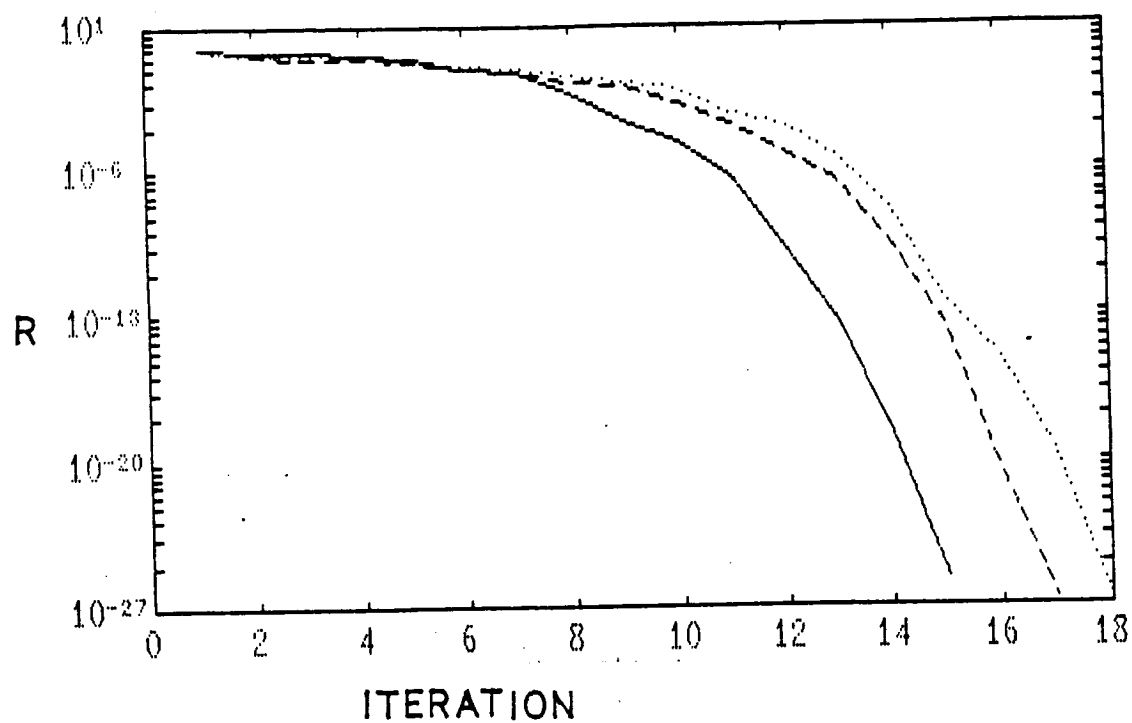
Figure 5-15: BFGS Method: Values of the Residual during Minimization
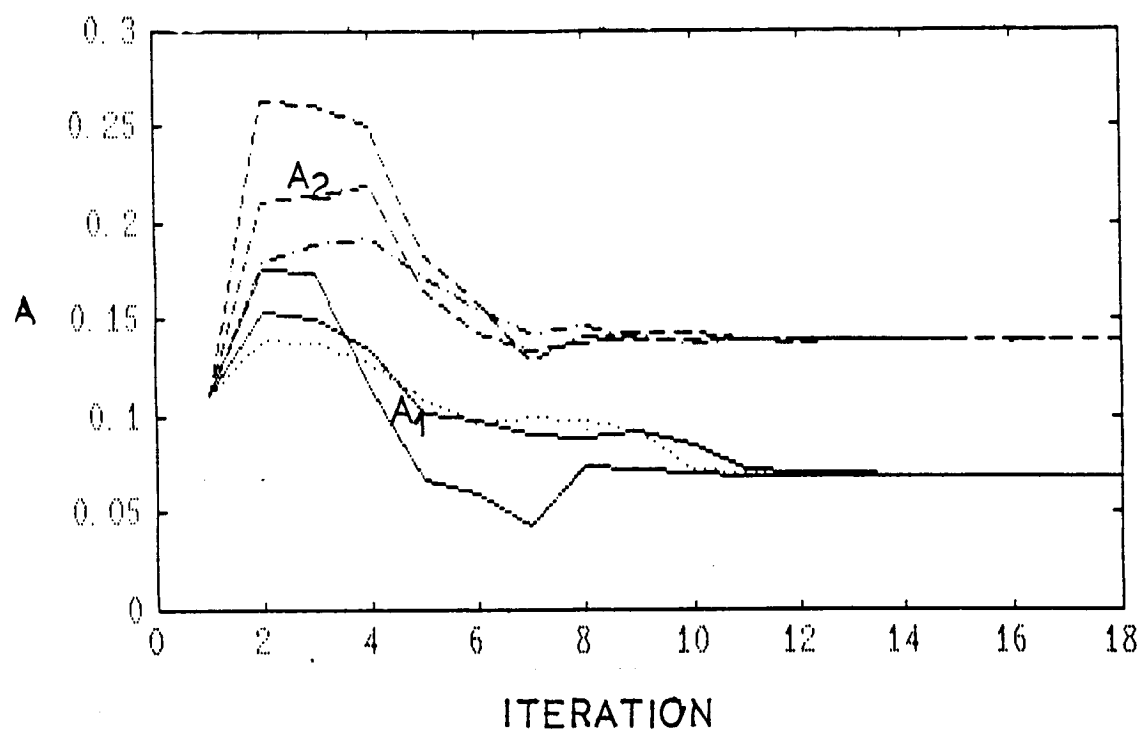with ϵ = 0.5, 0.1 and 10^{-3}, Remote Initial Point, Two Masses

Figure 5-16:   BFGS Method: A_1 and A_2 during Minimization with
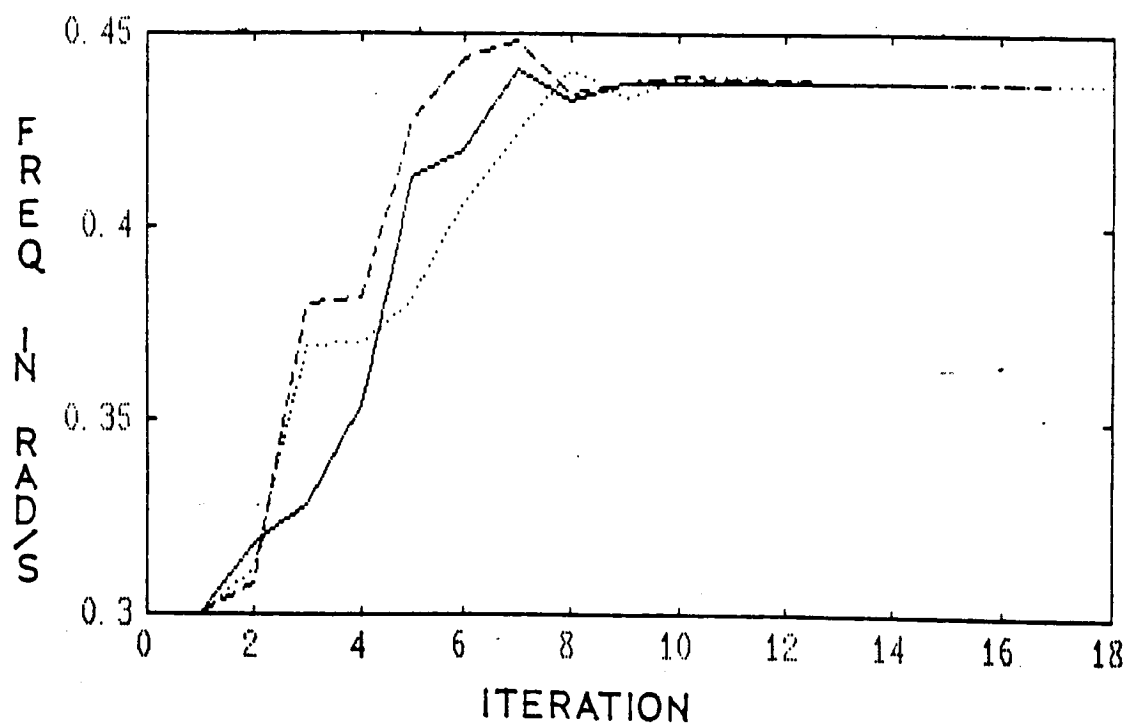$\epsilon = 0.5$, 0.1 and 10^{-3}, Remote Initial Point, Two Masses

Figure 5-17: BFGS Method: Frequency during Minimization with $\epsilon = 0.5$, 0.1 and 10^{-3}, Remote Initial Point, Two Masses
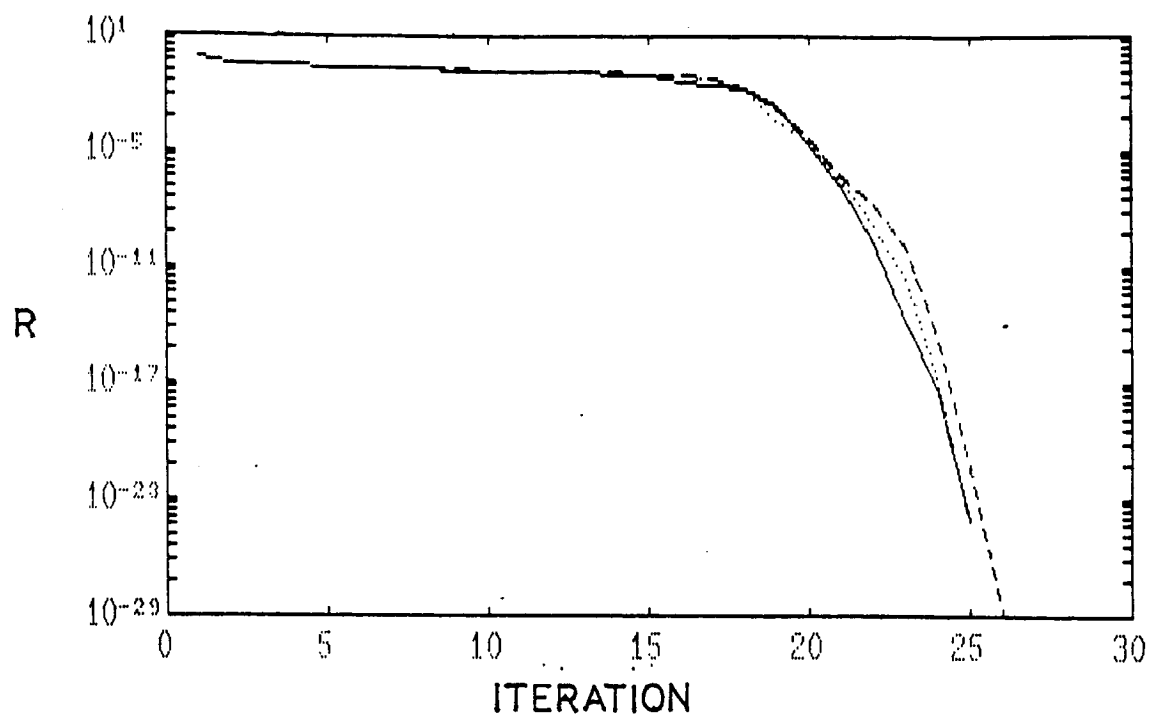
Figure 5-18: BFGS Method: Values of the Residual during Minimization with $\epsilon = 0.5$, 0.1 and 10^{-3}, Second Remote Initial Point, Two Masses

Figure 5-19: BFGS Method: Values of the Residual during Minimization
with $\epsilon = 0.5$, 10^{-1}, 10^{-2}, 10^{-3}, 10^{-4}, 10^{-5}, Accurate Initial Guess
Two Masses

Figure 5-20: BFGS Method: Values of the residual during Minimization with $\Phi = -\Pi/2$, 0, $\Pi/2$ and Π, $\epsilon = 0.5$, Two Masses

Figure 5-21: CG Method: Values of the Residual during Minimization
with $\epsilon = 10^{-1}$, 10^{-3}, 10^{-5}, 10^{-7}, One Mass

Figure 5-22: CG Method: Values of the Residual during Minimization

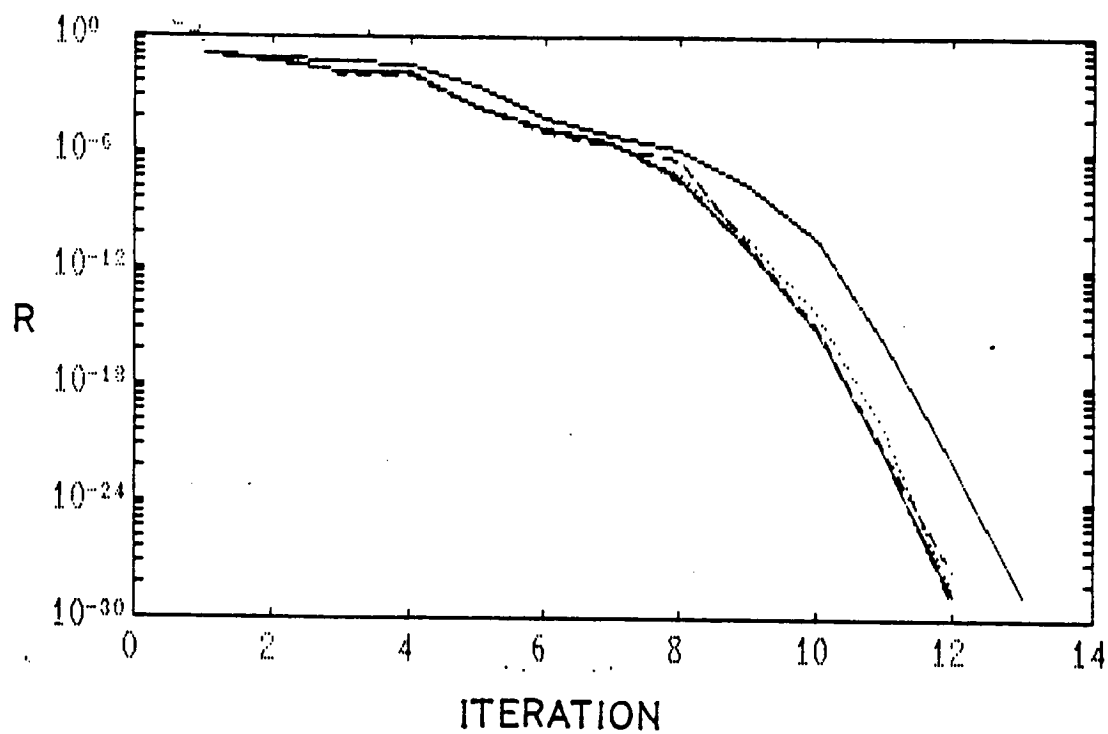with $\epsilon = 0.5$, 10^{-1}, 10^{-4}, Remote Initial Point, Two Masses

Figure 5-23: CG Method: Values of the Residual during Minimization with $\epsilon = 10^{-1}$, 10^{-2}, 10^{-3}, 10^{-4}, 10^{-5}, Accurate Initial Guess Two Masses
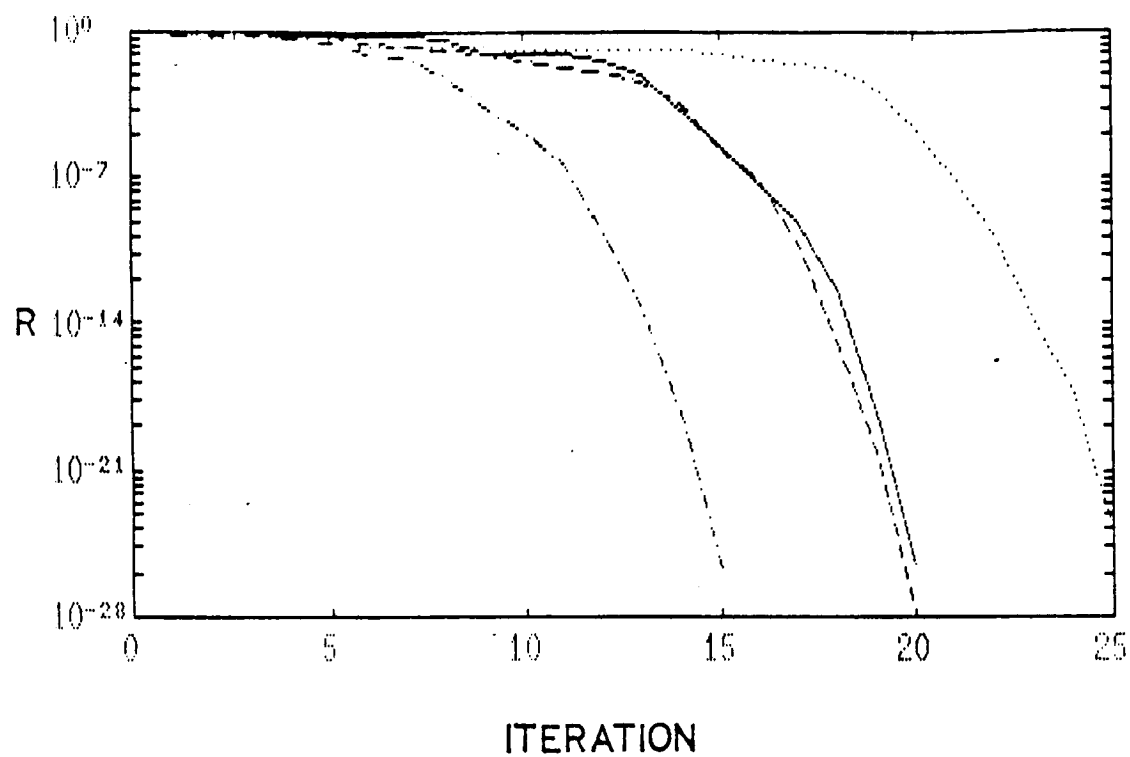
Figure 5-24:   CG Method: Values of the residual during Minimization

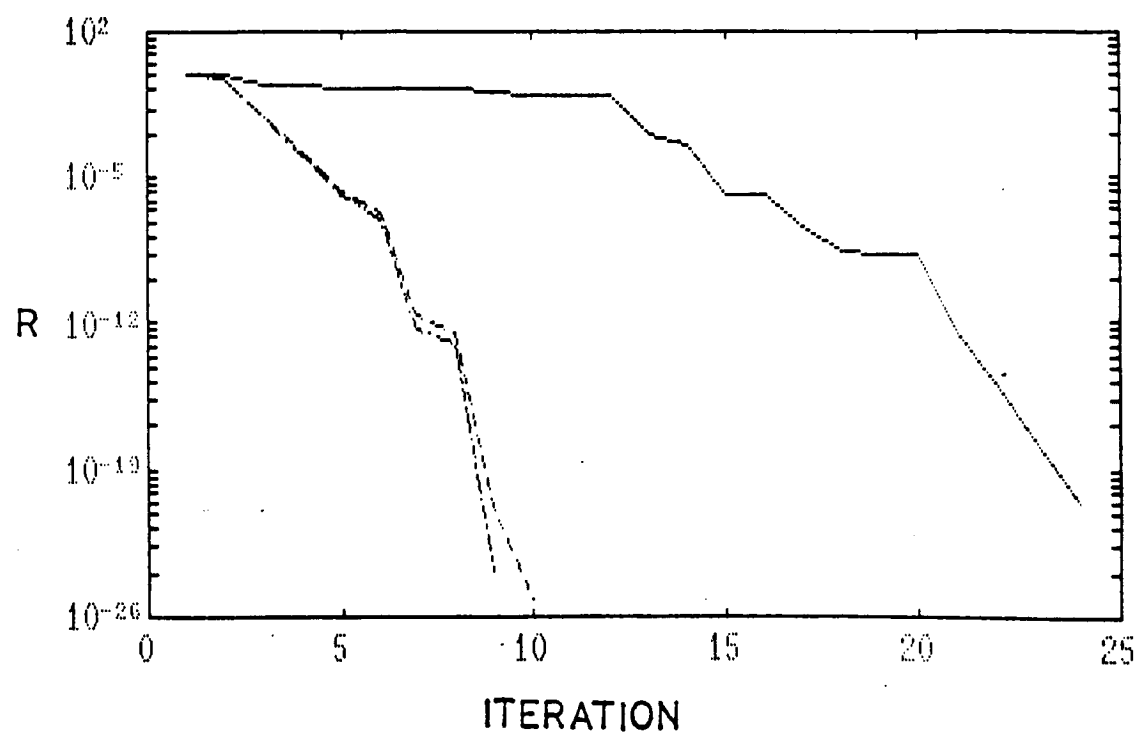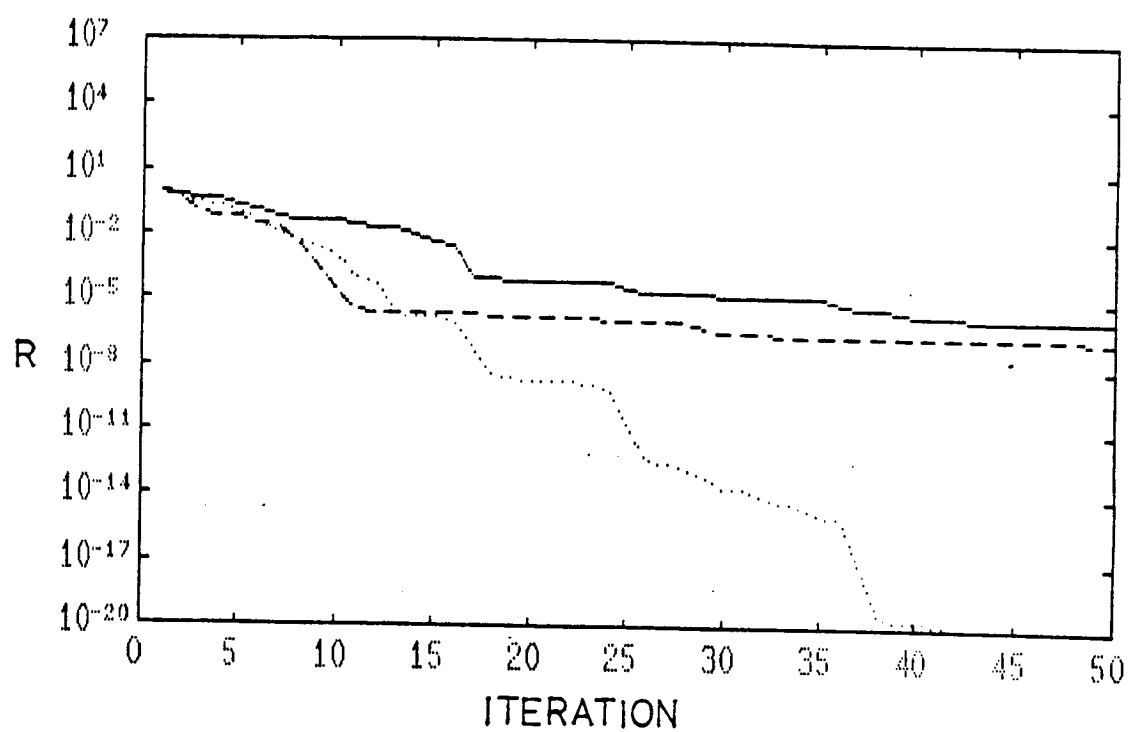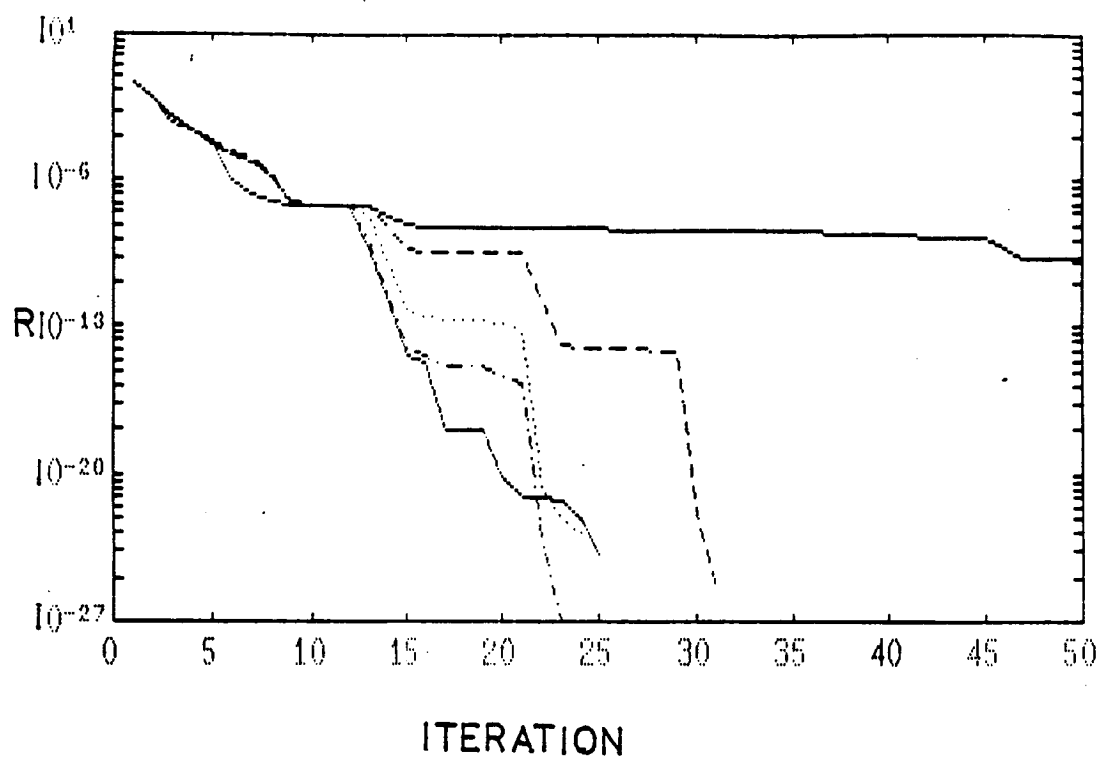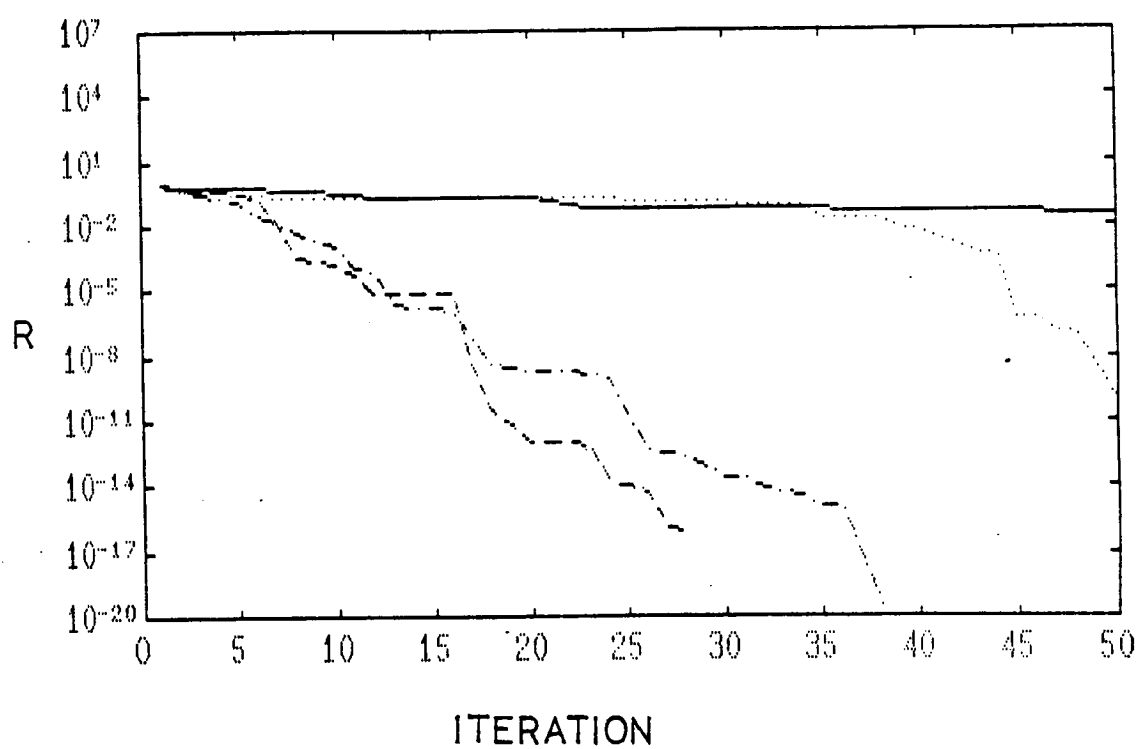with $\Phi = -\Pi/2$, 0, $\Pi/2$, Π, $\epsilon = 10^{-4}$, Two Masses

CHAPTER SIX

CONCLUSIONS AND RECOMMENDATIONS

6.1 Conclusions on the Modeling of Large Nonlinear Dynamical Systems.

In the field of Applied Mathematics, a theoretical answer to a problem is considered an acceptable solution only if the required derivations and calculations can be actually carried out, and even though computers keep enlarging the capability to solve complex problems, the study of large dynamical systems may result in problems whose size makes the implementation of a solution impossible. The object of this work was to show a possible approach to the study of the dynamics of large controlled structures with nonlinear joints that would allow the derivation of applicable resolution techniques, especially concerning the determination of limit cycles.

In Chapter 2, a general modeling framework for large structural systems having distributed nonlinearities was shown. The modeling included forming an equivalent linearized structure by replacing the nonlinear elements by linear ones, and performing a modal analysis on this altered structure, thus providing a finite state variable linear model. Nonlinearities were then fed back as forcing terms in the linear model. This modeling offers many advantages, among which are the use of existing modal analysis techniques to obtain a linear model, the global

way the entire system is treated, as opposed to cascading subsystems through nonlinear elements, the simplicity of the resulting representation with a linear model and a nonlinear feedback and the easiness to include a control feedback law. Its main disadvantage lies in the number of approximations that have to be made, such as taking approximate modes of an equivalent system, or taking only a finite number of them, but the accuracy can be increased at the cost of increasing the number of states. Hence, the modeling of the structure as a nonlinear feedback system appears very convenient. It can be readily done, requiring only a little additional work during a standard modal analysis, when one has to choose a linear model for each joint to include as the finite element equivalent stiffness.

6.2   Analytical Determination of Limit Cycles in Large Dynamical Systems.

The remainder of this work was concerned with determining analytically the existence of limit cycles, using the model derived in Chapter 2.

In Chapter 3, it was decided to keep only one harmonic to model the periodical behavior of the different state variables. This hypothesis is believed to be satisfactorily verified when dynamical systems such as a truss are considered, but should nevertheless be checked whenever the study of an actual structure is undertaken.

Under the single harmonic hypothesis, Dual Input Describing

Functions were used to model the nonlinear load-displacement law of the joints. Then, limit cycle conditions were derived, as well as stability conditions of the eventual limit cycles.

In Chapter 4, an applicable resolution method was derived to detect whether limit cycle conditions can be met in a given system, and what would be the limit cycle parameters, if one is detected. The methodology retained was based on the minimization of a scalar residual function. Two minimization algorithms were pointed out in the reviewed literature: the BFGS method was reported to be the fastest and most successful minimization algorithm, and the conjugate gradient method was reported to be the most applicable for very large problems. Rough evaluations of the computational task made in the same chapter showed that both methods require a considerable number of calculations, where the computation of the residual function and its gradient are the most important task, therefore making the calculation savings of the conjugate gradient method irrelevant.

The importance of the computation was found to come principally from the need to calculate the effect of each and every joint on each and every mode, and although the single harmonic analysis yields a simple model of each joint, the order of computation was shown to be an $O(24N_j n)$ to evaluate one residual in the minimization process, where N_j is the number of distributed nonlinearities and n the number of modes in the linear model. It was also shown that the gradient computation takes 3n times this number of operations. Furthermore, even efficient search techniques cannot converge in less than 3n iterations, which is the

number of variables that are necessary to describe a limit cycle, and groups of 3n, or major iterations may have to be repeated an important number of times.

Examples of search for limit cycles in simple systems (one and two nonlinearities) were made in Chapter 5, and they confirmed the overall superiority of the BFGS method. This latter approach was always found to be faster, and was also found very robust; that is, that the required number of iterations to converge only moderately depends on the initial conditions.

The influence of the line search accuracy on the performance of the different methods was investigated. Results showed that the BFGS algorithm performed better with a poor determination of the minima along the search directions, whereas the conjugate gradient method required a high accuracy in order to be successful.

The problem of finding sets of initial conditions that ensure fast searches was also addressed. The study showed that the first resonant peak of the linear part of the system plays a very important role in limit cycle occurrence. It led to the conclusion that the limit cycles must resemble the first resonant mode in terms of frequency, as well as phase between the oscillations, and relative amplitudes of the vibrations of the different parts of the structure. Most efficient sets of initial conditions should, accordingly, have a frequency below the first resonance, have small amplitudes in the neighborhood of the lower bounds given by the singular value test, and have initial phases derived from the ones found in the resonant mode directions.

The general conclusion of the thesis is, therefore, that the analytical determination of limit cycles is theoretically possible, and is applicable for systems of reasonable size. The computational task, however, rapidly grows as the number of nonlinearities N_j increases. The number of modes on which to approximate a solution is also an important factor since it fixes the number of variables on which limit cycles can depend, and if the typical data of the COFS I Mast experiment are taken, where about 1000 joints act on 100 modes, the estimates derived in Chapter 4 easily convince one that the size of the problem has become too large to be treated without further simplifications. It is therefore believed that only systems smaller than the Mast experiment can be studied with the method presented, where every single nonlinearity is being considered, and alternate approaches shall be taken for larger problems.

6.3 Alternate Approaches and Further Study.

6.3.1 Complementary Studies.

Only simple examples were derived in this study, and they brought no insight on the effect of the size on the performance of the technique. Hence, consistently larger models should be derived and studied, in order to consolidate the results and the conclusions presented before about the effectiveness of analytical methods to study limit cycles. More precisely, it would provide data to compare the

performances of different minimization algorithms, and enable to interpolate the number of major iterations and function evaluations required for very large problems. It would also allow the study of possible improvements of the algorithms, by introducing of hybrid methods for example.

6.3.2 Global and Reduced Joints Models.

A field of further study could be the investigation of techniques that enable the concentration of the effects of groups of nonlinearities. This would result in feeding back a smaller number of global non-linearities which would result in less nonlinear forcing terms than in the case where each and every nonlinear element is fed back. The computational task would be directly affected by a decrease in the number of nonlinear terms fed back, and could be drastically reduced.

A basic simplification that would occur in the treatement of real models would be to simplify the action of the forcing nonlinear terms, reducing it to one torque or one unique force, therefore limiting the action to a subspace of smaller dimension. Joints linking axial struts for example have only axial effects, and an elaborate routine could make use of this a priori information by avoiding the computation of their transverse components on the different modes, since those components are known to be zero. This could reduce considerably the computation. Only the action of the diagonal elements requires, in fact, a full numerical

treatment like the one described in figure 4.1, in order to be projected on the 3 dimensional space.

Thus, it might be possible to reduce the computation in the analysis of limit cycles in large truss structures by simplifying the action of the joints, and by making best use of the geometrical characteristics of the structure. It might also be possible to decrease it by finding ways to reduce the number of nonlinear forcing terms, and by deriving a global representation of the effects of clusters of joints. The influence of those further simplifications on the solution accuracy should also be investigated.

6.3.3 System Simulation.

Simulation is almost always used in the process of analyzing dynamical systems. However simulation has its limitations:

Firstly, it does not enable to forecast any trend in the behavior of the system, and it is theoretically necessary to try all possible initial conditions along with all other possible operating parameters to get a complete description of the system's behavior.

Secondly, simulation can be computationally expensive, due to the necessity of taking very small time steps in order to get a stable and accurate integration scheme. However, the cost associated with the analytical investigation of limit cycles may be more important than the one associated with the direct simulation of the system, and this latter approach might be worthwhile.

Very refined models using finite elements representation, like the ones shown in [2], can hardly be used to simulate very large dynamical systems, since they retain too many variables and cannot reasonably be implemented. Simple models have to be utilized, and the modeling derived in Chapter 2 appears to fit the purpose of simulation of large structures. The dynamics are approximated with the same degree of accuracy as when the analytical method is used, and both approaches should therefore yield the same solutions. The nonlinear feedback formulation can be readily employed in an integration scheme, and equation (2-22) needs very few changes to be implemented in a program.

The main task in a simulation would be again to calculate the forcing terms and their effects on the modes. The forcing term due to one single joint requires the knowledge of only the joint displacement and rate of displacement, if a simple model as presented in [2] is retained. The estimate of the number of operations associated with the calculation can be made in the same manner as in Chapter 4, and indicates that $O(8\ N_j n)$ multiplications are necessary to find the effects of all the nonlinearities on all the modes. The rest of the linear effects can be evaluated with $O(2n^2)$ operations, which is not preponderant when many nonlinearities are distributed in the system. The number of times the evaluation is performed depends on the integration scheme and the number of time it is called.

The range of integration can be expected to be long, and many oscillations are likely to be required in order to conclude on the existence of a limit cycle. A method having a small per-step truncation

error should therefore be used in order to minimize the cumulative error. Hamming's method ([28]) has such a property. The method is a predictor-corrector type of method. The recursive integration formula is stable, and it is also relatively stable, which means that the rate of growth of the total error during the process is always less than that of the solution. The use of a predictor and a corrector implies that the function must be evaluated twice per iteration. There is a benefit however in that the length of the step can be varied and in that the accuracy of the solution can be controlled. A fourth order Runge-Kutta scheme is usually chosen to start the process. The following estimates of the computational chore will be based on the use of Hamming's method.

Data from the COFS I mast experiment locates the lowest mode at 0.18 Hz, corresponding to the first bending mode, and places significant modes up to 100Hz. Even though the controls change the natural frequencies, those values indicate a reasonable order of magnitude for the closed-loop modes.

In order to obtain a sufficiently accurate solution, and because of the small per-step error of Hamming's method, the time step could reasonably be estimated in the order of $\tau = \dfrac{1}{20 f_{max}}$, where f_{max} is the maximum circular frequency. A reasonable value for the time step in the case of the Mast experiment should therefore be $\tau = 0.5$ milliseconds.

The frequency of the limit cycle is believed to be around the lowest linear mode's frequency, and a simulation may be run for as long as 50 cycles, depending on the speed with which the system tends toward zero, or a limit cycle. This time period corresponds to about 4.5

minutes in the case of the COFS I Mast, and the total number of evaluations of the nonlinear forcing term in that case can therefore be estimated to be equal to about 1,120,000.

Comparing this figure with the computation required by the analytical method, it must be recalled that a single major iteration of the analytical process requires $3n \times 3n \times 3$ times the determination of a nonlinear term equivalent to the nonlinear forcing term computed for the simulation. This means 270,000 evaluations of this equivalent nonlinear forcing term when the data of the Mast case are taken. Thus, the analytical procedure should converge in less than 5 major iterations to be faster than the simulation, and this is most unlikely as n keeps increasing.

According to these rough estimates, the simulation approach appears to be an interesting alternative to the analytical determination of limit cycles in dynamical systems having a large number of distributed nonlinearities. The determining factor in both approaches is to compute the effect of the numerous nonlinear forcing terms on a quite important number of modes. Simulating the system appears to require all together less evaluations of the linear forcing terms. Hence, it should to be faster to approach the problem by means of simulation.

The analytical method yields stable as well as unstable limit cycles. However, it fails to declare the absence of limit cycle, which can be seen more easily by simulating the system. Thus, the biggest advantage one method can have on the other is to be faster. Based on the estimates derived before, simulation was shown to be faster, but this,

however, might become untrue if the time step was to be reduced, and more importantly, if the model of the joints required more than two states, since it would increase the number of operations needed to calculate the nonlinear forcing term for every individual joint. Nevertheless, the effectiveness of simulation has to be considered, especially since alternate integration schemes such as the ones reported in [28] appear to be very promising, and shall result to be very appropriate for simulating nonlinear feedback systems. Those techniques are based on a better understanding of the specificity of the problem they try to solve. Approaches, such as Frowler's method, utilize as effectively as possible the linear character of the system. Those methods replace the linear continuous system by its discrete equivalent, thus yielding the exact homogenous response, whatever time step is used. The inputs to the discrete system are sampled versions of the continuous inputs, and compensation is used to reduce the distortion introduced by the sampling. Such integration schemes are always stable, and they are unusually accurate, even for large time steps.

Therefore, limit cycles should be analyzed in significantly larger systems with different simulation techniques. This study would allow to determine the best adapted one, and it would allow to compare its performance with the performance of the analytical methods. Definitive conclusions would then be made on the real efficiency of simulation techniques to determine limit cycles in large actively controlled dynamical structures.

REFERENCES

[1]   Lee, R.Y.-K.,   "Assessment of Linear and Nonlinear Joint Effects on Space Truss Booms",   S.M. Thesis, Dept. of Aero. and Astro., M.I.T., 1985.

[2]   Belvin, W.K.,   "Modeling of Joints for the Dynamic Analysis of Truss Structures",   S.M. Thesis, School of Engineering and Applied Science, George Washington University, 1985.

[3]   O'Donnell, K.J.,   "Identification of Nonlinear System Parameters in Space Structure Joints Using the Force-State Mapping Technique",   S.M. Thesis, Dept. of Aero. and Astro., M.I.T., 1985.

[4]   Meirovitch, L.,   "Modeling and Control of Distributed Structures",   Proc. of Workshop on Application of Distributed System Theory to the Control of Large Space Structures, J.P.L. Publ. 83-46, 1983.

[5]   Gelb, A. and Vander Velde, W.E.,   Multiple-Input Describing Functions and Nonlinear System Design,   McGraw-Hill, New York, 1968.

[6]   Atherton, D.P. and Dorrah, H.T.,   "A Survey on Nonlinear Oscillations",   Int. J. Control, Vol. 31, 1980, pp. 1041-1105.

[7]   Gray, J.O. and Nakhla, N.B.,   "Prediction of Limit Cycles in Multivariable Nonlinear Systems",   Proc. IEE, part D, Vol. 128, No. 5, 1981, pp. 223-241.

[8]   Athans, M., Multivariable Control Systems I & II: Coursenotes, School of Engineering, M.I.T., Fall 1985, Spring 1986

[9]   Guckenheimer, J. and Holmes, P.,   Nonlinear Oscillations, Dynamical Systems, and Bifurcations of Vector Fields, Springer-Verlag, New York, 1983.

[10]   Hahn, W.,   Theory and Application of Lyapunov's Direct Method, 1911, English Ed. Englewood Cliffs, N.J.,Prentice-Hall, 1983.

[11]   Aderibigbe, A.A. ,   "Methods for Predicting Limit Cycles in Multivariable Nonlinear Dynamic Systems",   Ph.D Thesis, Dept. of Mech. Eng., M.I.T., 1986.

[12]   Spannos, P-T.D. and Iwan, W.D.,   "On the Existence and Uniqueness of Solutions Generated by Equivalent Linearization",   Int. J. of Nonlinear Mechanics, Vol 13, 1978, pp. 71-78.

[13] Choudhury, B.E. and Atherton, D.P., "Limit Cycles in High Order Nonlinear systems," Proc. IEE, Vol. 121, pp. 717-724.

[14] Powell, M.J.D., "An Hybrid Method for Nonlinear Equations", Numerical Methods for Nonlinear Algebraic Equations, Rabinowitz Ed., Gordon and Breach Science Publishers, London 1970.

[15] More, J.J. , et al., User Guide for MINPACK-1, Argonne National Laboratory, Illinois, ANL-80-74, 1980.

[16] Scales, L.E., Introduction to Non-Linear Optimizations, Springer-Verlag, New York, 1985.

[17] Broyden, C.G., "The Convergence of a Class of Double-Rank Minimization Algorithms I: General Considerations", J. Inst. Math. Appl., Vol. 6, 1970, pp.76-90.

[18] Fletcher, R., "A New Approach to Variable Metric Algorithms", Computer J., Vol 13, 1970, pp. 317-322.

[19] Goldfarb, D., "A Family of Variable Metric Updates Derived by Variational Means", Math. Comp., Vol. 24, 1970, pp. 541-551.

[20] Shanno, D.F., "Conditioning of Quasi-Newton Methods for Function Minimization", Math. Comp., Vol 24, 1970, pp. 647-656.

[21] Himmelblau, D.M., "An Uniform Evaluation of Unconstrained Optimization Techniques", Numerical Methods for Optimization, Lootsma Ed., Academic Press, 1972.

[22] Polak, E. and Ribière, G., "Notes sur la Convergence de Méthodes de Directions Conjuguées", Revue Fr. Inf. Rech. Oper., Vol 16-R1, 1969, pp.35-43.

[23] Dixon, L.C.W., "The Choice of Step Length, a Crucial Factor in the Performance of Variable Metric Algorithms", Numerical Methods for Optimization, Lootsma, F.A. Ed., Academic Press, 1972.

[24] Wen, Y.-K., "Method for Random Vibration of Hysteretic Systems", J. of Eng. Mech. Div., ASCE, Vol. 102, No. EM2, April 1976.

[25] O'Connell, S.P., "The Influence of Heavy Vehicle Dynamics on Pavement Response", S.M. Thesis, Dept. of Mech. Eng., M.I.T., 1986.

[26]   Moler, C. , Little, J. , Barget, S. , Kleiman, S. ,
        _PC-Matlab User's Guide, The MathWorks Inc., November 1985.

[27]   James, M.L., Smith, G.M. and Wolford, J.C., Applied Numerical
        Methods for Digital Computation with Fortran and CSMP, Second
        Edition, Harper & Row, 1977

[28]   Smith, J.M., Mathematical Modeling and Digital Simulation for
        Engineers and Scientists, John Wiley & Sons, 1977